A NUMERICAL MODEL OF THE SURFACE ENERGY BALANCE
AND GROUND THERMAL REGIME IN ORGANIC PERMAFROST TERRAIN


by

DAVID HARRY HALLIWELL, B.Sc.


A Thesis

Submitted to the School of Graduate Studies

in Partial Fulfillment of the Requirements

for the Degree

Doctor of Philosophy


McMaster University

November 1989

# NUMERICAL MODEL OF THE GROUND THERMAL REGIME IN PERMAFROST

DOCTOR OF PHILOSOPHY (1989)                    MCMASTER UNIVERSITY
(Geography)                                     Hamilton, Ontario

TITLE:   A Numerical Model of the Surface Energy Balance and
         Ground Thermal Regime in Organic Permafrost Terrain

AUTHOR: David Harry Halliwell,   B.Sc. (Carleton University)

SUPERVISOR: Professor Wayne R. Rouse

NUMBER OF PAGES: xii, 195

## ABSTRACT

Measurements of the surface energy balance and
ground thermal regime were carried out near Churchill,
Manitoba at two sites in the summers of 1984 and 1985, and a
third site in the summer of 1987. The sites represented
unforested permafrost locations with a non-transpiring
organic surface cover. After examining the microclimatic and
ground thermal regimes, the measurements were used to
develop a physically-based one-dimensional model capable of
emulating the observed regimes. Sensitivity analysis of the
model was carried out to determine the relative importance
of processes and factors influencing ground temperatures at
the study locations, and to assess the validity of using
this modelling approach for prediction of changes in the
microclimatic or ground thermal regimes.

The data collected in this study represent a
complete, comprehensive, and accurate series of measurements
of the summer microclimatic regimes at the study locations.
On a descriptive basis, the data provides a strong knowledge
base of microclimatic processes in this type of terrain. The
major significance of the thesis lies in the results of the
numerical modelling. Although the general modelling approach
is similar to previous models in the literature, the model
developed in this study uses a more comprehensive
evaporation model which includes a thermal resistance factor

acting in the surface layer. Changes in the thermal resistance factor completely reverse the sensitivity of the model to surface moisture changes: with a high thermal resistance the soil cools in response to surface drying, while low thermal resistance values lead to soil warming in response to surface drying. This result is very important in assessing the response of permafrost conditions to local or global climatic change.

In addition, the field data indicate that both surface moisture and surface temperature vary widely over horizontal distances of only a few metres. This result indicates that one-dimensional models may not be capable of treating the evaporation process in a physically-based manner. Evaporation models previously used in the literature may be misleading in their predicted response to climatic change. Further study is required into the nature of the surface evaporative layer, and the validity of one-dimensional evaporation models in non-homogeneous terrain.

## ACKNOWLEDGEMENTS

Although only one name goes on a thesis, the effort involved requires the support of a large and varied cast of people. A thesis also represents much more than an academic accomplishment, and the contributions of the following individuals are just as varied. The longer the process takes, the longer the list gets, and I cannot pretend that it is comprehensive or complete.

First and foremost, I want to thank Dr. Wayne Rouse for his support, guidance, and patience over the last 6 years. From the day he received a letter out of the blue from France, he has been responsive and encouraging regarding my work. Dr. John Davies has borne the brunt of many long discussions, on topics ranging from climatology through to the joys of JET. Dr. John Drake provided additional help, especially during our Wednesday afternoon meetings. Dr. Ferouk Mirza also contributed to the guidance procedure, keeping me on the straight and narrow when it came to numerical work. All have contributed their knowledge to the manuscript.

I never would have made it into the field if it hadn't been for Steve Hardill: how on earth did you get all that equipment ready for us? Out in the field, help came from many places, but Arvids Silis, Paul Stalker, David

Joiner, Tim Papakyriakou, and Shelagh Gunn are all fixed in my memory banks (for good reasons). Dr. T.H.W. Baker filled a large gap in instrumentation with the provision of the TDR equipment. Without Veryan Bingham, 1985 would have been unmanageable, and her continued friendship has seen me through some difficult times. Dr. Peter Lafleur became an ideal place to bounce crazy ideas, and provided much stimulus through the analysis period. Anyone who was ever a Gannet must be thanked, as must the Friday morning hockey crew (except that tall blonde guy that came out one year and always hogged the puck). From the day I arrived as a new M.Sc. student, looking at the world through green eyes, to the day I left Mac as a "senior" Ph.D. student with new students that had never heard of who I thought of as "the old guard", I have had the benefit of socializing with a number of very good people. Thanks to all.

All of my efforts have been with the continued support of my family. Now they'll finally have another "Dr. Dave" to talk about.

## TABLE OF CONTENTS

# LIST OF FIGURES

# LIST OF TABLES

Chapter 1: Introduction

As human activities increase in permafrost areas, predictions are required of both the effect of development and the range of possible natural changes over the lifetime of the activities. For example, in the case of railways, bridges, or pipelines, the design engineer must consider the local effects of construction, and the possible range of conditions which will occur over the many years the facility is in use. A design which is stable after initial construction could be in danger if permafrost degrades as the result of local hydrologic changes or global warming. Adequate planning requires an understanding of the nature and characteristics of permafrost, and knowledge of its relationship to climate.

Permafrost is defined on the basis of ground temperature, and ground temperature is controlled by climatic conditions. On a regional scale, the most important factor is mean annual air temperature, which in lowland terrain varies only slowly over distances of hundreds of kilometers. At this scale, permafrost is commonly divided into continuous, and discontinuous zones - based on how extensive the permafrost is in the area. Figure 1.1 shows the southern limits of these zones in North America. Within each of these broad zones, variations in permafrost

1
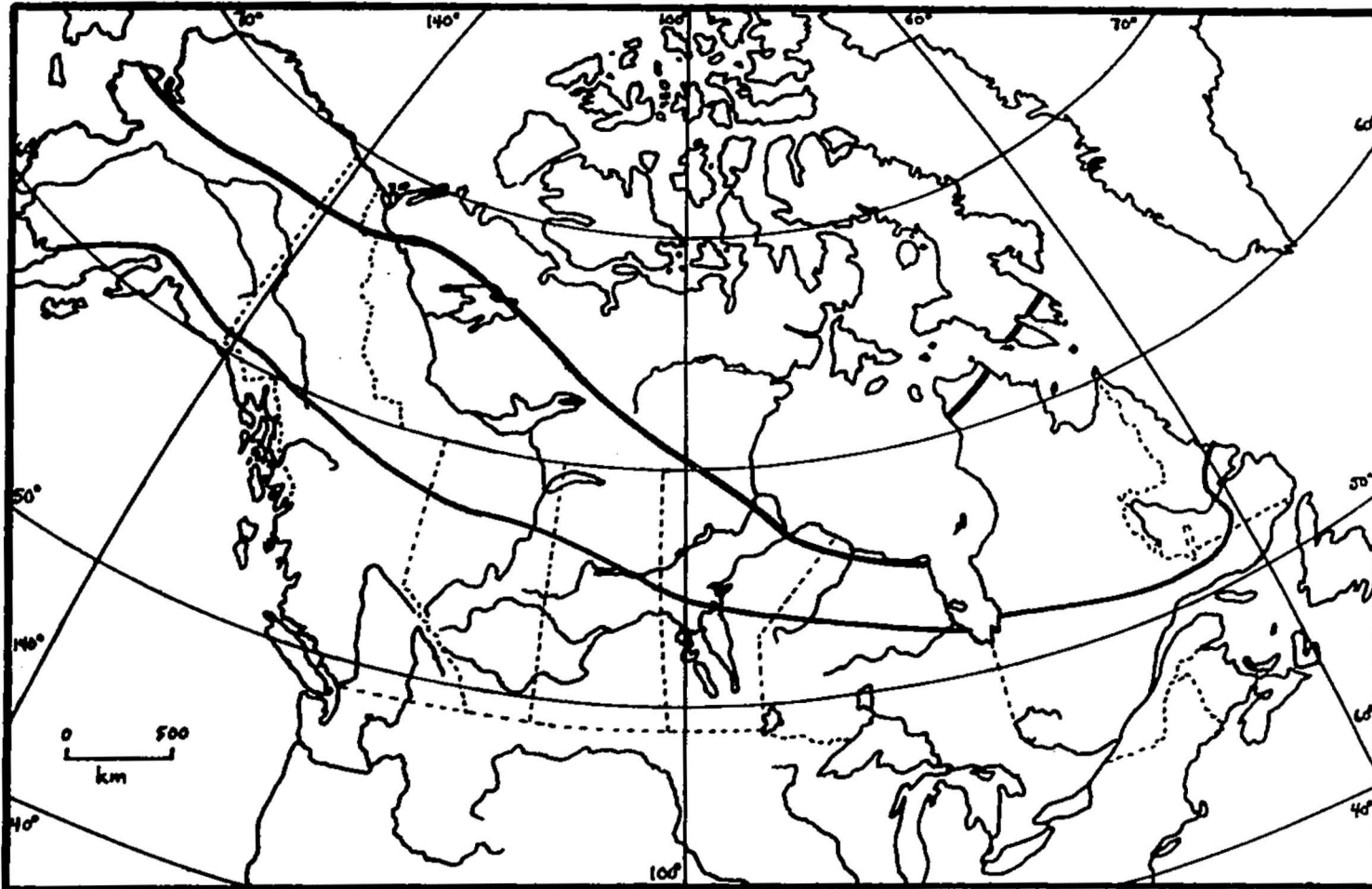
**Figure 1.1:** Southern limit of continuous permafrost (heavy line) and discontinuous permafrost (medium line) in North America. Permafrost may exist outside these limits at high altitude in mountainous regions.

conditions occur because of variations in surface microclimate. Differences in soil type, vegetation cover, snow cover, and other local factors alter the microclimate and affect the relationship between air temperature and ground temperature. In the continuous permafrost zone, these local differences lead to variations in active layer depth. In the discontinuous permafrost zone, these differences can also control whether permafrost is present or absent in a particular location.

On a descriptive basis, considerable work has been done in associating surface conditions with permafrost conditions (e.g. Brown and Péwé, 1973; Luthin and Guymon, 1974; Weller and Holmgren, 1974; Brown, 1978). Frequently, the presence or absence of peat (or organic soil) at the surface is identified as an important controlling factor, along with the hydrologic conditions related to evaporation. The influence of peat is explained by the large difference in thermal conductivity between the saturated, frozen state which occurs in winter, and the dry, unfrozen state which occurs in summer. The effect is to allow efficient removal of heat in the winter, but restrict warming of the soil in summer, thus promoting cooler ground temperatures and an increased likelihood of permafrost. The role of hydrological conditions is also important in determining the quantity of energy which will be utilized for evaporation. When moisture is readily available at the surface and evaporation rates

are high, surface temperatures should be cooler than they would be under dry conditions.

Descriptive models of this type are limited in their predictive or interpretive power. Although the nature of the system response can be described, it cannot be quantified, and interpretation becomes subjective. In complex situations where feedback processes are common, it is rarely possible to determine the overall response to a given condition using a purely descriptive framework. Mathematical or numerical models allow one to quantify the relationships between variables and examine the importance of individual processes. Feedback processes can be included or excluded at will, to assess their importance in the total system response. This aids identification of importance processes in interpretive studies, and facilitates a quantitative prediction in forecasting work.

For example, local measurements in regional climate studies incorporate purely local effects, which must be quantified in order to assess true regional conditions. A numerical model allows identification of the local influences, isolating the processes and conditions important at the regional scale. For predictions of the permafrost response to external changes, a numerical model is also of value; e.g. changes in surface conditions (such as plant cover, soil type, or hydrologic conditions) as the result of natural events or anthropogenic activities, or changes due

to regional or global climatic factors (such as atmospheric warming due to anthropogenic production of $CO_2$ and other trace gases).

Numerical computer models suitable for this type of study have been developed by several authors, e.g. Outcalt et al (1975), and Smith (1975, 1977). These models attempt to partition energy available at the ground surface into atmospheric and sub-surface components, allowing prediction of the ground thermal regime. The models incorporate radiation, evaporation, and atmospheric heating, along with soil thermal conduction. This surface energy balance approach can be used to examine the effect of any change which influences the energy partitioning. The only required meteorological input is incoming radiation (or cloud cover or similar data to allow modelling of incoming radiation), air temperature and humidity, wind speed, and precipitation. Various surface parameters must also be supplied to initialize the models.

One characteristic of the Outcalt et al (1975) and Smith (1975, 1977) models is the lack of water vapour movement in the soil. The thermal effects of vapour movement are assumed to be included in the thermal conductivity coefficients, and vapour movement is only considered at the surface (evaporation) as a boundary condition. Evaporation is treated as a purely atmospheric phenomenon, with local surface control.

Other authors have developed models for soil thermal diffusion which include vapour movement within the soil, e.g. van Bavel and Hillel (1976) and Outcalt and Nelson (1985). In a model of this type, evaporation is simply the rate of vapour transfer at the surface, so the influence of subsurface moisture conditions is handled directly. The model of van Bavel and Hillel includes the surface energy balance, but was not applied to permafrost problems. The model of Outcalt and Nelson is applied to palsas, but uses prescribed surface temperatures. The model was only used to simulate soil temperatures over a 24 hour period. These models require specification of soil vapour diffusion and hydraulic conductivity coefficients, and soil water characteristic curves. This type of information is rarely available, making it difficult to use these models for long-term predictions over periods of months or years in applied studies. As a result, authors examining long-term effects have used models of the type presented by Outcalt et al (1975) and Smith (1975, 1977) - e.g Smith and Riseborough (1983).

This study follows in the footsteps of these earlier works. The specific goals of this thesis are as follows: to examine the microclimatic and ground thermal regimes in an unforested permafrost location with organic surface cover; to develop a physically-based one-dimensional numerical model capable of emulating the observed microclimatic and

ground thermal regimes; use the model to interpret the physical processes and factors influencing the ground temperatures at the study locations; and to assess the validity of using this modelling approach for predictive purposes.

## Chapter 2 - Collection and Manipulation of Field Data

### 2.1 - Site Locations and Descriptions

The basic data used in this study come from two sites near Churchill, Manitoba. The first site, designated the Churchill Site, is located east of the town, about 2km from the coast of Hudson Bay. The second site, designated the Marantz Site, is located about 70km south of the town of Churchill and about 10km east of the Hudson Bay Railway. The locations of these sites are indicated in Figure 2.1. Data were collected during the summers of 1984 and 1985. In 1984, the collection period for both sites was from mid-May to mid-August. In 1985, the collection periods were from early May to late September at the Churchill site, and from early June to mid September at the Marantz site. (After mid-August, the Marantz Site was unattended, with only a limited number of instruments in operation.) In order to supplement the knowledge of the frozen soil characteristics, measurements of soil temperatures, water content, and thermal conductivity were carried out at each site in December, 1985.

The Churchill site is in a low-lying, poorly-drained area. The surface cover at this site is predominately sedge peat. The sedge cover is sparse, 0.05-0.2m in height, and
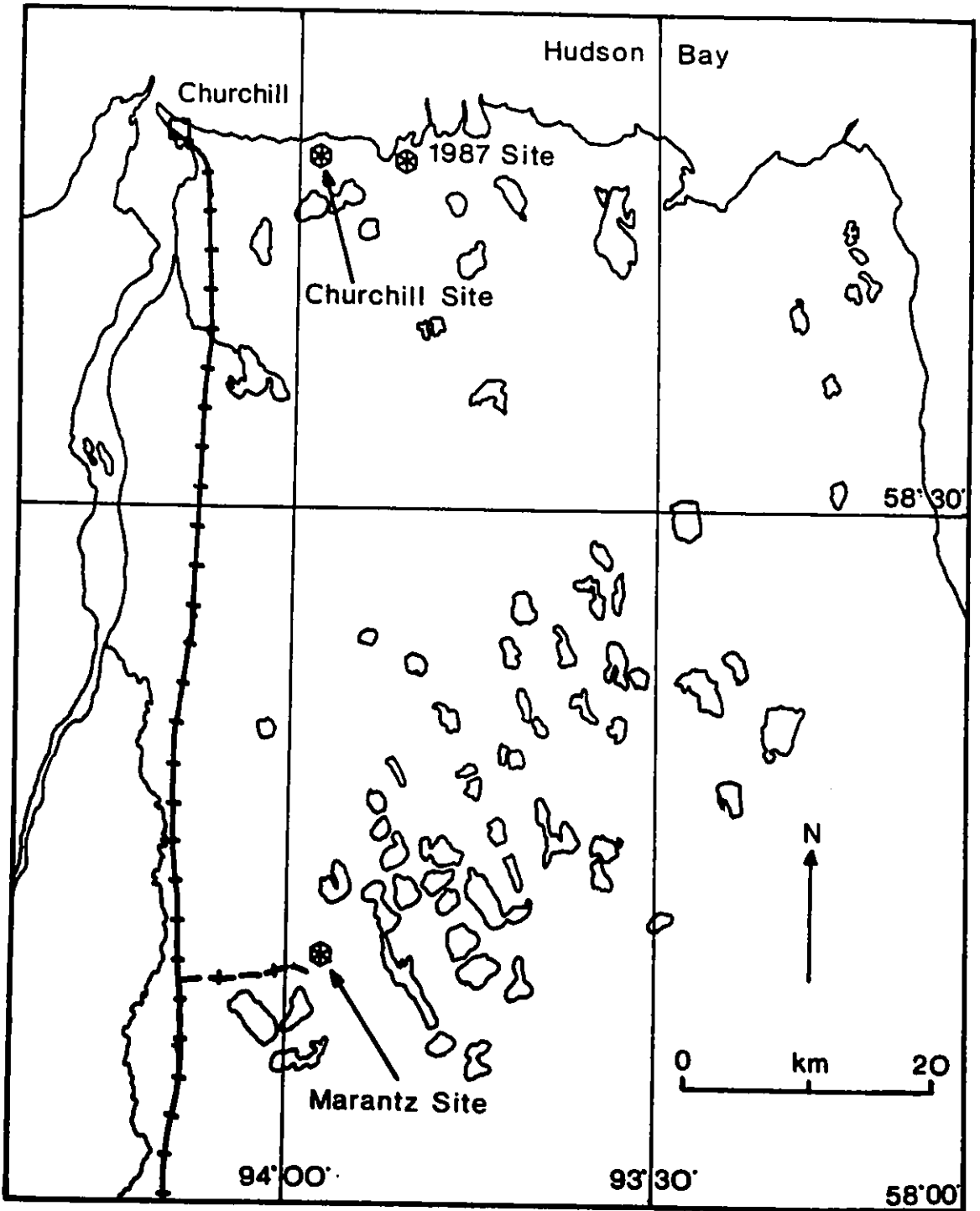
**Figure 2.1:** Map showing the location of the study sites, near Churchill, Manitoba.

there are occasional dwarf deciduous trees and small ponds. The soil profile consists of 0.25-0.3m of sedge peat overlying a sandy clay containing numerous cobbles. The Marantz site is on a polygonal peat plateau, with a moss- and lichen-dominated surface cover. Drainage from the peat hummocks is good. Approximately 1m of peat overlies a coarse, sandy mineral soil. Both sites have local surface irregularities in the order of 0.1-0.2m.

Information on soil moisture and density was obtained from core samples collected in May, 1984, during installation of soil temperature sensors and neutron probe access tubes. These sensors were installed in holes drilled using a modified USA-CRREL core barrel driven by a Stihl power auger. The CRREL barrel provides core samples with a nominal diameter of 3.8cm (Veillette and Nixon, 1980). At the Churchill site, three holes were drilled and four samples from various depths were recovered. At the Marantz site, two holes were drilled and four samples recovered. All samples were collected in early May, when the soil was still frozen. They were maintained in a frozen state until volume measurements and weights for moisture content determination could be carried out. The condition of the samples varied, but enough material was recovered in an undisturbed state to allow determination of the soil densities and volumetric water content. Borehole logs are provided in Figures 2.2 and 2.3.
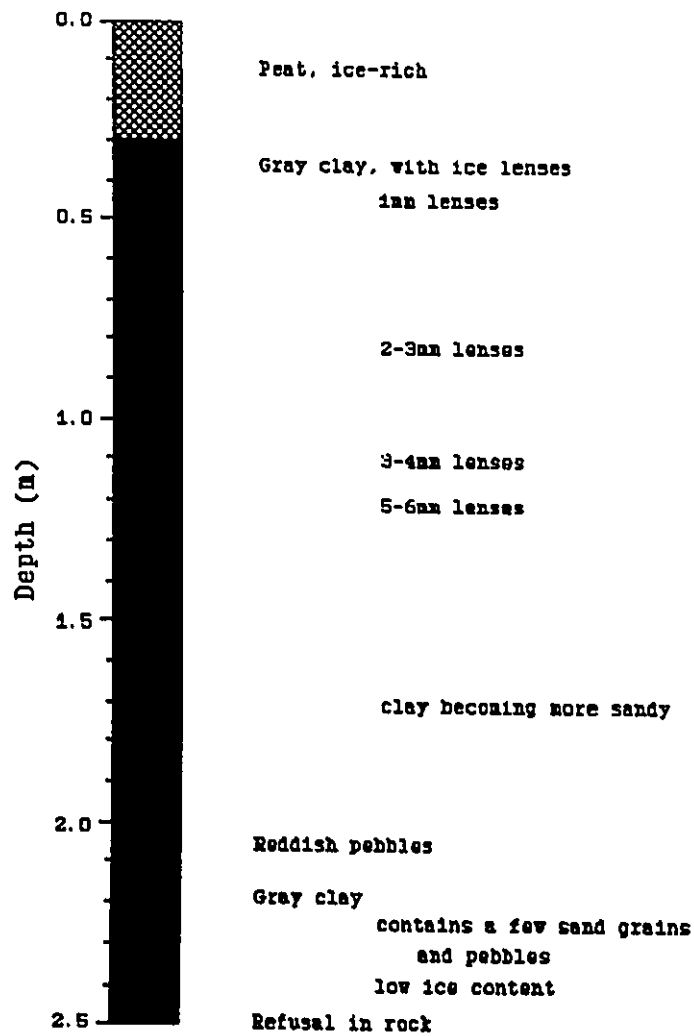
Figure 2.2: Borehole log for the soil profile at the Churchill Site. Composite of three boreholes.
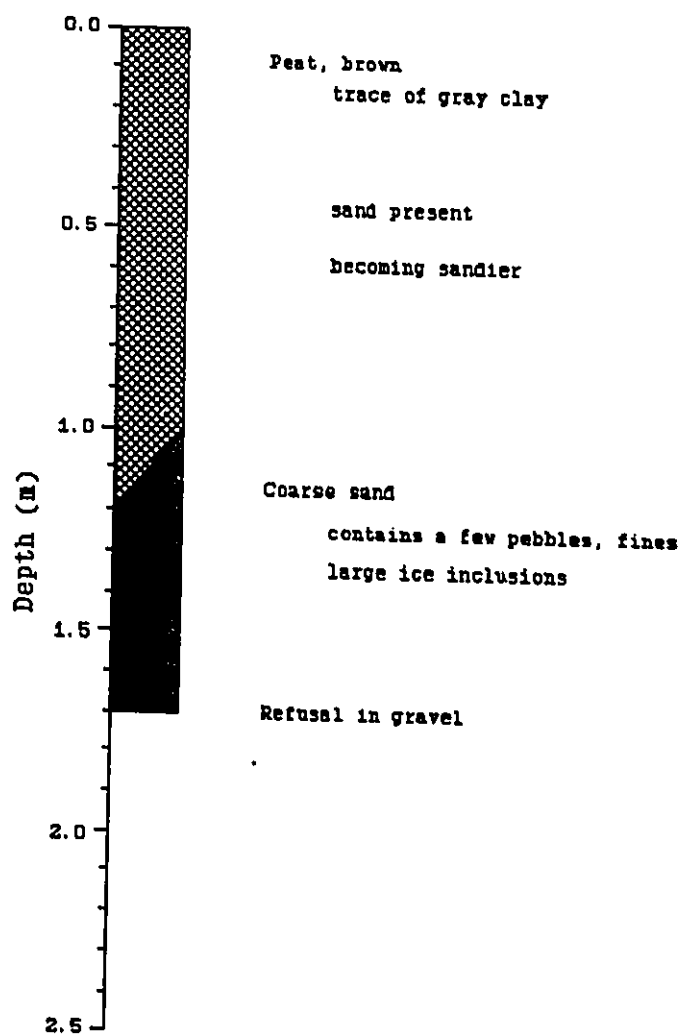
**Figure 2.3:** Borehole log for the soil profile at the Marantz Site. Composite of two boreholes. The peat contained occassional ice layers up to 45mm thick. The sand contained ice layers up to 45mm thick in one hole, and 350mm in the other.

After the 1984 and 1985 data had been analyzed, it became apparent that supplementary data on the spatial variability of surface and near-surface soil thermal characteristics would be useful. Logistical considerations made it impossible to instrument the 1984/85 sites again, but in 1987, measurements of this variability were carried out at another site located east of the Churchill site. This site had surface characteristics similar to the Churchill site, allowing comparison with the earlier data. This site is indicated on figure 2.1 as the 1987 site. The soil profile consisted of 0.1 to 0.15m of sedge peat overlying a cobbly mineral soil.

## 2.2 - Instrumentation

Instrumentation can be roughly divided into three categories: radiation, atmospheric variables, and soil variables. The basic instrumentation layout was established in 1984, and will be described first. Several additions were made in 1985. The 1987 site was instrumented in a similar fashion, but only the detailed soil information is used in this study.

### 2.2.1 - 1984 Instrumentation

Radiation instruments at each site consisted of one Middleton CN-1 net pyrradiometer for measurement of net all-wave radiation, and one Eppley black-and-white pyranometer

for measurement of incoming short-wave radiation. These instruments were placed at a height of about 3m. The Churchill site had, in addition, another Eppley pyranometer inverted for measurement of reflected short-wave radiation, and an Eppley PIR pyrgeometer with a silicon dome for measurement of incoming long-wave radiation. These instruments were placed at a height of about 1m. The net pyrradiometer domes were inflated with dry air. The air was desiccated by passing it through silica gel. At the Churchill site, the air supply was provided by an aquarium pump connect to AC power. The Marantz site lacked electrical power, so air was supplied from three truck inner tubes which were inflated by hand at each site visit.

The pyrradiometers and pyranometers had been recently calibrated by the Atmospheric Environment Service of Canada and compared well in pre- and post-season cross-checks. The overall error associated with these instruments is in the order of +/-5%.

The Eppley PIR pyrgeometer was modified from the original specifications. First, the internal temperature compensation circuit, which corrects for the radiation emitted by the sensor, had been removed and replaced by a thermocouple. The thermocouple allows direct calculation of the radiative loss by the pyrgeometer, and eliminates errors in the compensation circuitry. The second modification was to enclose the body of the instrument in a housing with a

fan, to provide ventilation of the silicon dome. This reduces the errors associated with solar heating of the dome (Enz et al, 1975).

The pyrgeometer calibration was checked prior to the field season by inverting it over a temperature-controlled circulating oil bath. Measurements of the pyrgeometer output were then compared to the radiative flux calculated using the bath temperature. The calibration coefficient determined in this manner was about 14% higher than the original manufacturer's calibration. The new calibration was used in the field. In 1985, a test was carried out to determine the effect of solar heating of the dome under field conditions. Alternately shading and unshading the pyrgeometer indicated a solar heating effect of about $15Wm^{-2}$ with incoming solar radiation of $750Wm^{-2}$. This compares well to values of 13-$30Wm^{-2}$ reported by Alados-Arboledas et al (1988) for an unventilated Eppley pyrgeometer. No correction was applied to eliminate this error.

Atmospheric variables included air temperature and humidity, wind speed and direction, and precipitation. Temperature and humidity measurements were made using a psychrometer design modified from that given by McCaughey and Brintnell (1984). Psychrometers were mounted on a mast at heights of 0.25, 0.5, 1.0 and 2.0m. Wind measurements used a Young propeller anemometer/wind vane with a stall speed of about 0.3m/s. The anemometer was positioned at a

height of 3.5m. Precipitation was measured using standard rain gauges with a diameter of 0.1m. At least two gauges were used at each site, and the values averaged.

Psychrometer temperatures were measured using copper-constantan thermocouples. Calibration of the thermocouples prior to the field season indicated that they were interchangeable to 0.01C°. Analysis of errors prior to the field season indicated that the greatest source of error in the thermocouple temperatures was the reference compensation provided by the data logger. The data logger design incorporated a platinum resistance sensor for each input card, but testing indicated that errors of several tenths of a degree could occur between opposite ends of the input card during periods of rapid warming or cooling. This error would be very large for measurements of temperature profiles.

In order to reduce errors associated with reference junction compensation, the psychrometer thermocouples were arranged so that the dry bulb sensor for each psychrometer was referenced to a single large thermal mass, which could be buried in the ground where thermal gradients and transient temperature changes would be small. This thermal mass was then referenced back to the data logger for an absolute temperature reading. Wet bulb thermocouples were referenced directly to the corresponding dry bulb, to provide a wet bulb depression. Since measured temperatures

still use the data logger input card reference temperature, the physical arrangement of thermocouple junctions did not improve the overall absolute accuracy of the temperature readings. However, it provided greatly reduced relative errors between dry bulb temperatures, giving better estimation of the temperature and humidity gradients.

Soil temperature data for the Churchill Site consisted of thermistor readings at nominal depths of 0.0, 0.05, 0.1, 0.2, 0.3, 0.5, 0.75, 1.0, 1.25, and 1.5m, and thermocouple readings at nominal depths of 0.0, 0.05, 0.1, 0.25, 0.5, and 0.75m. Each set of thermistor or thermocouple sensors was mounted on a single wooden rod, installed in a hole drilled in the frozen soil. As a supplement to the rod data, the soil surface temperature was measured using fine-gauge thermocouples imbedded just beneath the surface cover. Several thermocouples were connected in parallel, to provide a spatial average.

Soil temperature data for the Marantz site consisted of one thermocouple rod at the same nominal depths as the Churchill Site, one thermistor rod at nominal depths of 0.2, 0.35, 0.5, 0.65, 0.8, 0.95, 1.1, 1.25, and 1.4m, and the same method of soil surface temperature measurement. At each site, two Middleton CN-6 soil heat flow transducers were buried at a depth of about 0.01m. The two transducers were connected in series to provide a single average value. Periodic soil moisture readings were carried out using a

neutron probe lowered down a 0.1m diameter aluminum access tube.

All radiation and atmospheric sensors were connected to a Campbell Scientific CR-7 data logger. Each sensor was read every 10 seconds, and one-hour averages were output to magnetic tape for subsequent computer manipulation. Vapour pressures were calculated from the dry- and wet-bulb temperatures by the data logger at each ten-second interval, and the values averaged each hour. Wind direction was not averaged directly: the data logger computed a vector sum using wind speed and direction, thus providing a true hourly wind direction and magnitude. Soil thermocouples and heat flow transducers were read every 60 seconds, and averaged every hour.

The error in measurements introduced by errors in voltage measurements by the data logger is negligible when compared to the inaccuracy of the basic sensors themselves. The accuracy of the radiation instruments and the arrangement of psychrometer thermocouples have already been discussed. Field cross-checking of psychrometers for a 24-hour period indicated that they agreed to +/-0.05C° for dry bulb temperatures, with most values differing by less than this. Wet bulb temperatures were less accurate, with the resulting vapour pressures varying by up to 0.01kPa. No systematic variations were identified. Data logger resolution was 0.01C° or better for temperatures

(psychrometers and soil thermocouples), and 0.001kPa for vapour pressure.

The soil temperature thermistors and precipitation gauges were read manually once per day, usually in the morning (between 6 and 10 o'clock solar time). Thermistor resistances were measured using a hand-held multimeter. The resistances were then converted to temperatures using calibration curves established prior to the field season. Calibration procedures used a temperature-controlled oil bath and a platinum resistance sensor accurate to +/-0.01C°.The values measured in the field had a precision of at least +/-0.01C° and an accuracy of +/-0.05C°.

At the Churchill site, settlement of the thawed soil caused displacement of the thermistor and thermocouple rods, so that the zero mark on each rod was above the surface. The displacement at the end of August, 1984 was 0.03m for the thermistor rod and 0.04m for the thermocouple rod. This displacement had increased to 0.1m and 0.07m respectively by the spring of 1985. The displacement continued to increase through the 1985 field season, reaching 0.25m and 0.11m by the end of September, 1985. The displacement was measured periodically to provide a correction for the depths of the temperature sensors. No problems with rod displacement occurred at the Marantz site.

Each site was visited once or twice a day. At this time, all radiometers were checked for levelling and

moisture on domes, psychrometers were checked for correct operation, the data logger was checked to ensure correct reading of all sensors, and manual readings were taken.

### 2.2.2 - Additional Instrumentation (1985)

In 1985, two changes were made to the basic instrumentation setup: the psychrometer heights were changed to 0.5, 1.0, 1.5, and 2.0m, and the single propeller-anemometer at 3.5m was replaced by four cup anemometers at the same heights as the psychrometers. The anemometers were of two different types: the Churchill site used Weathermeasure anemometers, while the Marantz site used Young anemometers. Both types had a stall speed of about 0.3m/s. A common calibration curve was used for the four anemometers at each site. Cross-checking of the four anemometers at the Churchill site was carried out for a period of about three days in late June. The anemometers generally agreed to within +/-0.03m/s, when wind direction didn't cause shielding of any of the anemometers on the calibration stand.

The four anemometers were mounted on a separate mast, which could be rotated to reduce the shielding effect of the mast as wind direction changed. The propeller anemometer/wind vane combination was replaced by a simple wind vane, used in conjunction with the 2m anemometer for wind vector calculations of mean wind direction. In late

July, the four-level anemometer system at the Churchill site was replaced with a single anemometer at 2m, so that the 4-level system could be used on another project.

The Marantz site was fully instrumented until the middle of August in 1985. After this date, a reduced set of instruments was left running in an unattended mode until mid September. This site was visited only twice during this period. The reduced instrumentation consisted of net radiation and incoming short-wave radiation, wind speed and direction at 2m, temperature and relative humidity at 2m, and soil temperatures and heat flux. Wind speed was measured using a cup anemometer. Temperature and relative humidity were measured using a Campbell Scientific temperature/relative humidity probe.

Additional soil data was also collected in 1985. Water contents were measured using two methods: a neutron probe, and Time Domain Reflectometry (TDR). The neutron probe technique could not be calibrated for the organic materials, so its use was restricted to the Churchill Site for the depth interval 0.3-1.4m. It provided information on the total water and ice content in the soil. The TDR technique (Topp et al, 1980) is an electromagnetic method of determining soil water content, which responds only to water in the liquid state (Patterson and Smith, 1981).

The TDR technique does not require calibration for mineral soils, but the large range of water content and low

density renders the standard calibration useless for the organic soils. In order to use the technique for the organic soils, large samples (about 0.3m per side) were collected in 1985, and calibrated in the laboratory. The calibration involved adding known quantities of water to a sample of known volume, taking TDR readings at each step. The calibration started with air-dried samples, and proceeded until the samples became saturated. The samples were then allowed to drain, with additional calibration data collected during the drainage phase. The samples could only be subjected to soil moisture suctions of about 1m in the calibration apparatus, so the degree of drainage was not great. At this suction, the Churchill peat retained 72% water by volume, and the Marantz peat retained 67%. Curves were then fit to the calibration data, to allow calculation of the water contents from the field data. Separate curves were established for the Churchill and Marantz peat soils. The resulting water contents have an accuracy of $\pm 0.03 m^3 m^{-3}$.

At the same time that the TDR calibration measurements were taken, freezing characteristic curves were determined for each of the peat soils and the Churchill clay soil. This provided information on the unfrozen water content ($\theta_{uf}$) of each soil over the temperature range -0.05 to -10.75°C. Data were collected for both the freezing and thawing cycles. The TDR readings were converted to unfrozen water contents using the calibration curves established for

the peat soils, and the standard calibration (Topp et al, 1980) for the mineral soil. The calibrations for the unfrozen peat correspond to an air/water/peat mixture, so the curves were adjusted to account for the difference in electrical properties between air and ice before calculating the unfrozen water contents of the ice/water/peat mixture in the frozen samples. (The low ice or air content of mineral soils makes this correction unnecessary for the clay soil.) The results of these measurements are given in Figure 2.4. Since the laboratory results provide values at discreet points only, and the calculations require a continuous function, the data were fitted to an equation of the form:

$$\theta_{uf} = a \, e^{bT} + c \qquad\qquad\qquad (2.1)$$

Since the field data represent thawing conditions, laboratory data for a warming cycle were used. (The soils in question show varying amounts of hysteresis between freezing and thawing over the temperature range 0 to -1°C, as indicated in figure 2.4.) The parameters a, b, and c were calculated using a least-squares criterion. The value of c represents the lower limit for $\theta_{uf}$ at cold temperatures. The term (a+c) is the value of $\theta_{uf}$ at 0°C. (It is assumed that any water in the unfrozen soil in excess of this value will freeze at 0°C.) The value of b is the slope of the curve: it will decrease as the soil texture becomes finer. The fitted parameters are given in table 2.1.

In the field, probes for the TDR technique were
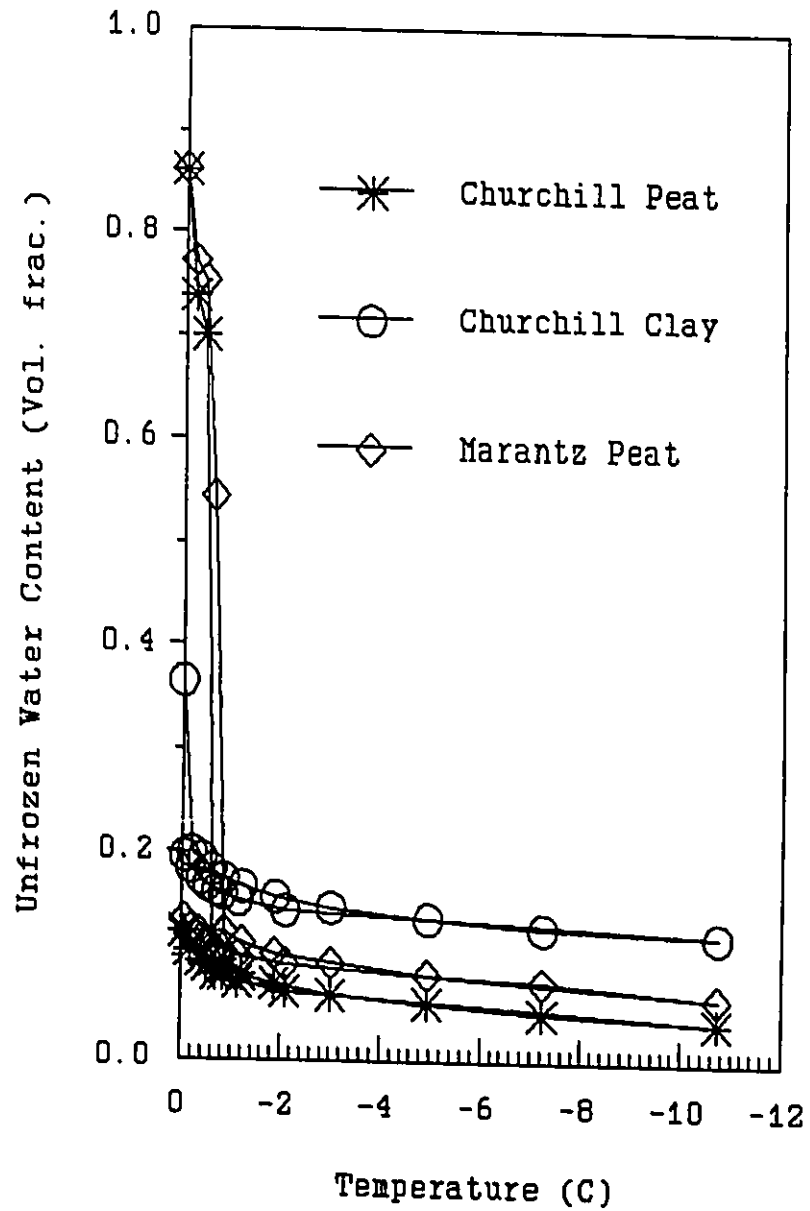
**Figure 2.4:** Unfrozen water content versus temperature for the three tested soils. Results are from laboratory TDR measurements.

Table 2.1: Coefficients for freezing characteristic
curves (equation 2.1), Churchill soils.

| Soil | a | b $(c.^{-1})$ | c |
|------|-----|-----|-----|
| Churchill peat | 0.076 | 0.782 | 0.042 |
| Churchill clay | 0.070 | 0.772 | 0.125 |
| Marantz peat | 0.067 | 0.525 | 0.064 |

installed vertically from the surface, to obtain integrated values with depth, and horizontally in the sides of pits dug in the active layer, to determine values at specific depths. The TDR measurements extended to a depth of 0.6m. The neutron probe and TDR measurements were taken approximately twice a week at the Churchill Site, and every 2 to 3 weeks at the Marantz site.

The horizontal TDR probes were of the design given by Baker and Goodrich (1984), and incorporated a thermal conductivity probe so that simultaneous water content and thermal conductivity determinations could be made. The conductivity readings were made using the transient line-source technique. These probes were installed in the unfrozen soil over the course of the 1985 season, as the active layer deepened, and thermal conductivity determinations were carried out periodically through the summer. Since no measurements could be obtained on the frozen soils during the summer, one set of thermal conductivity readings was taken at the Churchill Site in

December, 1985, to provide an indication of the values for the frozen soil. TDR readings were taken at both the Churchill and Marantz sites at this time. The measured thermal properties for both the frozen and unfrozen soil fall within the ranges given by Brown and Williams (1972) for similar soils.

### 2.2.3 - 1987 Data

The 1987 field program was designed to establish the degree of spatial variation in soil thermal properties and regimes. Although complete atmospheric and radiation data are available, only the soil data are considered here. The results do not apply directly to the previous field sites, but the similarity between this site and the Churchill site allows a qualitative comparison with the 1984 and 1985 data.

The 1987 data consisted of soil temperature profiles, soil heat flux, thermal conductivity and water contents from the surface to a depth of 0.15m. Three locations were instrumented at the site: a dry location at the top of a hummock, a wet location at the bottom of a depression, and an intermediate (mesic) location situated in a low area between the other two. The locations were separated horizontally by distances of 1 to 2m, with a total elevation difference of about 0.2m. Although the elevation difference is small, the contrast in surface moisture regimes was large. The wet location was covered with 1 to

2cm of water when instruments were installed in late June. The dry location was almost completely dry at the surface at this time.

Each location was instrumented with six soil temperature thermocouples at depths of 1 to 13cm, a surface temperature thermocouple consisting of four fine-wire thermocouple junctions wired in parallel, a soil heat flux transducer at 1cm, and a combined TDR/thermal conductivity (TDR/TC) probe at 5cm. The heat flux transducers and TDR/TC probes were the same ones used in 1984 and 1985. The wet and dry locations also had a second soil heat flux transducer at 10cm, and a second TDR/TC probe at 10cm. To avoid interference between the various types of sensors, the instruments were arranged in three vertical planes: soil temperatures in one plane, soil heat flux transducers in a second, and TDR/TC probes in a third. The three planes were about 0.25m apart. The three sets of instruments were installed by cutting a section of peat out of the ground and inserting the sensors in the side of the exposed pit. Additional water content readings were taken using vertically-installed TDR probes of lengths 0.025, 0.05, and 0.1m. These probes were not permanently installed: they were inserted at each location when readings were taken, and five or six readings were taken at each location for each length of probe. This provided an indication of the variability in water content at each location.

Soil temperatures and soil heat flux were recorded by a CR-7 data logger at 7 second intervals, with 10 minute averages stored on cassette tape. TDR and thermal conductivity readings were taken once or twice a week. TDR readings were converted to volumetric water content using the calibration determined for the peat soils from the Churchill and Marantz sites. The 1987 measurement period extended from late June until mid August.

## 2.3 - Data Manipulation

Much of the data collected in the field was stored in a format ready for direct use. However, derivation of several values required adjustment of raw data, or calculations based on the raw data. Three items will be described here: net radiation corrections for the Churchill site due to problems in 1984; soil heat flux corrections for all 1984 and 1985 data; and energy balance calculations.

### 2.3.1 - Net Radiation Corrections

Problems were encountered with the measurement of net radiation at the Churchill site at the start of 1984. Initially, the net pyrradiometer was connected to the data logger as a floating voltage measurement. Due to inadequate grounding of the data logger, the net pyrradiometer voltages occasionally exceeded the permissible voltage ranges on the data logger, and zero values resulted. Once identified, the

problem was fixed by grounding the pyrradiometer to the data logger and providing a local ground for the data logger. However, for earlier data it was necessary to identify erroneous data and provide an alternate estimate of net radiation. Problems were again encountered in late July and early August, due to a loose input card in the data logger.

Net radiation (Q*) can be expressed in the form of the sum of short- and long-wave radiative fluxes by:

$$Q* = K\downarrow - K\uparrow + L\downarrow - L\uparrow \qquad (2.2)$$

where K is the shortwave flux, L is the longwave flux, and the arrows indicate incoming or outgoing fluxes. At the Churchill site, measured values of $K\downarrow$, $K\uparrow$, and $L\downarrow$ were available. Outgoing longwave radiation, $L\uparrow$, is the result of two components: the reflected portion of $L\downarrow$, and longwave radiation emitted by the surface. Reflected $L\uparrow$ can be estimated from the surface emissivity, $\varepsilon$, as $(1-\varepsilon)L\downarrow$, and emitted longwave radiation can be estimated from the surface temperature, $T_S$, and $\varepsilon$ using the Stefan-Boltzmann law $(E = \varepsilon\sigma T_S^4)$. Equation 2.2 can then be rewritten as:

$$Q* = K\downarrow - K\uparrow + \varepsilon(L\downarrow - \sigma T_S^4) \qquad (2.3)$$

Equation 2.3 was used to calculate Q* for the period June 18 to July 6, 1984, when the net radiometer was working correctly. It was found that the agreement between measured and calculated values was good when $\varepsilon = 0.85$ was used: regression analysis gave an $r^2$ value of 0.9983 and a standard error of 8.48 $Wm^{-2}$, with the mean measured flux

being $162 Wm^{-2}$. Therefore, equation 2.3 was used to calculate Q* during the periods of pyrradiometer problems. Erroneous net radiation measurements were identified as times for which the measured and calculated values showed large deviations. In total, nearly 200 hours of measured data were replaced with calculated values of Q*, out of a total of about 2200 hours of observations. (Note: the use of $\epsilon = 0.85$ does not imply that this is an accurate estimate of the true surface emissivity. Errors in radiometer and surface temperature readings have not been considered. The value of 0.85 is simply the value that provided the best agreement between measured values of Q* and values of Q* calculated from equation 2.3.)

## 2.3.2 - Soil Heat Flux Corrections

The second correction applied to the raw data was correction of the soil heat flux transducer readings. Heat flux transducers disturb the thermal regime of the soil in which they are placed, because they do not have the same physical properties as the soil itself. The thermal conductivity of the transducers used in this study is approximately 0.2W/mC·, based on the manufacturer's calibration and the voltage output per unit temperature difference across the transducer. This is less than the values measured at both sites in wet and saturated peat (0.33-0.64W/mC·). Several authors that have examined the

effect of heat flux transducer size, shape, placement, and thermal properties (e.g. Schwerdtfeger, 1976; Fritschen and Gay, 1979; Penney, 1979) have indicated that underestimation by the heat flux transducer is expected when the thermal conductivity of the transducer is less than that of the soil. A second potential source of problems is the lack of good thermal contact between the porous peat soil and the transducer, especially at low water contents. A third source of error would be the transfer of energy in conjunction with large vapour fluxes in the porous peat. Heat flux transducers would not respond to this energy transfer, and since they present a barrier to vapour flow they would further alter the thermal regime in the surrounding soil.

Recently, Rouse (1984) suggested that heat flux transducers seriously underestimated the soil heat flux in permafrost terrain, and recommended an alternate approach. He outlined a method in which the observed changes in soil temperature and active layer depth were used to calculate the change in storage of sensible and latent heat within the soil profile. By estimating a seasonal total soil heat flux using this calorimetric method, he was able to determine a correction factor which could be applied to the heat flux transducer readings. The method used in this study is modified from the method used by Rouse (1984). The method is best described after reviewing basic soil heat flux theory.

Thermal conduction of heat in soils is governed by

the Fourier equation, which is given for one-dimensional heat flow by:

$$C \frac{\partial T}{\partial t} = \frac{\partial}{\partial z}\left(-\lambda \frac{\partial T}{\partial z}\right)$$

(2.4)

where T is the temperature at time t, and both heat capacity (C) and thermal conductivity ($\lambda$) can be functions of depth (z).

In soils, energy can also be transferred by mass movement, with or without phase change. The most common example of this is vapour diffusion, which can significantly augment the transfer of heat in moist soils. Generally, this vapour transport cannot be separated from purely conductive transport, and the term "apparent thermal conductivity" is used to describe the value of $\lambda$. Equation 2.4 is then assumed to incorporate all energy transfer, so that separate vapour diffusion need not be considered.

Since equation 2.4 gives the change in thermal storage at a point in the soil, it must be integrated with depth to determine the storage in a layer of soil:

$$-\lambda \frac{\partial T}{\partial z}(z_1) + \lambda \frac{\partial T}{\partial z}(z_2) = \int_{z_1}^{z_2} C \frac{\partial T}{\partial t} \partial z$$

(2.5)

The two terms on the left side of the equation represent the soil heat flux at the two depths $z_1$ and $z_2$. By setting $z_1 = 0$, the surface flux is given by:

$$Q_g(0) = -\lambda \frac{\partial T}{\partial z}(0) = \int_0^{z_2} C \frac{\partial T}{\partial t} \partial z - \lambda \frac{\partial T}{\partial z}(z_2)$$

(2.6)

Using equation 2.6, methods of measurement of soil heat flux can be divided into two basic classes. The first class uses the left side of the equation and involves determination of the thermal conductivity and temperature gradient in the material under study. This could be carried out on the soil itself, but the temporal and spatial variability of soil thermal conductivity, and the difficulty of measuring the thermal gradient at the soil surface render this approach impractical for many purposes. The heat flux transducer is a modification of this approach, in which a portion of the soil is replaced by an object of known thermal properties incorporating a direct measurement of the thermal gradient across it. The heat flux transducer cannot be placed directly at the surface however, so that the thermal storage in the soil above it will be missed. This could be significant if the burial depth is great and the heat capacity of the soil above the plate is high.

The second class of measurement methods utilizes the right side of equation 2.6. The calorimetric method of Rouse (1984) falls in this class. He measured soil temperatures to a depth of 1.6m, and ignored the heat flux at the base of the soil column. The value of C was based on estimates of the volume fractions of soil solids, water and ice, and their respective heat capacities. The latent heat of phase change was incorporated as a separate value, based on the volume of water which froze or thawed in the soil column in

each time interval. For this, Rouse assumed that all soil water changed phase at 0°C.

In fine-grained soils, there exists a quantity of unfrozen water, $\theta_{uf}$, at temperatures below 0°C, and the latent heat of fusion is liberated over a temperature range. In order to incorporate this into calculations of thermal storage, the concept of "apparent heat capacity" (Williams, 1977) can be used, where the latent heat is included in the definition of heat capacity, such that:

$$C' = C + \frac{d\theta}{dT}uf \tag{2.7}$$

This is then substituted for C in equation 2.6.

In practice, equation 2.6 must be integrated numerically. This can be done using the trapezoid method or Simpson's method, applied directly to the observed temperatures, but the latent heat effect would be missed if the temperature data were not very detailed in the region of the freezing or thawing front. To avoid this problem, the temperature data can be fitted with a suitable interpolating function, and the integration can be carried out using calculated temperatures at any desired depth interval.

Problems can also arise in the use of equation 2.6 where the heat capacity changes rapidly with temperature. Depending on the temporal resolution of the temperature data, the heat capacity at subsequent data intervals may be very different. This is the case for temperatures at or

slightly below 0°C, where the latent heat term dominates. The rapid change in unfrozen water content causes a dramatic increase in the apparent heat capacity. If most latent heat is liberated very close to 0°C - as would be the case for coarse-grained soils - temperature readings could possible fall on either side of the latent heat "hump" in the C vs. T curve, and the latent heat would be missed. This problem can be eliminated by expressing the apparent heat capacity in terms of the enthalpy of the soil, H, where

$$C' = \frac{dH}{dT} \tag{2.8}$$

We can then substitute this in equation 2.6, and thus evaluate H instead of C' for each value of T. Integration of equation 2.8 yields:

$$H(z) = \int_{T(H=0)}^{T(z)} C' dT \tag{2.9}$$

which can be used to evaluate H. This approach has been used in the numerical modelling of heat conduction problems with phase change, using finite element techniques (Comini et al, 1974). Since we are concerned only with changes in H, the selection of a temperature for H=0 is arbitrary. For convenience, 0°C is suggested.

Other variations of calculating soil heat flux can be derived from equation 2.6. By calculating the thermal storage to some intermediate depth, and then adding the heat

flux at the base, one can eliminate the problem of measuring $\lambda$ and $dT/dz$ at the surface without requiring detailed knowledge of soil properties at greater depths. Alternatively, the calorimetric method can be used to correct the value measured by a heat flux plate placed at some depth in the soil. Kimball and Jackson (1975) provide an excellent discussion of the various techniques.

For this study, calorimetric calculations were carried out to various depths using both the thermistor and thermocouple soil temperature readings. The basal flux was then calculated from the observed temperature gradient and measured thermal conductivities. The sparseness of the soil temperature data with depth required the use of an interpolating scheme to get continuous soil temperature profiles at each point in time. This was done by fitting a cubic spline to the observed temperatures, after correcting the sensor depths for vertical rod displacement. Temperatures were then calculated at 0.01m intervals, followed by calculation of the corresponding enthalpy values. The change in enthalpy between two times was then calculated and integrated (using the trapezoidal rule) from the surface to the base depth, obtaining the total calorimetric storage in the soil layer. The basal flux was then added to get the total surface flux.

The soil profiles and thermal properties used in the calculations are given in table 2.2. The coefficients used

Table 2.2: Soil profiles and physical/thermal properties used in the calorimetric heat flux calculations. The soil solid fraction ($X_S$) is based on borehole samples collected in 1984. Moisture contents ($\theta_V$) and thermal conductivities ($\lambda$) are based on field measurements taken in 1985.

| Depth (m) | Soil Type | $X_S$ $C_S$ ($MJ/m^3C\cdot$) | | $\theta_V$ | $\lambda_t$ $\lambda_f$ ($W/mC\cdot$) | |
|---|---|---|---|---|---|---|
| **Churchill Site** | | | | | | |
| 0-0.3 | Peat | 0.15 | 2.5 | 0.85 | 0.6 | 1.6 |
| 0.3-1.0 | Clay | 0.65 | 1.9 | 0.35 | 2.3 | 2.9 |
| >1.0 | Clay | 0.57 | 1.9 | 0.43 | 2.3 | 2.9 |
| **Marantz Site** | | | | | | |
| 0-0.05 | Peat | 0.10 | 2.5 | 0.30 | 0.1 | 0.4 |
| 0.05-0.08 | Peat | 0.12 | 2.5 | 0.50 | 0.3 | 0.6 |
| 0.08-0.15 | Peat | 0.12 | 2.5 | 0.70 | 0.43 | 1.4 |
| >0.15 | Peat | 0.13 | 2.5 | 0.87 | 0.56 | 1.6 |

to calculate unfrozen water content as a function of temperature were given in table 2.1. The water contents were based on 1984 borehole samples and 1985 TDR and neutron probe measurements. Soil densities and profiles were based on the 1984 borehole samples.

An example of temperature profiles fitted to the measured values is given in Figure 2.5. Variations in interpolated frost line depth gave rise to large latent heat storage calculations when hourly thermocouple data were used. To reduce the error associated with this, the soil heat flux values were integrated over time to give a cumulative soil heat flux. Errors do not accumulate in this
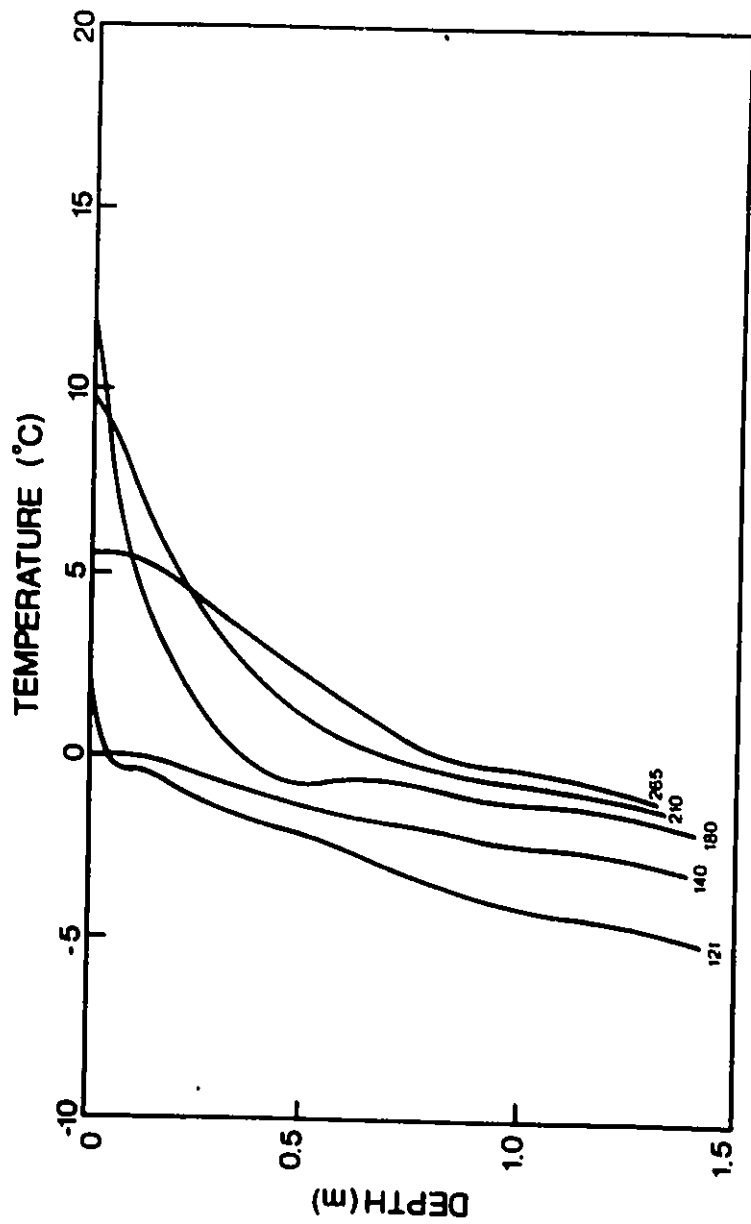
**Figure 2.5:** Temperature profiles interpolated from thermistor readings. Churchill site, 1985. Numbers on curves are Julian day.

Table 2.3:   Soil heat flux plate correction factors.

| Site | 1984 | 1985 |
|------|------|------|
| Churchill | 2.22 | 1.72 |
| Marantz | 2.44 | 1.92 |

procedure because the cumulative calorimetric storage depends only on the temperature profiles at the start and end of the time period. Intermediate profiles only affect the basal flux calculations. The resulting cumulative flux was then compared to the cumulative values indicated by the heat flux transducers to obtain a correction factor. Examples of the comparison are given in Figure 2.6.

Care was required in selecting base depths for the calorimetric calculations. Errors were introduced if the base depth lay between two temperature sensors which spanned changes in soil type (either peat/mineral transitions or unfrozen/frozen transitions). Details of the various calculations for the Churchill site (1984 and 1985) and the Marantz site (1985) are given in Halliwell and Rouse (1987). The final correction factors used in this study are given in table 2.3. The 1984 values are significantly higher than the 1985 values. The reasons for this may be due to differences in installation, or differences in soil moisture conditions between the two years.

The correction factors were applied to the soil heat
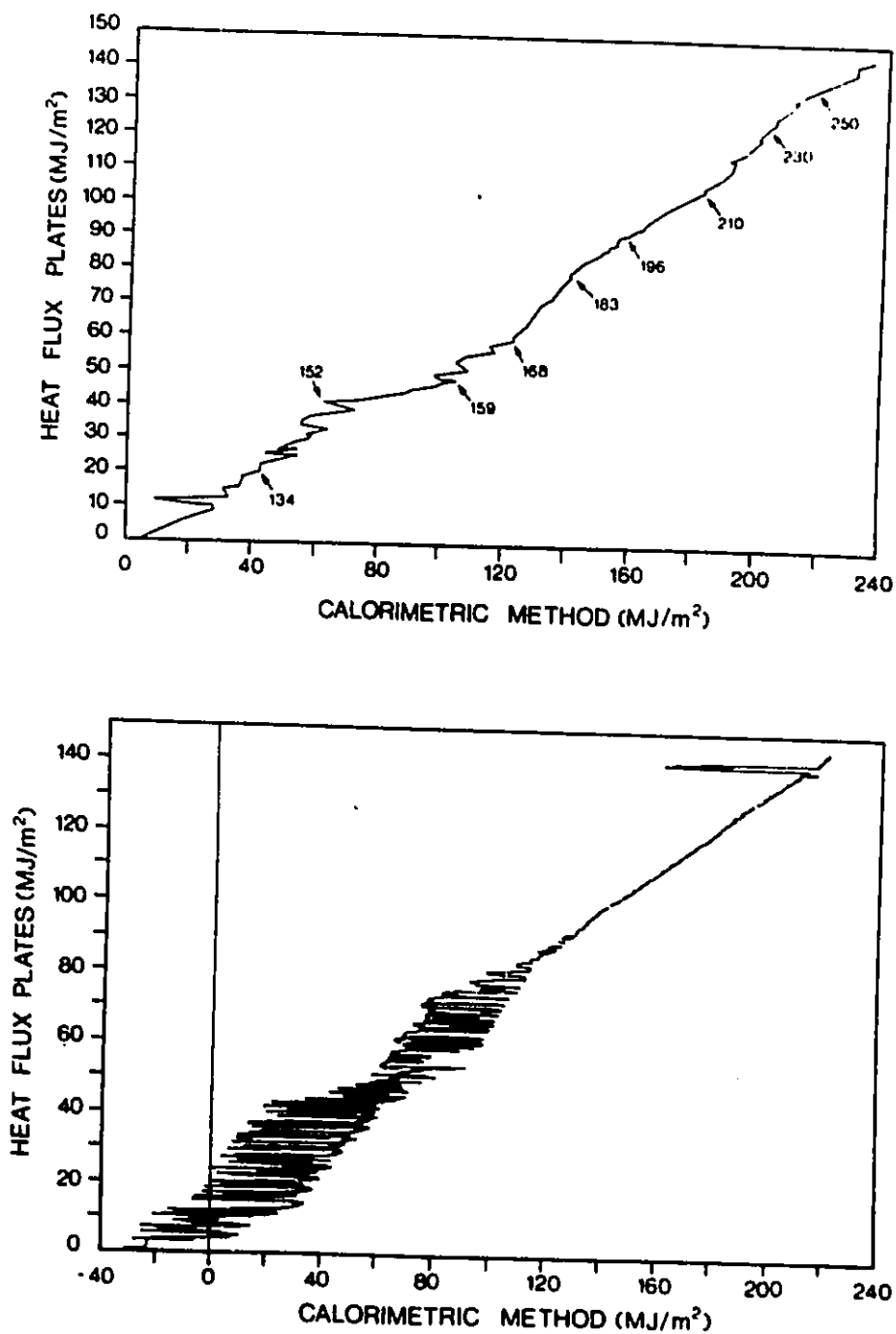
Figure 2.6:   Cumulative heat flux calculations; comparison
of heat flux plates and calorimetric method,
Churchill Site, 1985. Top: thermistors
(numbers indicate Julian day). Bottom:
thermocouples.

flow transducers on an hourly basis. The method of deriving the correction factor eliminates the average error, but the errors associated with individual readings may still be quite high. The 1987 data from the soil heat flux plates indicate a spatial variability in Qg of a factor of 2, with higher values in the wet area. In the 1984 and 1985 data, the hourly response of the plates depends on very local conditions, while the calorimetric adjustment is based on long-term soil temperatures which reflect Qg over a much greater area.

### 2.3.3 - Energy Balance Calculations

The field measurement program provided temperature and humidity profiles from which the atmospheric sensible and latent heat fluxes (QH and QE) could be calculated. In this section, the method of analyzing the profiles to calculate QH and QE will be described.

The two methods which can be used to calculate the fluxes from the profile measurements are the aerodynamic method and the Bowen ratio method. The data requirements for each method are similar: in addition to profile measurements of temperature and humidity, the aerodynamic method requires measurement of the wind profile, and the Bowen ratio method requires measurement of net radiation and soil heat flux. In 1985, wind speed profiles were measured at both sites, but only a single wind speed measurement was available for the

Churchill site after late July, 1985, and for both sites in the 1984 season. The 1984 instrumentation was designed with the expectation that only the Bowen ratio method would be used. However, problems with the Bowen ratio approach often occur in early mornings or late afternoons, and the wind profile measurements were added in 1985. A method of analysis was developed which incorporated both the Bowen ratio and aerodynamic methods, and could be extended to the 1984 data with minimal loss of accuracy resulting from the use of a single anemometer. The method combines the best features of both methods, and allows the use of any number of levels of temperature, humidity, or wind speed.

A number of papers and books in the literature have reviewed flux-profile relationships. For a detailed discussion, the reader is referred to works by Sellers (1965), Dyer (1974), Thom (1975), Yaglom (1977), and Oke (1978), amongst others. However, in order to outline the details of the calculation procedure used in this study, it is desirable to review the basic concepts involved in the two profile methods.

Using a flux-gradient approach, the fluxes of sensible heat (QH), latent heat (QE), and momentum ($\tau$) in the surface boundary layer can be expressed as functions of the time-averaged temperature (T), vapour pressure (e), and wind speed (u) profiles:

$$QH = -\rho c_p K_h \frac{dT}{dz} \qquad (2.10a)$$

$$QE = -\frac{\rho c}{\gamma} p \, K_w \frac{de}{dz} \qquad (2.10b)$$

$$\tau = \rho \, K_m \frac{du}{dz} \qquad (2.10c)$$

where $\rho$ is the density of air, $c_p$ is the specific heat of air at constant pressure, and $K_{h,w,m}$ are turbulent transfer coefficients for sensible heat, latent heat (water vapour) and momentum respectively. (The use of temperature, $T$, in equation 2.10a and subsequently is restricted to situations where changes in height are small. In cases where height variations exceed several metres, adiabatic temperature changes become important and potential temperature should be used.)

Under conditions of neutral stability, wind speed increases linearly with the logarithm of height $(z)$, such that:

$$u(z) = \frac{u}{k}* \, \ln(\frac{z}{z_0}) \qquad (2.11a)$$

and

$$\frac{du}{d\ln z} = \frac{u}{k}* \qquad (2.11b)$$

where $k$ is the von Karman constant, and $z_0$ is the surface roughness length. The friction velocity, $u_*$, is related to the momentum flux by:

$$u*^2 = \frac{\tau}{\rho}$$

(2.12)

For non-neutral conditions, the profiles depart from a log-linear form as the result of buoyancy effects. This curvature is incorporated in the flux equations using the dimensionless stability functions $\emptyset_h$, $\emptyset_w$, and $\emptyset_m$. These stability functions are typically expressed as a function of either the Monin-Obukhov parameter (z/L), or the gradient Richardson number (Ri). (See Appendix 1.) Combining equations 2.10-2.12 and incorporating the stability functions yields the following:

$$QH = - \rho c_p k^2 \frac{du}{d\ln z} \frac{dT}{d\ln z} (\emptyset_h \emptyset_m)^{-1}$$

(2.13a)

$$QE = - \frac{\rho c}{\gamma} p \, k^2 \frac{du}{d\ln z} \frac{de}{d\ln z} (\emptyset_w \emptyset_m)^{-1}$$

(2.13b)

$$\tau = \rho k^2 (\frac{du}{d\ln z})^2 (\emptyset_m \emptyset_m)^{-1}$$

(2.13c)

Typically, the stability functions in the literature are expressed as functions of z/L, but these can be transformed into functions of Ri using the relationship:

$$Ri = \frac{z}{L} \frac{\emptyset_h}{\emptyset_m^2}$$

(2.14)

The practical advantage of using Ri instead of z/L is that

Ri can be evaluated directly from the observed temperature and wind speed profiles, allowing direct calculation of the fluxes. In this study, the stability functions used are those recommended by Dyer (1974). Transformed into functions of Ri, these become:

$$\emptyset_h = \emptyset_w = (1-16Ri)^{-0.5} \qquad\qquad (2.15a)$$

$$\emptyset_m = (1-16Ri)^{-0.25} \qquad\qquad (2.15b)$$

for the unstable regime, and

$$\emptyset_h = \emptyset_w = \emptyset_m = (1-5Ri)^{-1} \qquad\qquad (2.15c)$$

for the stable regime.

Equations 2.13a and 2.13b constitute the aerodynamic method for calculating the surface fluxes of QH and QE. The ratio between these two fluxes, QH/QE, is the Bowen ratio, β. If it assumed that $\emptyset_h = \emptyset_w$ under all stability conditions, (2.13a) and (2.13b) give:

$$\beta = \gamma\frac{dT}{de} \qquad\qquad (2.16)$$

Combining β with the energy balance equation:

$$Q^* - Q_g = QH + QE \qquad\qquad (2.17)$$

yields:

$$QH \; = \; \frac{\beta(Q* - Qg)}{(1+\beta)} \qquad\qquad (2.18a)$$

$$QE \; = \; \frac{(Q* - Qg)}{(1+\beta)} \qquad\qquad (2.18b)$$

The Bowen ratio method comprises equations 2.16, 2.18a, and 2.18b. The measurements required for its use are temperature and vapour pressure at a minimum of two levels, plus net radiation (Q*) and soil heat flux (Qg).

The application of the aerodynamic and Bowen ratio methods is typically carried out by measuring the desired properties at two levels in the atmosphere, and applying a finite difference representation of the gradients in (4) and (7). The identity

$$\frac{d}{d\ln z} \; = \; z \frac{d}{dz} \qquad\qquad (2.19)$$

is often used to transform the aerodynamic equations so that simple differences in height can be used. Note that this approximation is only valid over a limited range of z, and that the geometric mean height should be used for z, rather than the arithmetic mean. (The geometric mean height will correspond to the value of z found by averaging the lnz values.)

The inaccuracy associated with using a finite difference formulation at two heights to calculate the

slopes (dT/dz, de/dz, or du/dz) is usually avoided by using height-integrated forms of the profile equations. Paulson (1970) and Holtslag (1984) provide integrated equations which include a general form of the stability functions. This consideration applies only to the aerodynamic method, since the height terms disappear in the Bowen ratio equations.

Any method which uses two height levels exclusively for calculation of the gradients will be highly sensitive to equipment malfunction or errors in measuring temperature, humidity, or wind speed. Fuchs and Tanner (1970) provide an error analysis of the Bowen ratio method in this context, and Ohmura (1982) expands on this to outline a method of identifying invalid data. Systematic error between sensors can be eliminated by using a reversing system, such as that described by McCaughey and Brintnell (1984), but random error remains.

The analysis in this study combines multiple levels into the calculation process in a simple but fundamentally sound manner. For the Bowen ratio method, Thom (1975) recommends that B be calculated from a plot of T versus e, using several levels. This plot should be a straight line under any stability conditions (assuming no flux divergence), and deviations from the straight line can be assumed to be instrumental error. For the aerodynamic method, profiles of temperature or humidity versus log

height will be linear only under neutral conditions. However, for a limited height interval the curvature introduced by non-neutral stability will be small, and it is possible to assume that the true profile is linear against log height. Deviations from linearity will be due to measurement errors.

A tall vegetation cover can also introduce curvature into the log-height profiles, but this effect can be incorporated into the aerodynamic equations by replacing z with z-D, where D is the effective zero plane displacement. No zero plane displacement was apparent at either the Churchill or Marantz sites, so this correction was not required.

The procedure used to analyze profiles in this study assumes that temperature, vapour pressure, and wind speed all are linear functions of log height, for the limited height interval over which the measurements are taken. Linear regression of these properties versus log height provides the values of dT/dlnz, de/dlnz, and du/dlnz for use in (2.13a) and (2.13b). In addition, the Richardson number is evaluated by substituting (2.19) into the standard formulation for the Richardson number to get:

$$Ri = \frac{g}{T} z \frac{(\frac{dT}{dlnz})}{(\frac{du}{dlnz})^2}$$

(2.20)

One advantage of this approach is that the three

properties need not be measured at the same heights: the only requirement is that each series of measurements represents the same height interval. As a result, it is possible to eliminate an individual sensor (e.g. a wet bulb that has dried out) from the calculations when it is obvious that the sensor is in error. It is also possible to complete the calculations with only a single anemometer, if a reliable estimate of $z_0$ is available.

To carry out the data analysis, a graphics program was written in Turbo Pascal to provide 5 graphs for analysis:

.    - vapour pressure versus temperature (for ß determination);

- temperature versus log height (dT/dlnz);

- vapour pressure versus log height (de/dlnz);

- wind speed versus log height (du/dlnz);

- wet bulb depression versus log height.

For each time period, the program calculates all fluxes using the Bowen ratio and aerodynamic methods as outlined above. For $Q_g$, the soil heat flux transducers were corrected using the values in table 2.3. The program also provides other variables such as $u_*$, Ri, ß, and $z_o$. The user of the program can then select plots to examine the data. If necessary, individual data values can be eliminated from the analysis (e.g. a single wind speed, temperature or vapour pressure) and the flux values recalculated. The best-fit

line for the appropriate graph is shown on the screen, along with the calculated fluxes. Once the user is satisfied with the results, the values are written to a disk file for further analysis or printing. Recalculation and replotting after addition or removal of a data value takes approximately one second, allowing rapid comparison of the effect of including or excluding an individual data value.

The purpose of examining the data for each time period is to identify individual data values which appear to be in error and eliminate their effect on the final calculated fluxes. The most common problem encountered in the field data was the drying out of wet-bulb wicks. This would normally occur only during extremely dry conditions, when the rate of water feed could not be maintained in all wicks. Wet-bulb depressions at these sites can exceed 12C·, and are often in the range 8-10C·. Under these conditions, adjustment of the water feed mechanism becomes critical and the likelihood of one or more wet bulbs malfunctioning increases.

Identification of erroneous vapour pressure readings was most readily carried out through examination of the wet-bulb depression versus log height. Experience indicated that this variable changes slowly and smoothly with height, so that any irregularities could be attributed to instrumental problems. In addition, a notebook was used to record any instrument malfunctions observed during daily visual

inspections of the field site.

In analyzing the profiles, identification of which levels to exclude from the calculations can become subjective. Identification of a single level amongst four is not difficult, but once two levels become suspect, the decision is not always easy. At these times, notes recording field observations are important, and the patterns of reliability over the preceding or following time periods can be helpful. Generally, a single level would be eliminated if it departed from a straight line through the other three points and its exclusion led to a change of more than a few percent in the calculated fluxes. Errors of this type appear to be random, rather than systematic. If it appeared that more than one level was in error (i.e. no combination of three levels showed a strong linear trend), then all four levels were used, unless wet-bulb depressions or field observations indicated that specific sensors were in error.

Generally, the Bowen ratio and aerodynamic methods agreed well for values of QH and QE, using the 1985 data when four anemometers were in use at each site. Error analysis was carried out using the mean bias error (MBE) and root mean square error (RMSE), as used by Davies et al (1984). The MBE is a measure of systematic difference, and the RMSE is a measure of non-systematic error. The errors can be calculated from the difference or deviations between the two methods (d) by:

$$\sigma(d)^2 = \left(\frac{d_i^2}{N}\right) - \left(\frac{d_i}{N}\right)^2$$

$$= (RMSE)^2 - (MBE)^2 \qquad\qquad (2.21)$$

where $\sigma(d)$ is the standard deviation of the deviations, and N is the number of observations.

The Bowen ratio method is known to provide inaccurate results and can give fluxes with the wrong sign when $\beta$ approaches -1 (and $Q*-Q_g$ approaches zero). When data for hours with $-1.4<\beta<-0.7$ or Bowen ratio fluxes with the wrong sign were eliminated from the comparison, the Bowen ratio and aerodynamic methods gave MBE values of less than $8Wm^{-2}$, and RMSE values of less than $40Wm^{-2}$. The absolute errors during stable conditions were lower than those during unstable conditions (although the relative errors were larger for stable conditions). The errors for the Churchill Site were lower than those for the Marantz site, likely due to greater errors in soil heat flux estimates at the Marantz site. Figures 2.7 to 2.10 show the comparisons. Differences in magnitudes between the two methods may be due to errors in $Q*$ and $Q_g$, upon which the Bowen ratio values depend, or errors in the wind profile, upon which the aerodynamic values depend. The differences are within the range of errors in the radiation and soil heat flux values. Further details on the comparisons are provided in Halliwell and
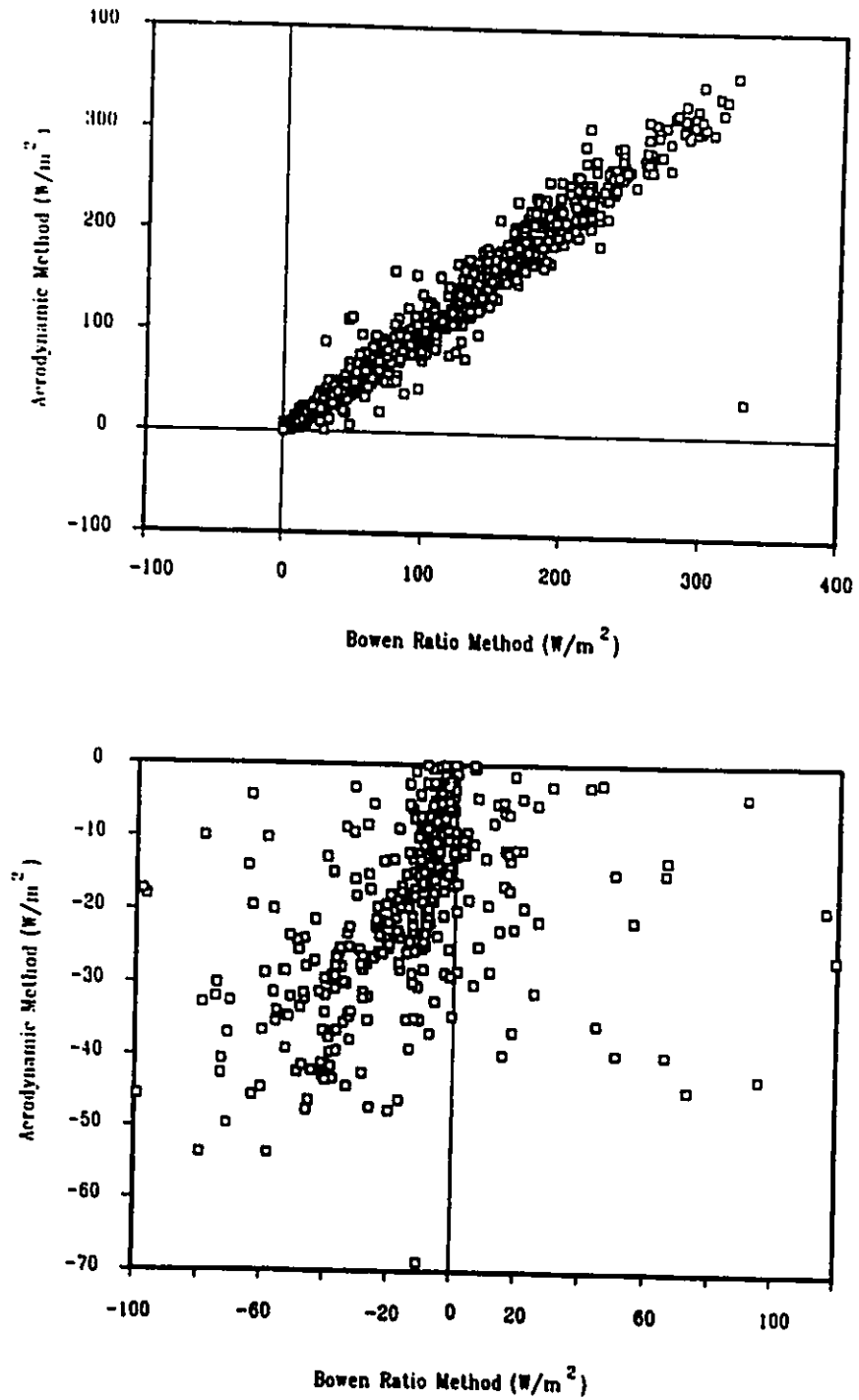
Figure 2.7: Comparison of sensible heat flux (QH) calculations for unstable (top) and stable (bottom) conditions. Churchill Site, 1985.
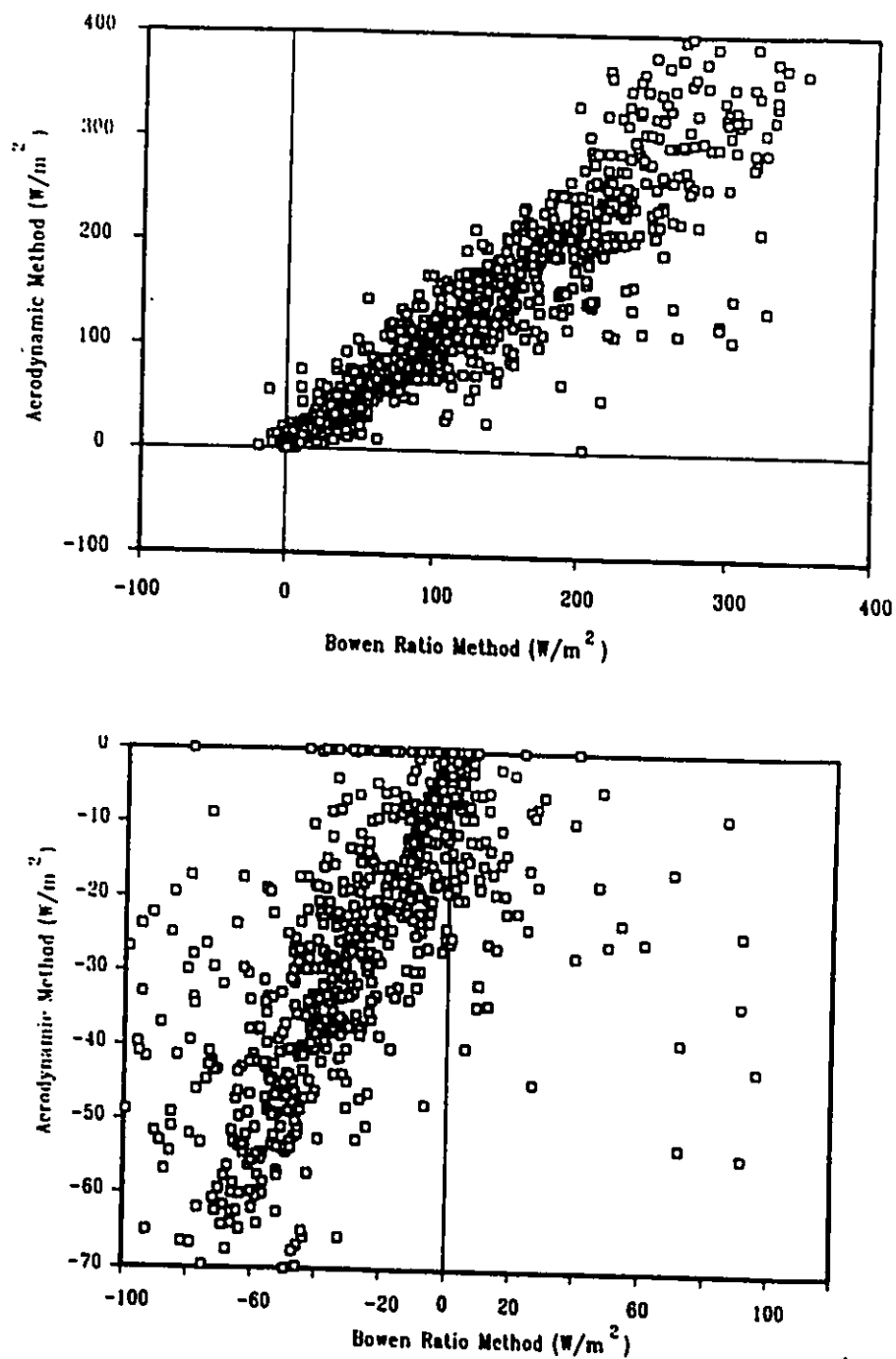
**Figure 2.8:** Comparison of sensible heat flux (QH) calculations for unstable (top) and stable (bottom) conditions. Marantz Site, 1985.
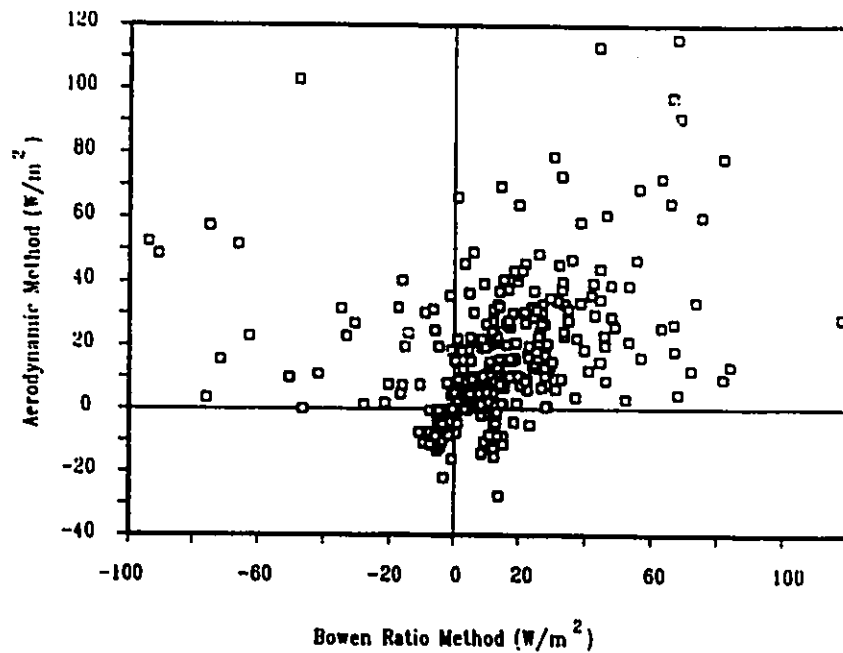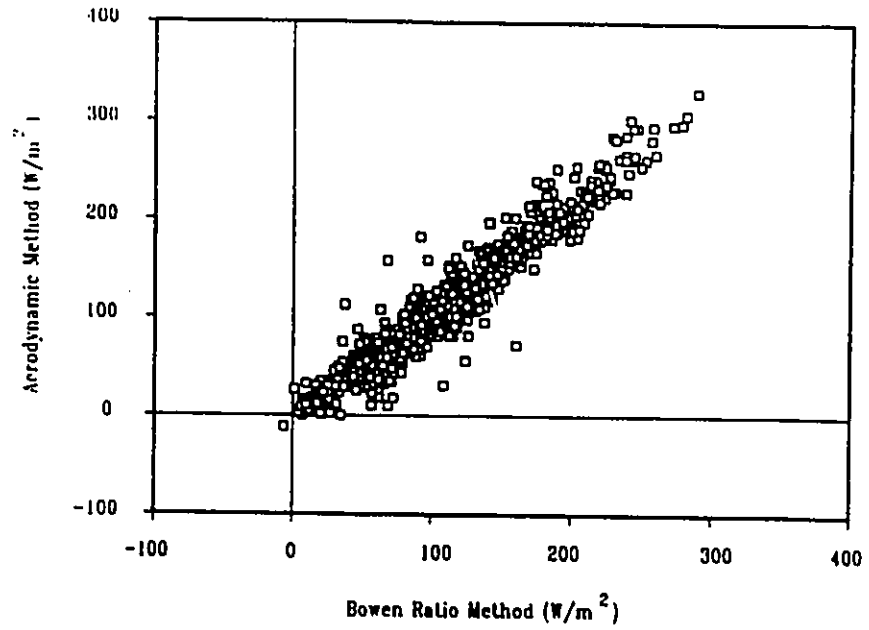
**Figure 2.9:** Comparison of latent heat flux (QE) calculations for unstable (top) and stable (bottom) conditions. Churchill Site, 1985.

56
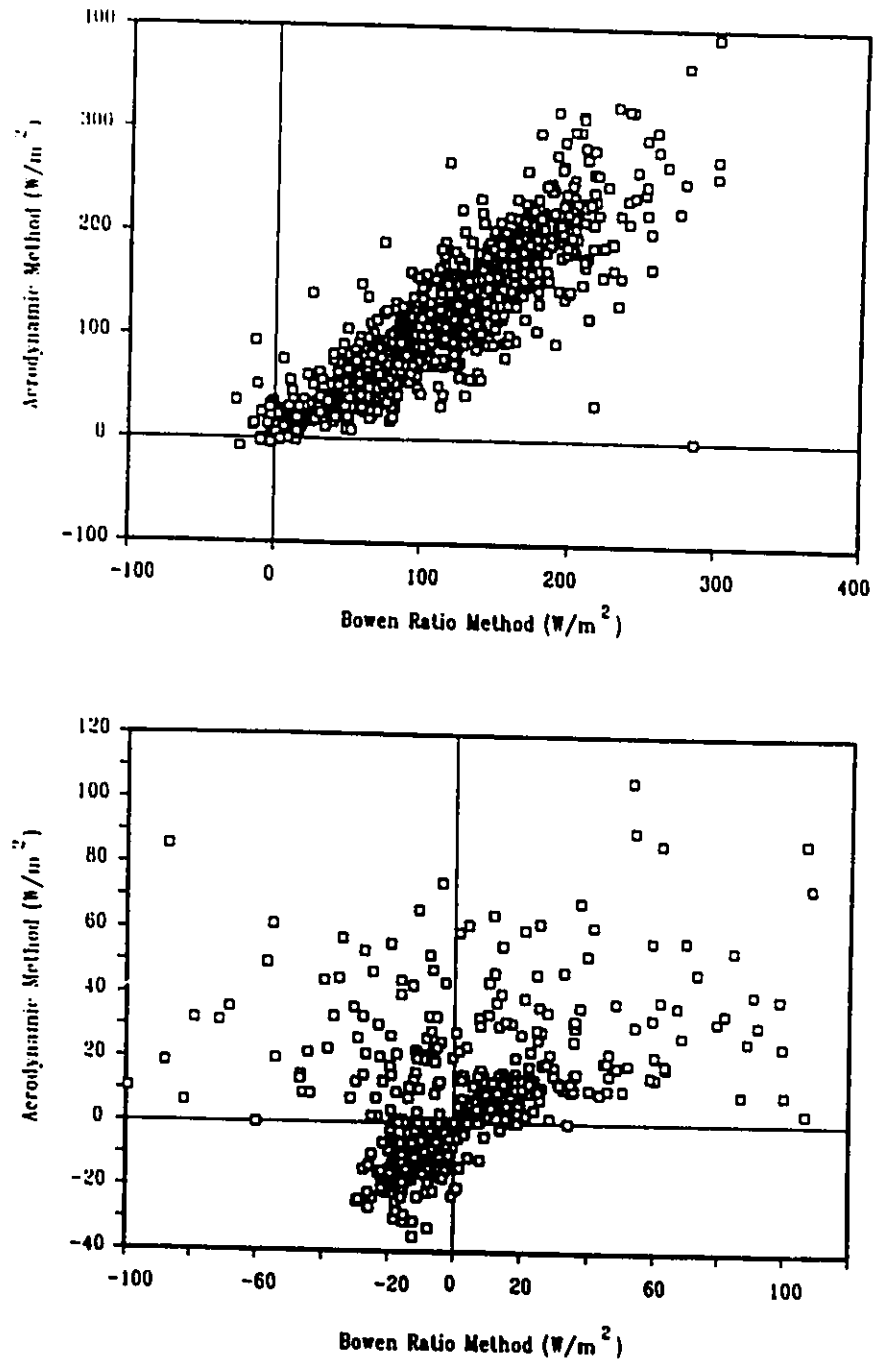
**Figure 2.10:** Comparison of latent heat flux (QE) calculations for unstable (top) and stable (bottom) conditions. Marantz Site, 1985.

Rouse (1989).

For periods when only a single wind speed was available (both sites in 1984, and the Churchill site after July 28, 1985) a fixed value of $z_0$ was used to calculate du/dlnz for the aerodynamic method. Determination of $z_0$ requires wind profile measurements under neutral conditions (Ri=0). Since it is rare to get completely neutral conditions over a one hour period (the averaging time of the data logger), the value of $z_0$ was determined by graphing the apparent $z_0$ against Ri. The true $z_0$ value was taken from the graph at Ri=0.

The use of a single wind speed introduces an error into the calculations of $u_*$ and Ri, but the effect on the calculated values of QH and QE (from the aerodynamic method) is large only during stable conditions. The reason for this is as follows:

The effect of using a single anemometer appears in two places in the aerodynamic calculation of the fluxes: in the estimate of $u_*$, and the estimate of Ri. The relative error in $u_*$ will translate directly into an equivalent relative error in the flux, but a relative error in Ri will work through the stability function. The total error effect can be estimated by differentiating (2.13a) and (2.13b) with respect to du/dlnz, after making the appropriate substitutions for Ø and Ri. By doing this, the relative error in the flux calculation (dQ/Q) can be expressed as a

function of the relative error in the measurement of du/dlnz, giving:

$$\frac{dQ}{Q} = (1 + \frac{24Ri}{1-16Ri}) \; (\frac{d\frac{du}{dlnz}}{\frac{du}{dlnz}}) \qquad (2.22a)$$

for unstable conditions, and

$$\frac{dQ}{Q} = (1 + \frac{20Ri}{1-5Ri}) \; (\frac{d\frac{du}{dlnz}}{\frac{du}{dlnz}}) \qquad (2.22b)$$

for stable conditions.

The effect is to multiply the error in du/dlnz by a factor that is a function of the true value of Ri. This multiplier is graphed in figure 2.11. In stable conditions (Ri>0), the error growth is rapid. The tendency during stable conditions is to underestimate du/dlnz and overestimate Ri. Since the stability function reduces the size of the flux, the errors are additive and the calculated fluxes rapidly tend towards zero. In unstable conditions (Ri<0), the error introduced directly by du/dlnz is offset by the indirect error from Ri and the stability function. The overall error is reduced. At Ri=-0.125, the two sources of error cancel out, and the flux will be calculated correctly. Since the largest fluxes are in the unstable regime, the net result is that using a single anemometer introduces only small errors in flux calculations. The relative errors are greatest in stable conditions, when the absolute magnitude of the fluxes is small. As the true value
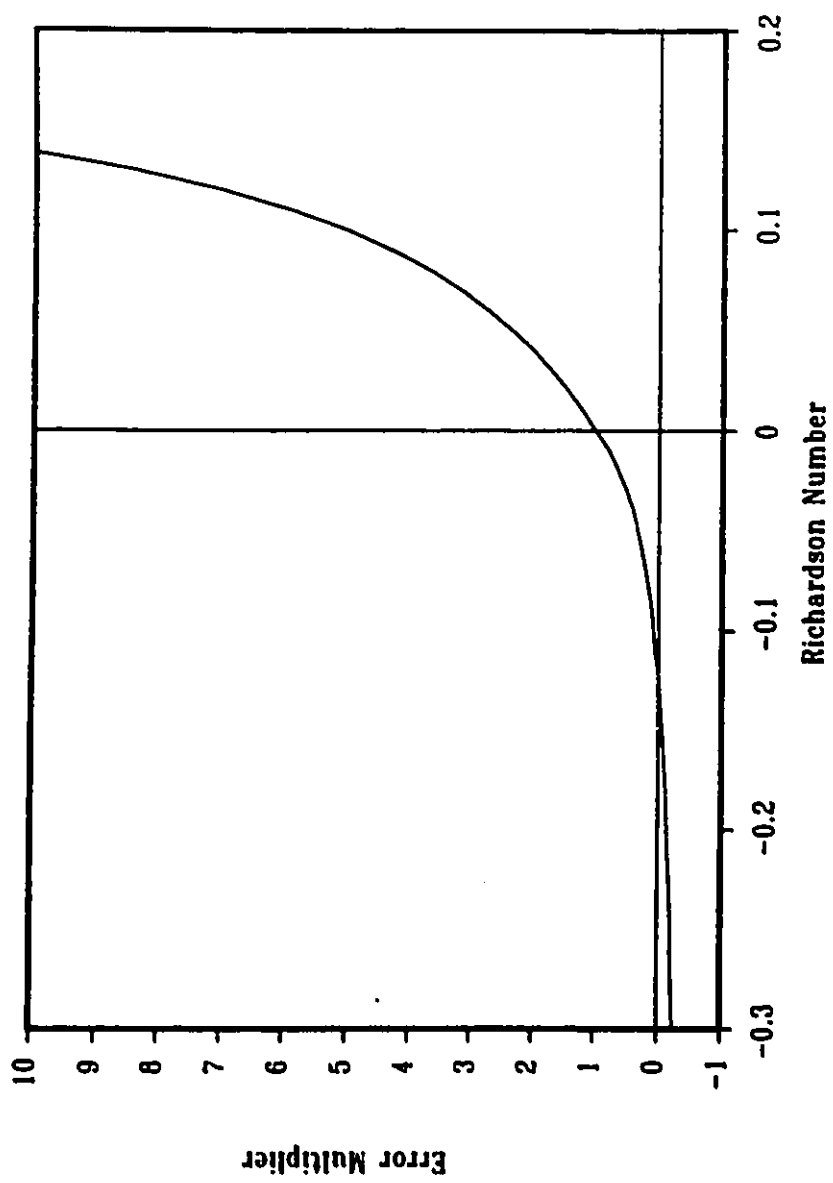
**Figure 2.11:** Error multiplication factor for aerodynamic flux calculations using a single anemometer. The multiplier is plotted as a function of the true Richardson number.

of Ri increases under stable conditions, the value of Ri estimated using a single anemometer will rapidly approach the critical value of 0.2, at which the aerodynamic method gives QH=QE=0. The aerodynamic method will become unreliable in this situation and the Bowen ratio method will give more reliable estimates of the surface fluxes. Comparisons of flux calculations using a single anemometer and using four anemometers are given in Halliwell and Rouse (1989). Except for very stable conditions, the errors introduced by using a single anemometer are less than 2% for both QH and QE.

For most of the field data, either the Bowen ratio method or aerodynamic method should give acceptable results. Since only a single anemometer was used at each site in 1984, and at the Churchill site in August and September, 1985, it was decided to use the Bowen ratio values as the "correct" ones. This allows direct comparison between the 1984 and 1985 values, without questions regarding differences in analysis. The Bowen ratio values were discarded and the aerodynamic values used when the Bowen ratio method gave fluxes of the wrong sign, or a β value close to -1 indicated that the magnitude of the Bowen ratio fluxes was incorrect. These times generally corresponded to near-neutral stability, when errors in the aerodynamic method would be minimal.

Several other situations resulted in alternate methods of calculating QH and QE. Periods when Q* readings

were unavailable required use of the aerodynamic values. In May and early June, periods of sub-freezing weather eliminated the use of the wet bulbs for humidity measurements. During this time, QH was calculated using the aerodynamic method, and QE was calculated as a residual using the energy balance equation (2.17). QE was not calculated as a residual if there was snow on the ground, or the soil surrounding the heat flux transducers was freezing or thawing, as the transducers would not indicate the correct flux in the snow or freezing soil. At these times, QE is not available.

During very short periods of instrument "down-time" when profile measurements were not available (e.g. during changing of wet-bulb wicks), the values of QH and QE were calculated using the Bowen ratio method with an estimated value of β. These periods never exceeded 2 hours in length (2 consecutive time periods) and constituted only 10-20 hours per season.

Based on the differences between the Bowen ratio and aerodynamic methods, it is estimated that the standard errors in the measurement of QH and QE at the Marantz site are less than $35 Wm^{-2}$ under all conditions. At the Churchill site, the errors are less than $20 Wm^{-2}$. Individual values may have greater or lesser errors. The errors in individual values would be proportional to the errors in regression slopes for the profiles in question. Additional errors are

introduced by the errors in $Q*$ and $Q_g$ for the Bowen ratio method. Since two methods are available for estimation of QH and QE at any time, the large errors associated with one or the other under particular conditions can be avoided. when long term averages are considered, the errors in QH and QE are likely less than $10Wm^{-2}$.

# Chapter 3: Characteristics of Field Observations

The purpose of this chapter is to examine the meteorological conditions, energy balance, and soil thermal and hydrologic regimes at the Churchill and Marantz sites during the 1984 and 1985 measurement seasons. This will include comparisons between the two sites, comparisons between the two years at each site, and comparisons between the Churchill site and Atmospheric Environment Service (AES) climate normals from the Churchill weather station where applicable.

The ultimate reason for examining these various conditions is to identify the characteristics of the energy balance and soil thermal regime which are important in modelling the system. The model must be capable of duplicating these characteristics.

To allow comparison of the various factors on a continuous time basis, it was decided to use cumulative values from an arbitrary date, rather than mean values over specified periods. Cumulative values show short-term variation without obscuring long-term trends. If mean values for selected periods were used, a large number of periods (e.g. periods of only a few days) would make overall comparisons difficult, while using longer periods (e.g.

Table 3.1.   Climate Normals, Churchill weather station.

| | | June | Month July | August | Sept. |
|---|---|---|---|---|---|
| Temp. | (°C) | 6.2 | 11.8 | 11.3 | 5.4 |
| VPD | (kPa) | 0.203 | 0.335 | 0.285 | 0.157 |
| wind | (km/h) | 20.7 | 19.3 | 20.5 | 23.7 |
| precip. | (m) | 0.0435 | 0.0456 | 0.0583 | 0.0509 |
| K | (MJ/m$^2$/day) | 21.92 | 20.36 | 15.28 | 8.80 |

monthly means) would provide few values and give no indication of variability within the period. The mean value for any period is represented on a graph of cumulative values by the slope of the line over that period.

For Churchill weather station (AES) data, usually only monthly means are available. The AES station is located only 3km west of the Churchill site, so most variables can be readily compared. Relevant values are given in table 3.1.

Calculation of cumulative values requires continuous data. Data collected in May of each year is incomplete, since extended periods of sub-freezing weather prevented the use of wet-bulb psychrometry for humidity measurement. This meant that energy balance data was lacking, so comparisons were started as of June 1 in each year. (Note that 1984 was a leap year, so that June 1 has a Julian day number of 153 in 1984 and 152 in 1985.) The Marantz site was not operational until June 3 in 1985, so cumulative values were set on that date to be equal to the 1984 values.

### 3.1 - Meteorological Conditions

#### 3.1.1 - Radiation

Cumulative radiation values represent the total radiative flux from June 1 to the date in question. Figure 3.1 shows the values of $K\downarrow$, $L\downarrow$, and $Q*$ for the Churchill site, and $K\downarrow$ and $Q*$ for the Marantz site. The Churchill site receives more solar radiation than the Marantz site, and as this is the dominant control on net radiation in this case, Churchill also has greater net radiation.

Incoming solar radiation was greater at both sites in 1984 than in 1985, but only the Marantz site showed a difference in net radiation. Since the Churchill site also showed greater incoming longwave radiation in 1984, the lack of a difference in net radiation requires some explanation. Measurements at the Churchill site indicate that surface albedo varies with surface moisture, ranging from 0.12 for a very wet surface (when large puddles are present) to 0.18 when dry. In 1984, when dry conditions prevailed, albedo generally ranged from 0.16 to 0.18. In 1985, under wetter conditions, the albedo was typically in the range 0.14 to 0.17. This albedo difference is enough to offset the higher $K\downarrow$ in 1984, leaving $K*$ unchanged. The greater $L\downarrow$ in 1984 was also offset by higher surface temperatures and greater $L\uparrow$, leaving $L*$ unchanged. This resulted in very little difference in $Q*$ for the Churchill site between the two years.
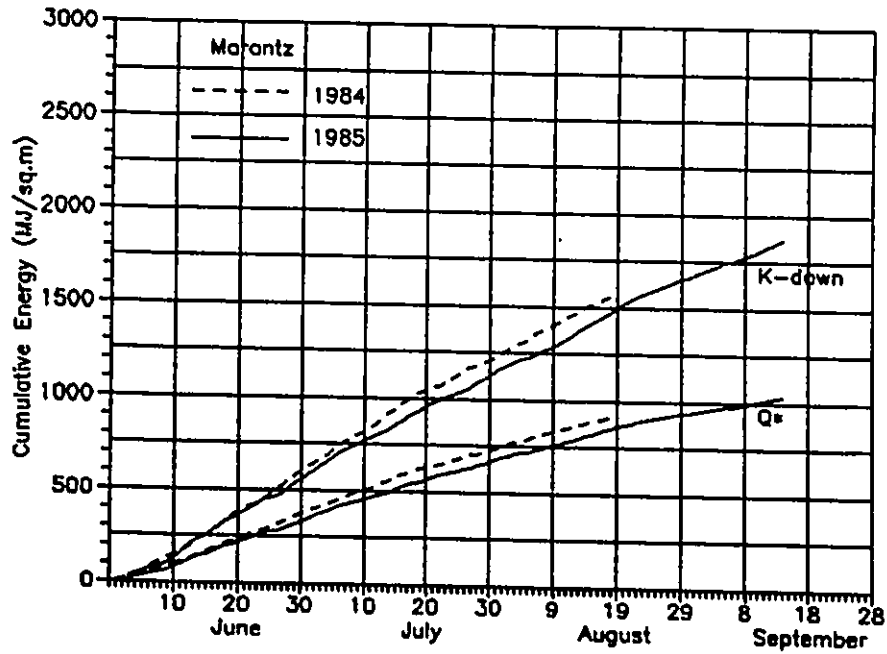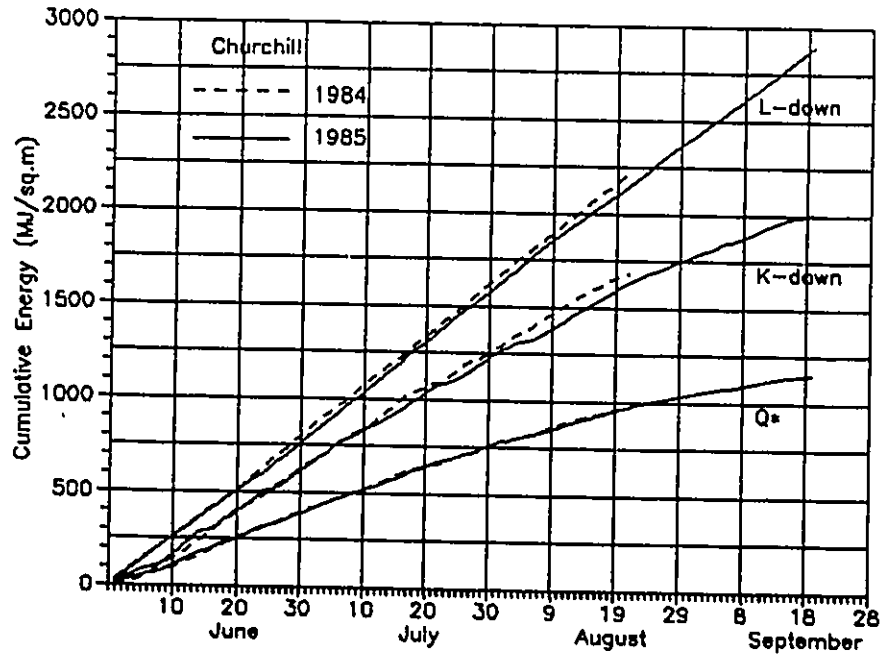
**Figure 3.1:** Radiative fluxes for the Churchill and Marantz Sites during the 1984 and 1985 measurement seasons.

No measurements of reflected (outgoing) shortwave radiation were made at the Marantz site, but we can speculate on the changes which may have occurred. Unlike the Churchill site, the Marantz site is well-drained and puddles do not tend to form after rainfall. The albedo is less likely to show significant variation with surface moisture, so the albedo would likely be similar between the two years. The greater K↓ in 1984 would lead to greater K*, resulting in greater Q*. The differences in Q* between the two years are consistent with the expected change in K*, assuming that L* is relatively unchanged. The ratio between K↓ and Q* is very close to that of the Churchill site, suggesting that the albedos at the two sites are similar in magnitude.

The values of K↓ for the Churchill site are close to the AES normals, indicating that both 1984 and 1985 are "normal" years. Although the Churchill AES station collects Q* data, this data cannot be compared to data from the research site because Q* depends on surface albedo.

### 3.1.2 - Temperature

Cumulative temperature values are given in figure 3.2a. The cumulative values were calculated using mean daily temperature at 2m. Summing on a daily basis provides a value in degree-days. Since the temperatures are in °C, the values in figure 3.2a are equivalent to thawing degree days (noting that daily mean temperatures <0°C are included and will
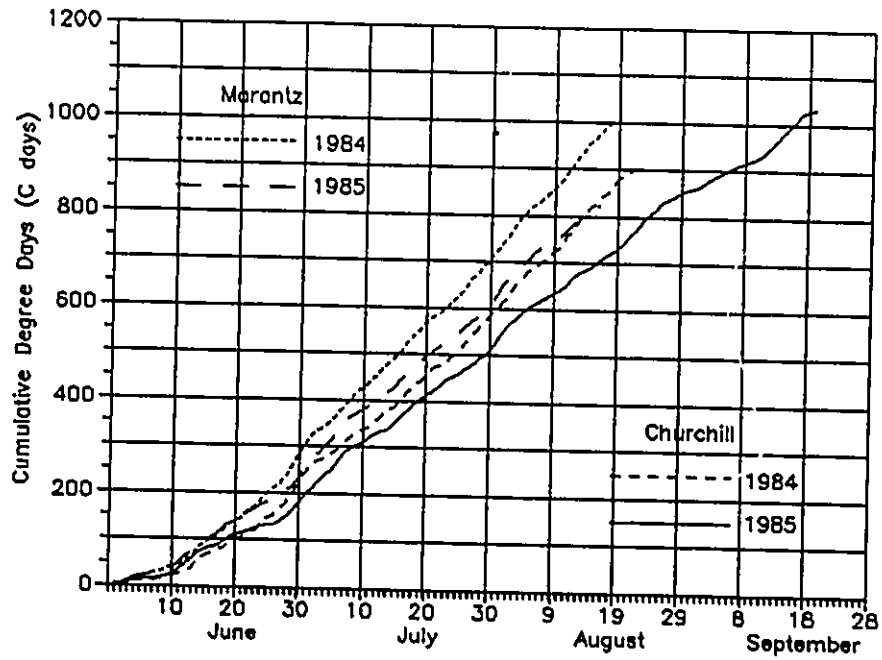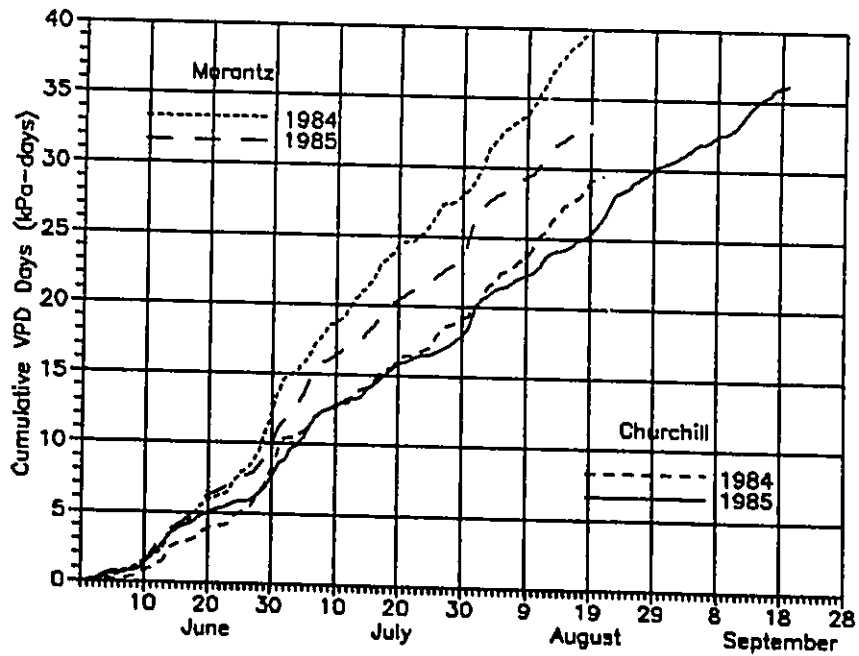
Figure 3.2: Air temperature and humidity measurements for the Churchill and Marantz Sites during the 1984 and 1985 measurement seasons.

lower the cumulative total, rather than being ignored).

The Marantz site, located inland, is significantly warmer than the Churchill site located close to Hudson Bay. For the period June through August, the difference in mean temperature is about 2° in both years. At both sites, 1984 was significantly warmer than 1985. Comparing the Churchill site to AES normals, 1984 was warm in each of June, July, and August. 1985 was normal in June, slightly cool in July and August, and warm in September.

### 3.1.3 - Humidity

Humidity can be quantified in a number of ways. In evaporation studies, the vapour pressure deficit (VPD) is often used as an indicator of the "drying power" of the air, and this value has been selected to compare the various sites and years. Mean daily temperature was used to calculate saturation vapour pressure, and then mean daily vapour pressure was subtracted to get a daily vapour pressure deficit. These daily values were then summed to get VPD-days (analogous to degree-days). Although VPD varies throughout the day, the values should allow some comparison between data sets. (Calculating VPD on an hourly basis, then summing or averaging would likely yield different values, since the relationship between temperature and saturation vapour pressure is not linear. However, comparisons between sites should yield the same results.) The results are

plotted in figure 3.2b.

The Marantz site is considerable drier than the Churchill site. The Marantz site was generally drier in 1984 than in 1985. The Churchill site was similar in 1984 and 1985 for June and July, but somewhat drier in August 1984 than August 1985.

Comparing the Churchill values directly to AES values suggests that Churchill was dry in June, normal in July, and very dry in August in both 1984 and 1985, and very dry in September. However, these comparisons may not be valid, since AES normals do not include VPD. The "normal" values were calculated from AES data giving mean monthly temperature and vapour pressure at 100, 700, 1300, and 1900 hours Local Standard Time. The effect of using monthly average T and e to calculate VPD would tend to yield a lower VPD than that calculated using daily T and e. The difference would depend on the variability in T and e. If some shift is allowed for, it seems more likely that June was close to normal, July more moist, and August and September somewhat dry.

### 3.1.4 - Wind

Cumulative wind values are calculated as the total wind passage, in km. These values are given in figure 3.3a. Care must be taken in comparing 1984 values to 1985, as the anemometer heights are not the same. In 1984, both sites had
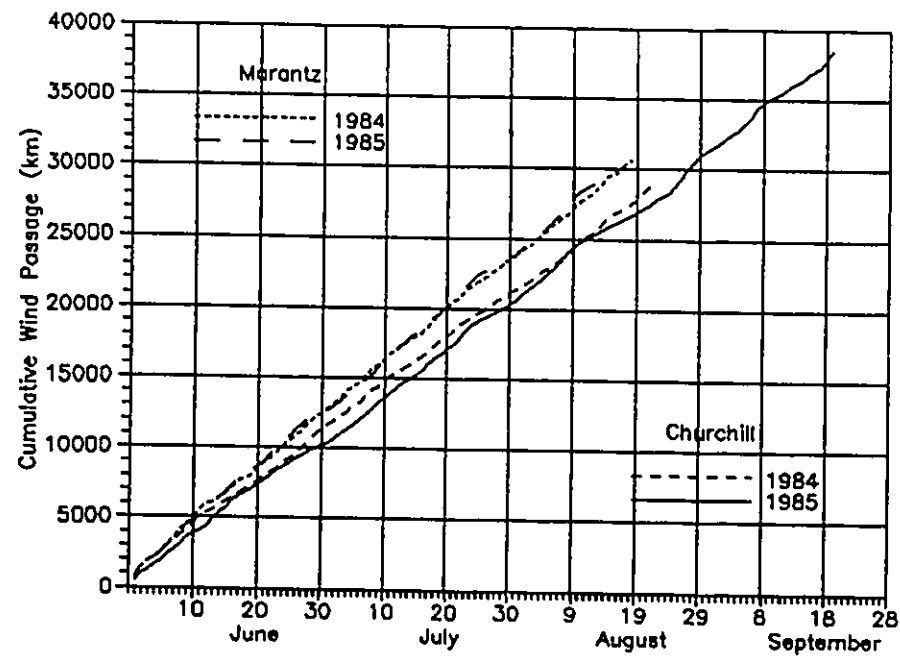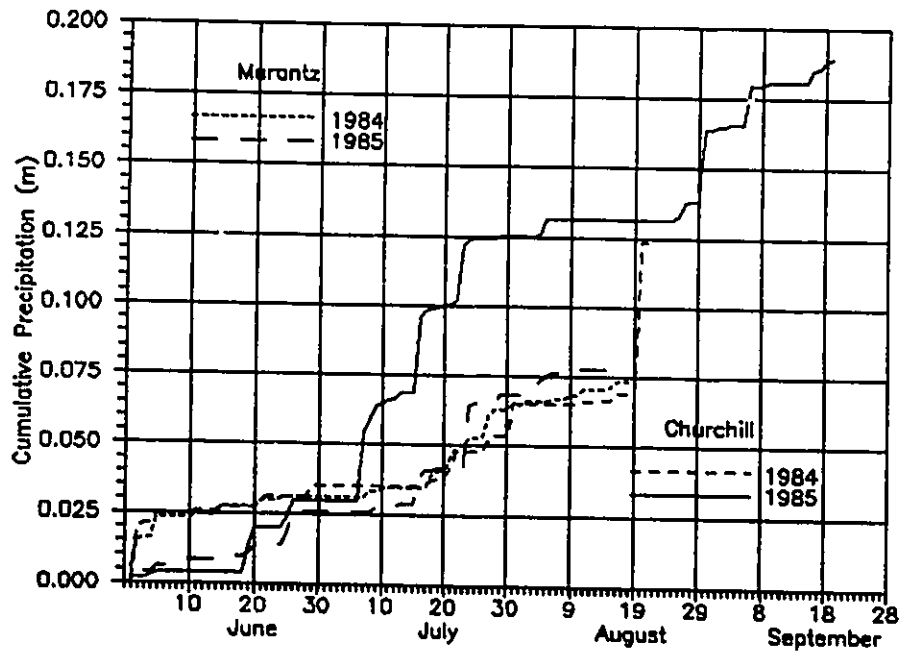
**Figure 3.3:** Wind and precipitation measurements for the Churchill and Marantz Sites during the 1984 and 1985 measurement seasons.

a single anemometer at about 3.6m height. In 1985, 4 anemometers were used at each site; the highest (2m) were used to calculate the values given in figure 3.3b. Using equation 2.10a (wind speed as a function of height and surface roughness length), we can estimate the wind speed at 2m from the wind speed at 3.6m. The ratio between the wind speeds would be about 0.9, so if we reduce the 1984 values by 10%, we can compare them to the 1985 values. In the same manner, the AES wind speeds (at 10m) should be reduced by 25% to compare with winds at 2m.

On this basis, 1984 wind speeds appear to be less than 1985 wind speeds. Both years appear to be below normal, comparing the Churchill data to the AES data. However, variations in wind speed appear to be minor at each site. The Marantz site does appear to be significantly windier than the Churchill site in both years.

### 3.1.5 - Precipitation

Precipitation is a measurement that varies considerable in both time and space. This is shown by the irregular nature of the lines in figure 3.3b, showing cumulative precipitation. In 1984, both sites received similar quantities of precipitation at similar times, shown by the small separation between lines in figure 3.3b. Half of the total rainfall measured at the Churchill site fell in a single storm on August 20/21. (The Marantz site was closed down just before this event.)

In 1985, the two sites differed considerably in both quantity and timing of rainfall. Early June was dry at both sites, with the Marantz site receiving slightly more precipitation. (Note: this is the only graph for which the 1985 Marantz values do not start at the same point as the 1984 Marantz data on June 3. The rain gauge was operational on June 1, 1985.) By the end of June, the Churchill site had received more, and both sites were close to the 1984 values. In July, the Churchill site received much more precipitation than Marantz. Both received similar quantities in August, leaving Churchill with a much greater total. The Marantz values for July and August were slightly greater than those in 1984, while the Churchill values were much larger (up until August 21, when the 1984 storm brought the total precipitation close to the 1985 values).

In comparing the Churchill data with AES normals, 1984 was a dry year prior to the August 20 storm. 1985 was dry in June, wet in July, dry in August, and slightly dry in September. Overall, 1985 was close to normal.

### 3.2 - Effects on Energy Balance

From the above discussion, it can be seen that the main differences between 1984 and 1985 are in the temperature and moisture regimes. 1984 was a relatively warm, dry summer. The higher temperatures and lower precipitation coincide with greater vapour pressure

deficits. As a result, a greater proportion of Q* is removed from the surface as QH in 1984. On a seasonal basis, the Bowen ratio (ß) is greater in 1984 than in 1985. The effects on the energy balance can be seen in Figure 3.4.

At the Churchill site, with equal Q* in both years, QH=QE in 1984, but QH<QE in 1985. The difference between years is most noticeable in July. In 1984, QH and QE have similar values throughout the season. In 1985, QE<QH in June, but warm, wet weather in July leads to large QE values, and QE is considerable greater than QH. Through August and September, QE continues to exceed QH.

At the Marantz site, Q* was less in 1985 than in 1984. As a result, the change in ß from 1984 to 1985 is seen in similar QE values, with significantly reduced QH values. Again, QE and QH are close in magnitude throughout the 1984 season. In 1985, the QE and QH values are similar in June, with QE exceeding QH in July and August.

Both sites show similar values of Qg in both years. Considering the accuracy of the heat flux plate measurements, discussed in chapter 2, little can be said about the small differences between sites and years.

### 3.3 - Active Layer Development

Figures 3.5 and 3.6 show the thaw depth within the active layer for both years at the Churchill and Marantz sites respectively. The graphs cover the entire data
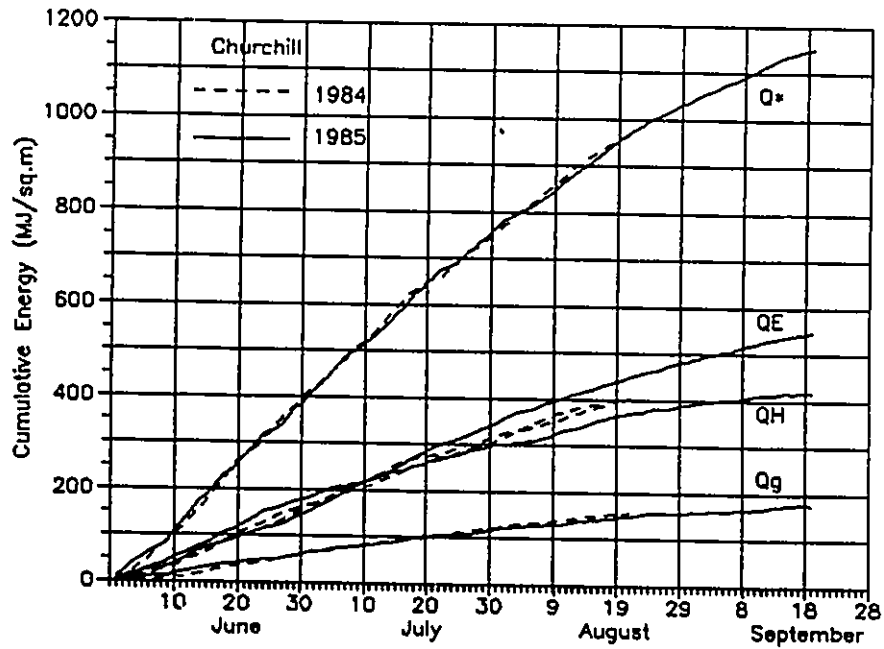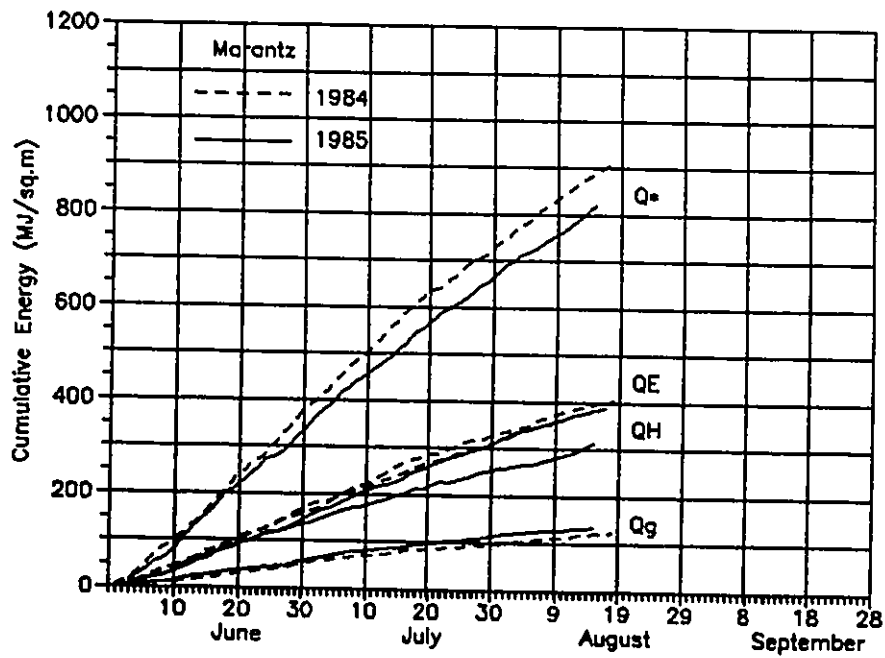
**Figure 3.4:** Energy balance measurements for the Churchill and Marantz Sites during the 1984 and 1985 measurement seasons.

a)

b)
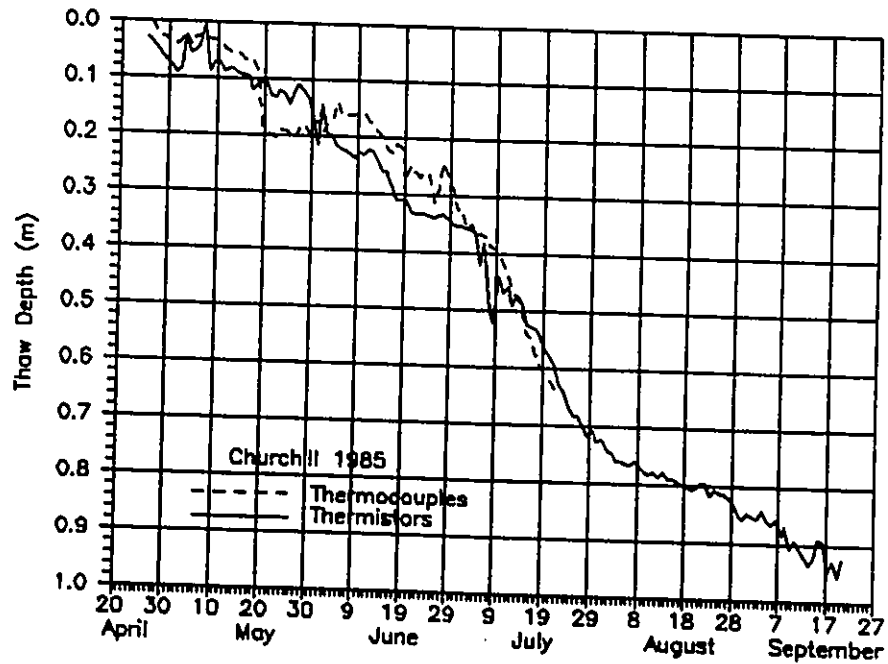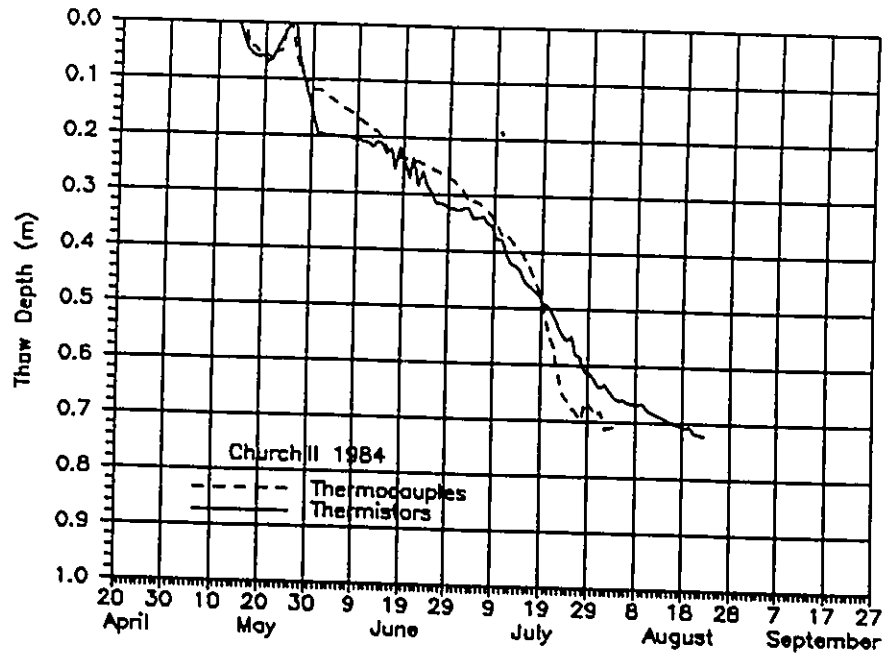
**Figure 3.5:** Thaw depths interpolated from thermistor and thermocouple temperature profiles, Churchill Site, 1984 and 1985.
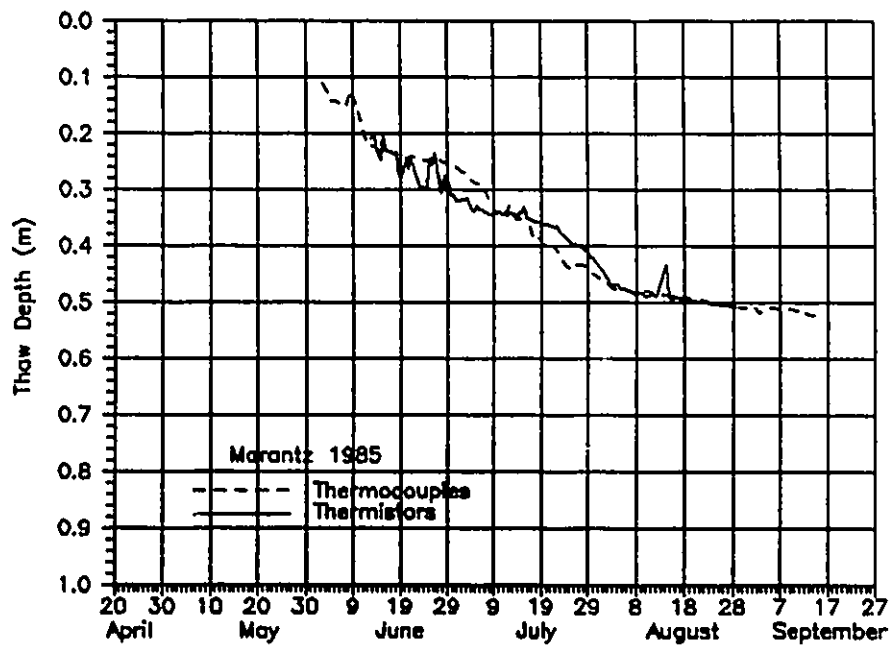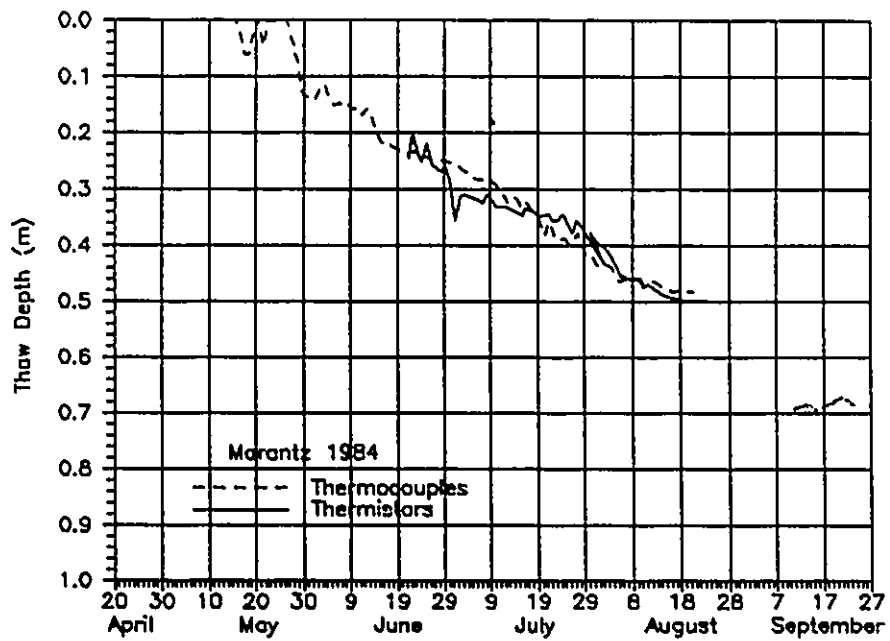
**Figure 3.6:** Thaw depths interpolated from thermistor and thermocouple temperature profiles, Marantz Site, 1984 and 1985.

collection period at both sites: from mid-May to mid-August in 1984, and from late April to late September at the Churchill site and early June to mid-September at the Marantz site in 1985.

Each site had both a thermocouple rod and a thermistor rod installed in the soil. The thermistor rods were measured manually each day, whereas the thermocouple rods were read automatically by the data logger. The thaw depths given in Figures 3.5 and 3.6 were determined by fitting an interpolating function to the observed temperature profile, followed by a root-finding procedure to calculate the $0°$ isotherm. All thermistor profiles were interpolated on an individual basis. Thermocouple readings were averaged on a daily basis to provide daily mean soil temperatures, and the mean profile was used in the interpolation routine.

At the Churchill site, the thermistor and thermocouple rods were installed in different holes. The thermistor rod was located at the top of a small hummock, where the ground surface was exposed in the early stages of snowmelt and where drying occurred rapidly after a rainfall. The thermocouple rod was located in a flat area between hummocks, which retained snow for several days after the hummock tops, and which tended to accumulate puddles of water after rain. As a result, the differences in thaw depth indicated in figure 3.5 may be real, as the two locations

experience different moisture regimes and surface temperatures. Periodic probing of thaw depth using a thin (3mm) steel rod adjacent to each set of temperature sensors showed differences of less than 2cm with the 0° isotherm interpolated from the temperature profiles.

At the Marantz site, the thermistor and thermocouple rods were both installed in the same hole, so they should have been measuring the same soil temperature profile. However, the depths of temperature sensors on each rod were different, and as a result the interpolating functions fitted to each profile would differ. The small differences in thaw depth indicated in figure 3.6 are the result of the inaccuracy of the fitting procedures. The interpolating functions are least accurate when the 0° isotherm is furthest from the fixed sensor depths. The first thermistor was located at a depth of 20cm, so the thermistor rod could not be used to estimate thaw depth until it exceeded this value.

Although Qg was similar at both the Churchill and Marantz sites, figures 3.5 and 3.6 show quite different thaw depths because of the different soil profiles. Most of Qg is consumed in the thawing of ground ice. During the period where the peat is thawing at the Churchill site, both sites have similar thaw depths. However, once the thawing front reaches the clay soil at the Churchill site, ice content is much lower and the same quantity of energy can thaw a

greater depth of soil. Figure 3.5 shows that the rate of increase of thaw depth is much faster below 0.3m at the Churchill site. As a result, the total thaw depth at Churchill greatly exceeds that at Marantz.

It is interesting to compare the thermistor and thermocouple thaw depths at the Churchill site. Initially, the thermistor rod shows a greater thaw depth, which could be due to the earlier loss of snow cover and more rapid soil warming. With the snow cover gone, the thaw depth indicated by the thermocouples catches up to that indicated by the thermistors, and then later appears to move deeper. This can be seen in late July 1984, and appears to be happening again in July 1985. Unfortunately, the 1985 thermocouple data stops when the thaw depth reaches the last thermocouple, and it cannot be verified if the trend continues. If the trend is real, it appears that the wetter location (thermocouples) experiences greater Qg values and thawing, even though the increased evaporation from the wet surface should keep the surface cooler.

A similar correlation between thaw depth and surface moisture is indicated in comparing the 1984 and 1985 Churchill data. 1985 was cooler and wetter, yet the thaw depth is greater. Thaw begins at an earlier date in 1985, but the depths are similar in early June when the previous comparisons of meteorological conditions were started.. By early July the 1985 thaw depth is about 0.1m greater than in

Table 3.2.  Hydrologic Balance. Total values from June 1
           to indicated date.

| Site | | 1984 | 1985 |
|------|------|------|------|
| Churchill | last date | Aug. 21 | Sept. 20 |
| | QE   $(MJ/m^2)$ | 405.9 | 548.56 |
| | Evap.   (m) | 0.165 | 0.223 |
| | Precip.(m) | 0.123 | 0.189 |
| Marantz | last date | Aug. 19 | Aug. 17 |
| | QE   $(MJ/m^2)$ | 395.3 | 382.7 |
| | Evap.   (m) | 0.161 | 0.156 |
| | Precip.(m) | 0.074 | 0.089 |

1984, and the thaw depth remains greater throughout the summer. At the Marantz site, where precipitation was similar in both years, thaw depth is similar in both years.

## 3.4 - Water Contents

Table 3.2 shows the seasonal totals for evaporation (in mm and energy equivalent) and precipitation for each site in each year. It can be seen that evaporation exceeds precipitation at each site. The difference is large enough that significant soil drying should occur over the season, but 1985 soil moisture measurements do not support this. Figure 3.7 shows the trends in soil moisture for the first three TDR probes at each site. As can be seen, the Churchill site remains at or near saturation at a depth of only 10cm. There appears to be a slight drying at 10 and 20cm in mid-
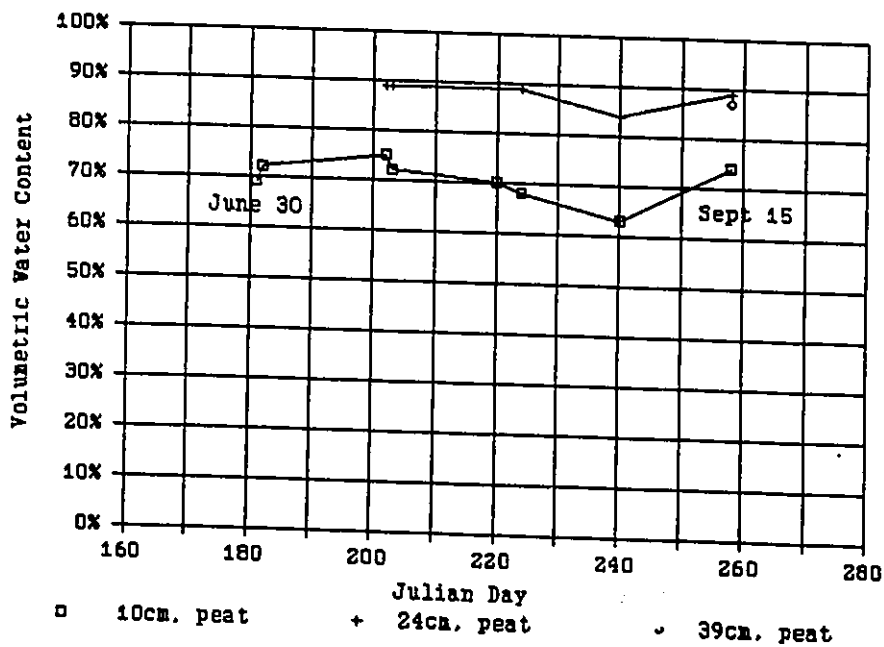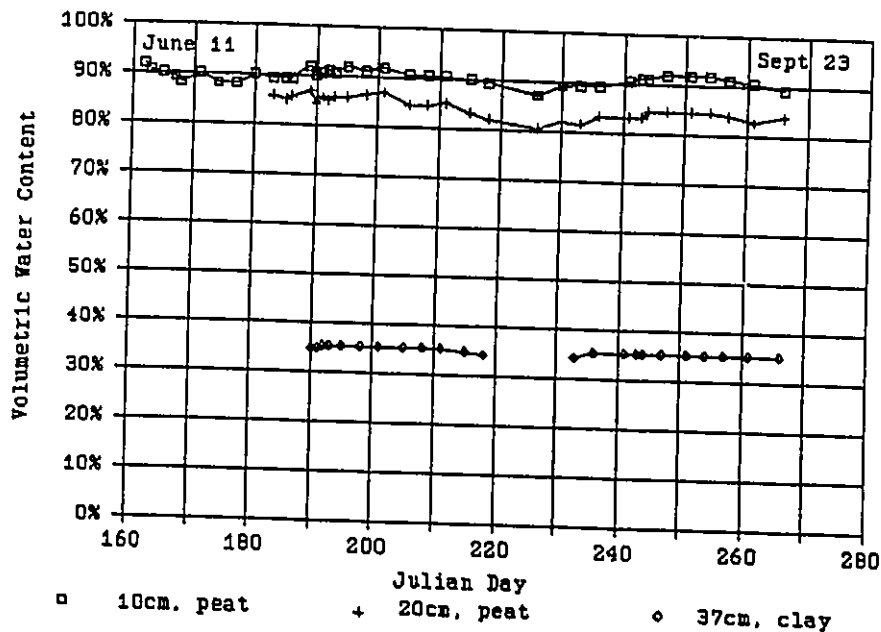
**Figure 3.7:**    Water contents measured using horizontal TDR probes. Top: Churchill Site, 1985. Bottom: Marantz Site, 1985.

### 3.4.1 - Moisture Availability for Evaporation

The moisture content measurements from 1985 indicate that both sites have large quantities of water close to the surface of the soil. Although 1984 was a drier year at the Churchill site, the topographic effect on drainage would maintain fairly high water levels during that season as well. Visual observations of pond levels in 1984 indicated considerable lower water tables - perhaps 10-15cm lower- but the moisture retention characteristics of the Churchill peat are even greater than the Marantz peat. (72% at 1m suction.)

The energy balance data, on the other hand, is indicative of a relatively dry surface. Bowen ratios are relatively high, with QH values approaching QE values. In part, the low ß values can be attributed to cool temperatures, since the reduced saturation vapour pressure at cooler temperatures causes the partitioning of Q*-Qg to shift from QE towards QH. However, the ß values are still rather high. Low ß values are observed just after rainfall events, but the ß values generally rise again after only a few hours.

In order to assess the dryness of the surface, the temperature and vapour pressure profiles recorded for the energy balance measurements were extrapolated to the surface. The technique is described by Thom (1975), and assumes similarity between the temperature, vapour pressure,

and wind speed profiles. Either the temperature or vapour pressure profile can be extrapolated to the height where wind speed becomes zero (at $z_0$) to get an apparent surface value. This procedure was carried out in the same program that was used for energy balance calculations, as described in chapter 2. Apparent surface temperature was then used to calculate saturation vapour pressure, which was then combined with apparent surface vapour pressure to determine the apparent surface relative humidity.

The results of this calculation are given on an hourly basis for July 1985 in figures 3.8 (Churchill) and 3.9 (Marantz). Both sites show a strong diurnal cycle, with high relative humidities at night, and low relative humidities in the day. The figures also indicate which hours experienced condensation at the surface (QE<0, indicated by a "+"), or precipitation (indicated by a box). Either of these events should correlate with an apparent surface relative humidity of 100%. (Hourly assignments of precipitation events at the Churchill site were based on the Churchill weather station hourly observations of weather conditions and three-hour totals of precipitation, with quantities scaled to agree with the daily precipitation measurements at the site. Generally, the weather station precipitation amounts were within 10% of the site totals, except when heavy scattered showers occurred. Hourly assignments at the Marantz site were based on logbook
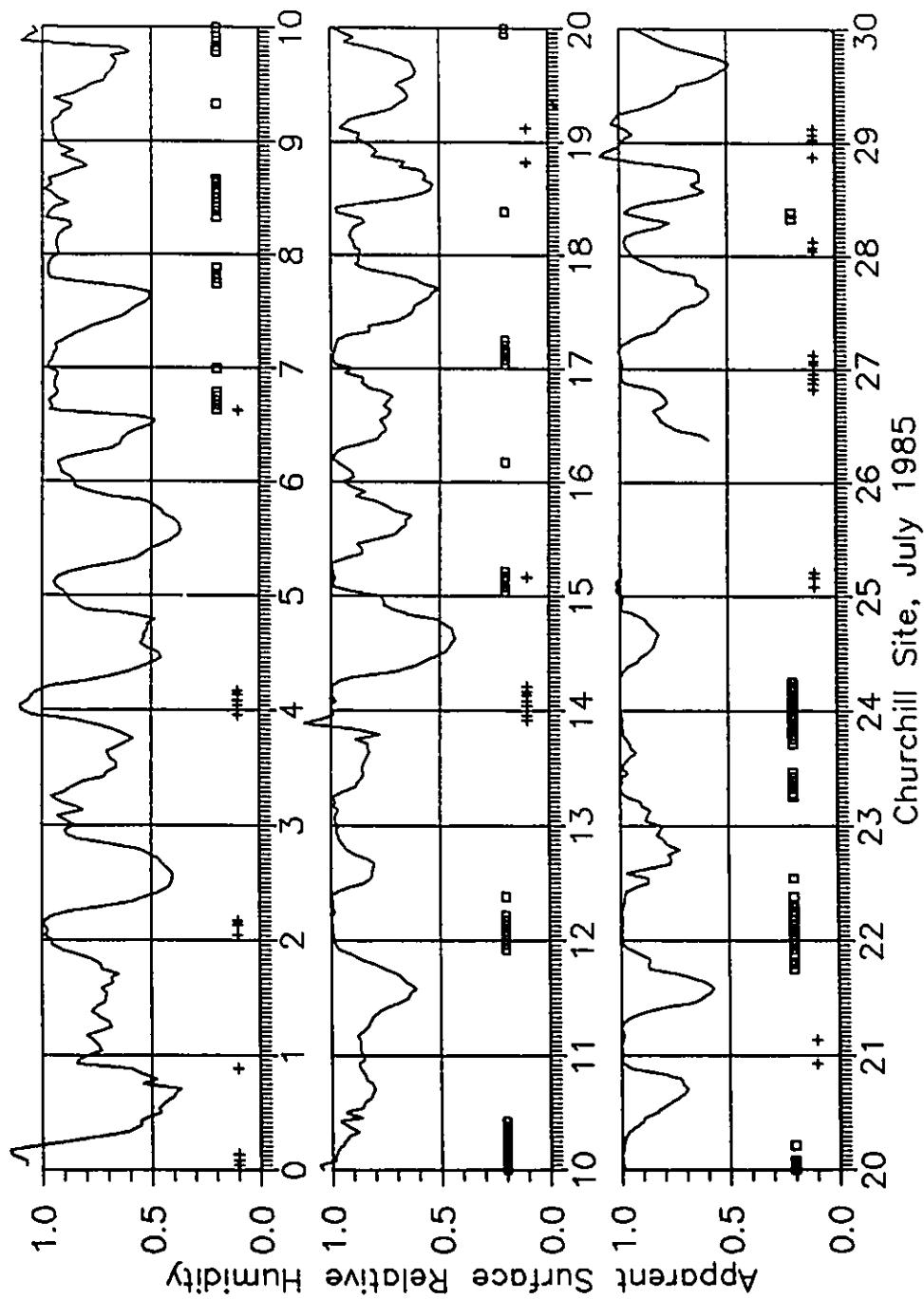
**Figure 3.8:** Apparent surface relative humidity. Churchill site, July 1985. A square indicates an hour with precipitation. A cross indicates an hour with QE<0 (i.e. condensation).
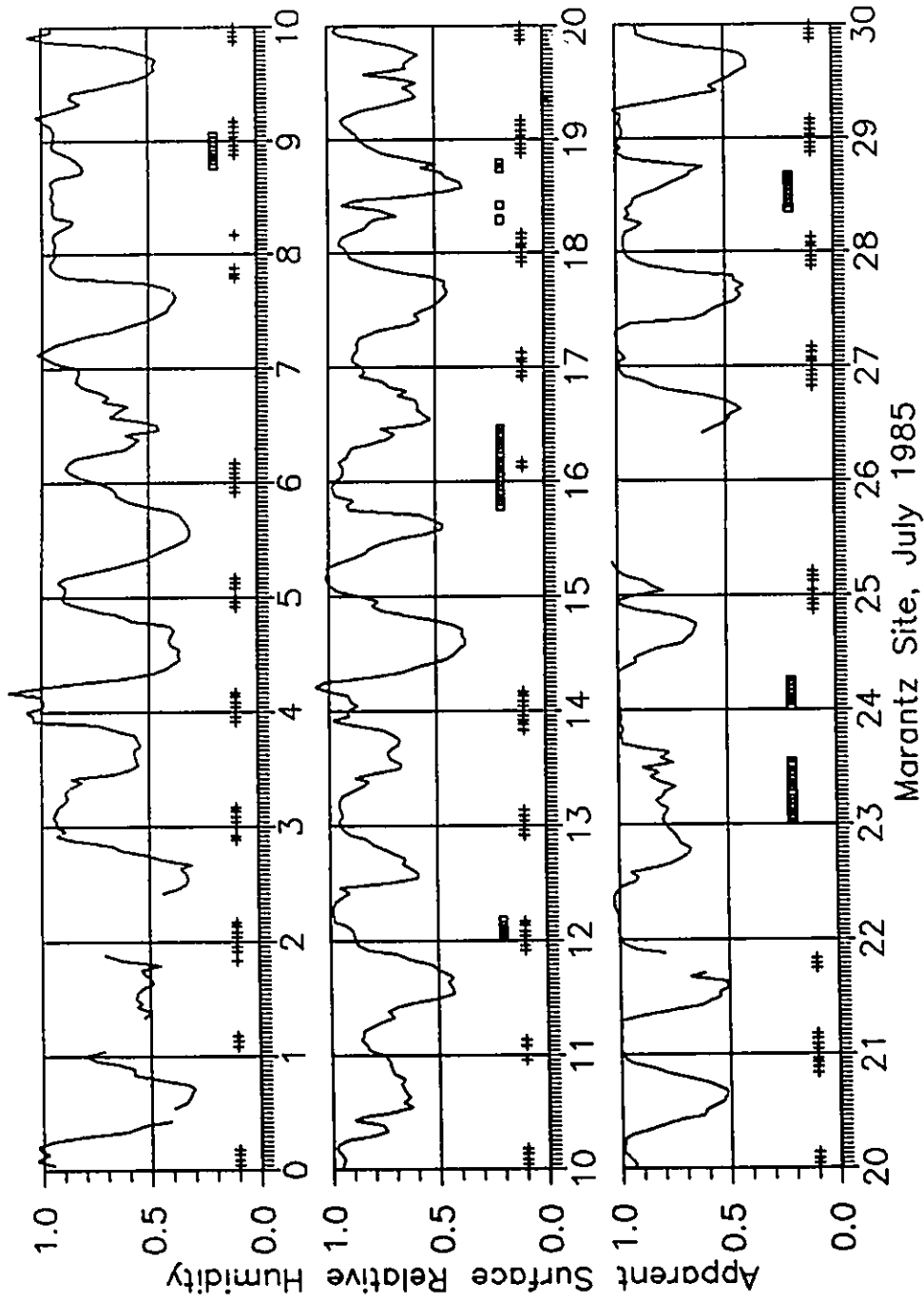
**Figure 3.9:** Apparent surface relative humidity. Marantz Site, July 1985. A square indicates an hour with precipitation. A cross indicates an hour with QE<0 (i.e. condensation).

entries by personnel at the site. These are less accurate, as they only indicate sky conditions and whether rain was falling at the time of twice-daily site visits. Rarely was the starting or ending time of rainfall events recorded.)

Figures 3.8 and 3.9 show that generally the apparent surface relative humidity approaches 100% during rainfall or condensation periods. However, two things are noted: relative humidity is usually close to 100% at night, even if there is no rainfall or condensation, and there are a large number of night-time hours during which evaporation occurred, rather than condensation. It appears, therefore, that the surfaces are behaving like moist surfaces at night, and like dry surfaces during the day. Since evaporation rates are greatest during the day, total evaporation quantities give the appearance of a relatively dry surface.

Two explanations are possible for the behaviour of the surface. First, both sites have peat at the surface, which has a high porosity and a high vapour diffusivity compared to mineral soils. Since large quantities of water are available close to the surface, it is possible that vapour diffusion and capillary flow can provide sufficient water transport towards the surface to sustain low rates of nighttime evaporation. As long as the evaporative demand at the surface is low, upward movement of water towards the surface maintains surface saturation with respect to water vapour. In the day, high evaporation rates exceed the

transport capability of the soil, and water stored near the surface is depleted, leading to low surface humidities.

The second explanation relates to the spatial variability of surface soil moisture. It is possible that the low, wet areas experience less warming during the day than higher dry areas, but also cool to a lesser degree at night. The wet areas provide the primary source for evaporated water, while a greater proportion of QH comes from the dry areas. In the day, the cooler wet areas evaporate at a lower rate (due to the lower saturation vapour pressure), leading to a low apparent humidity in comparison to the warm, dry areas. At night, the situation would be reversed, in which the warmth of the wet areas enhances evaporation, giving a high apparent humidity when compared to the dry areas. The extrapolated profiles only provide an apparent mean temperature and vapour pressure.

The 1984 and 1985 data did not include measurements of the variability of surface temperature. Although surface temperature was measured, the multiple-junction thermocouple was wired to provide a single mean surface temperature over an area of $1-2m^2$. Figure 3.10 shows the relationship between measured surface temperature and apparent surface temperature (from the extrapolated temperature profile) for the two sites in July 1985. At the Churchill site, the measured temperature is generally cooler in the day than the extrapolated temperature, and warmer at night. At this site,
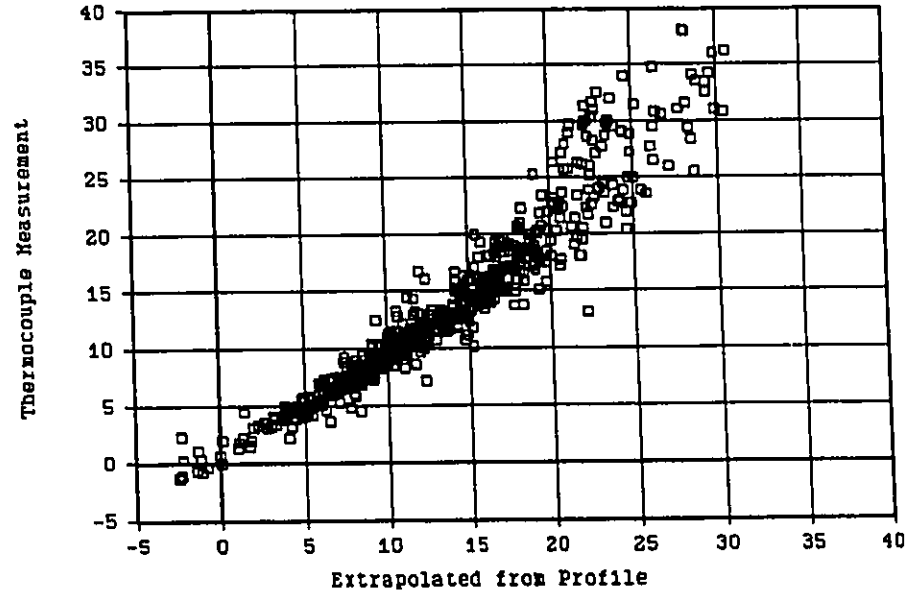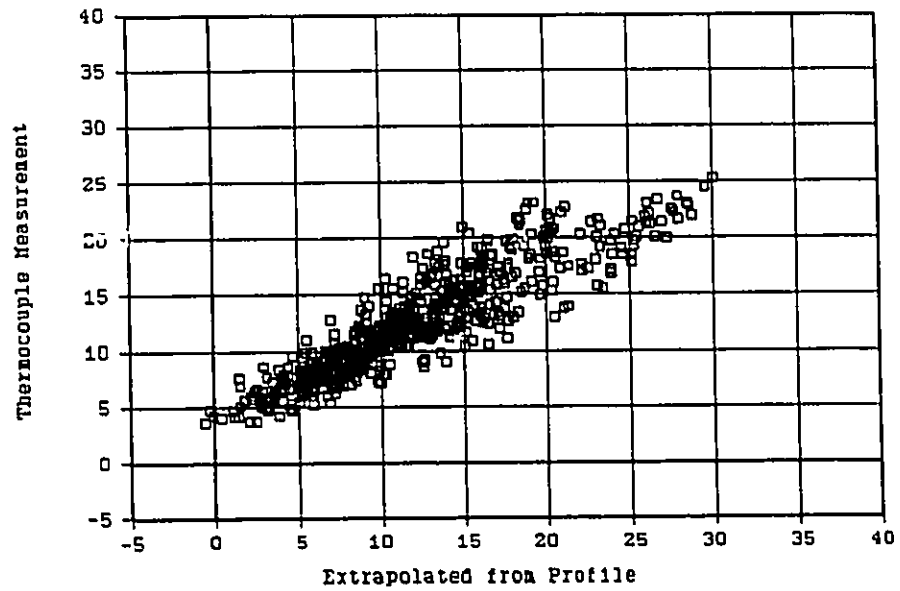
**Figure 3.10:** Surface temperature measurement comparison, July 1985. Top: Churchill Site. Bottom: Marantz Site.

the surface temperature thermocouple was located close to the heat flux plates and soil temperature thermocouple rod, in a relatively wet area. The figure indicates that the wet area experiences less daily variation in surface temperature than the mean (extrapolated from the profile). For the Marantz site, where surface soil moisture is less variable spatially, the agreement between measured and extrapolated surface temperature is better, except at the higher temperatures. Comparing the temperatures yields an MBE of -0.2°C (extrapolated - measured) and an RMSE of 2.49°C for the Marantz Site, and -0.39°C and 2.63°C for the Churchill Site. Although this suggests the errors for the two sites are similar, most of the error for the Marantz Site is at the higher temperatures, whereas at the Churchill Site it is spread more evenly. At the Marantz Site, 51% of the values are within 1° and 86% within 3°, while at the Churchill Site only 35% are within 1° and 75% within 3°.

Since there is uncertainty regarding how representative the surface temperature measurements are, the 1984 and 1985 values have not been compared at the two sites. Since sensor placement was not identical in the two years a comparison would not be valid. Differences could be due to sampling error rather than real.

One of the purposes of the 1987 field season was to examine in greater detail the spatial variation in surface temperature. Figure 3.11 shows July surface temperature
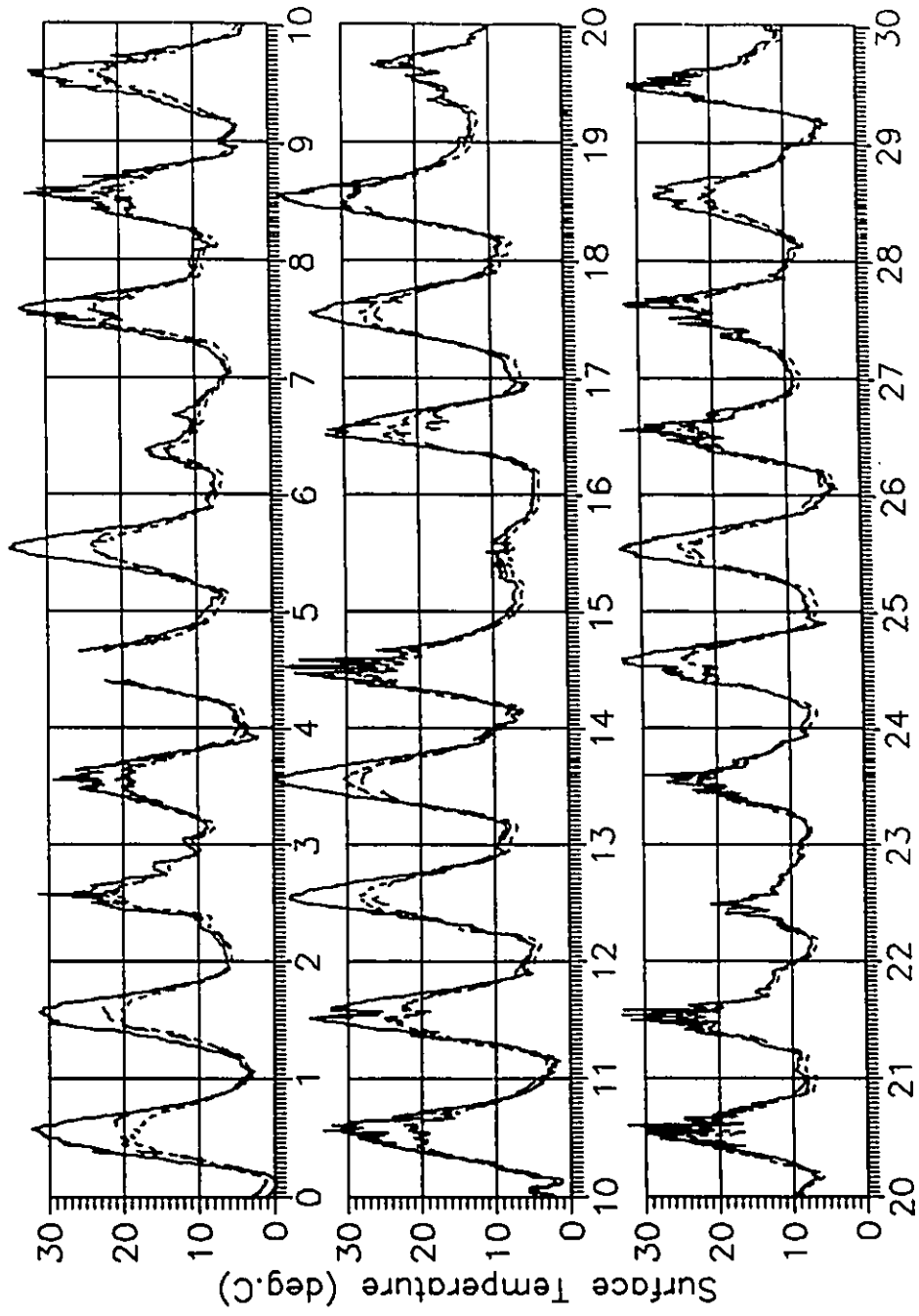
**Figure 3.11:** Surface temperature measurements at the dry (solid line), mesic (long dash), and wet (short dash) locations, 1987 site, July 1987.

measurements averaged over 10-minute intervals at the dry, mesic, and wet locations of the 1987 site. The dry location is up to 10° warmer during the day than the wet or mesic locations (which are similar). Temperatures at the dry location are also much more variable on a short time scale during the day. At night, differences in surface temperature between locations are small. These results indicate that spatial variability in surface temperature will have an important influence on the average energy balance during the day, but that at night the entire surface behaves in a uniform fashion. During the day, the coolness of the wet areas reduces evaporation, while at night the upward movement of water by vapour diffusion or capillary flow allows the dry areas to behave as if they are saturated.

# Chapter 4: Development of a Numerical Model

In this section, we will develop and verify a numerical model capable of simulating the surface energy balance and ground thermal regime of the sites described in chapters 2 and 3. To a large extent, the model will be physically-based, so that its applicability is not limited to just the research sites used here. It should also be applicable to any location of a similar physical nature.

## 4.1 The Surface Energy Balance Approach

The modelling approach is similar to that used by Outcalt, et al (1975) and Smith (1975,1977). The time-dependent soil temperatures are assumed to follow Fourier's law of heat conduction in one dimension (equation 2.4). A numerical solution of Fourier's law is used to model ground temperatures between the surface and an arbitrary depth in the soil, given boundary conditions at the ground surface and the base of the profile. With a knowledge of the soil thermal properties, the initial temperature profile, and the time-dependent boundary conditions, the entire temperature history of the soil profile can be calculated.

Given a non-varying soil profile, variations in the thermal history of the soil depend solely on variations in

94

the boundary conditions, so accurate modelling of the soil temperatures requires accurate modelling of the boundary conditions. In the soil, temperature variation is greatest at the surface and diminishes with depth, so that the basal boundary condition is easily established if the soil profile is deep enough. This boundary condition can be specified simply as a fixed temperature or fixed heat flux. At the surface, the boundary condition becomes much more complex, as the surface temperature or surface heat flux is the result of all surface energy exchanges. The surface energy balance includes net radiation, sensible and latent heat transfer into the atmosphere, and the surface soil heat flux, as described by equation 2.17.

If all components of the surface energy balance can be expressed such that surface temperature is the only unknown variable, then substitution into equation 2.17 would yield a single equation with one unknown, and could be solved for that unknown. Following Outcalt and Smith, this temperature is referred to as the equilibrium surface temperature. This temperature is then used as the boundary condition in the numerical solution of Fourier's law.

Three of the four terms in equation 2.17 are easily described in terms of surface temperature. Q* is described as the sum of incoming and outgoing fluxes of shortwave and longwave radiation in equation 2.2. If the incoming fluxes are known, then the outgoing fluxes can be calculated if the

surface albedo, emissivity, and temperature are known, as indicated in equation 2.3. Albedo and emissivity tend to be fairly constant over a given surface, so that the unpredictable factor in the outgoing flux is the surface temperature.

Soil heat flux also depends largely on surface temperature. From equation 2.6, Qg can be expressed by the surface temperature gradient and soil thermal conductivity. Given knowledge of the soil thermal properties and the existing internal soil temperatures, equation 2.6 can be reduced so that the only unknown value is surface temperature.

Sensible heat flux into the atmosphere can also be reduced to an equation involving surface temperature. Using equation 2.10a, describing QH as a function of the temperature gradient in the air, and assuming that QH is constant with height, we can integrate 2.10a from the surface to an arbitrary height in the air to get:

$$QH = \rho c_p (T_s - T_a)/r_a \qquad (4.1a)$$

where $r_a$ is the aerodynamic resistance and represents the integrated diffusion coefficient. If $r_a$ and $T_a$ (the air temperature at the reference height) are known, then surface temperature ($T_s$) remains the only unknown.

## 4.2 Evaporation modelling

The evaporative, or latent, heat flux is the only

remaining component of the surface energy balance which has not yet been included. As was done for QH, the turbulent transfer equations for QE and $T$ (equations 2.10b,c) can be integrated with height to get equations dependent on surface values:

$$QE = (\rho c_p / \gamma)(e_s - e_a)/r_a \qquad (4.1b)$$

and

$$\tau = \rho c_p(u/r_a) \qquad (4.1c)$$

In equation 4.1c it is assumed that wind speed becomes zero at the surface $(z_0)$. Equation 4.1c allows determination of $r_a$ using wind speed at a single height (and knowledge of $z_0$). In applying equations 4.1a and 4.1b it is assumed that $T_s$ and $e_s$ occur at $z_0$.

Equation 4.1b would enable calculation of QE if $e_a$ (vapour pressure at the reference height) and $r_a$ are known, and if we can estimate the surface vapour pressure $(e_s)$. In practice, the greatest difficulty in modelling the surface energy balance is the determination of $e_s$. If we could link $e_s$ to $T_s$, then we would have all components of the energy balance expressed with surface temperature as the controlling variable, and calculation of the equilibrium surface temperature would follow. If the surface is completely saturated, then $e_s$ is the saturation vapour pressure at the surface temperature, $e^*(T_s)$. However, if the surface is not saturated, then $e_s < e^*(T_s)$.

## 4.2.1 Surface Vapour Resistance

The most common technique to link $e_s$ to $T_s$ is to assume that there is a resistance to evaporation (water vapour movement) at the surface, in the same manner that the aerodynamic resistance is used in the atmosphere between the surface and the reference height. It is usually further assumed that the temperature across the layer creating this difference is uniform, so that the evaporation rate (or vapour flux) across this layer can be expressed by:

$$QE = (\rho c_p/\gamma)(e^*(T_s)-e_s)/r_s \tag{4.2}$$

where $r_s$ is the surface resistance to vapour transfer. Combining equation 4.2 with 4.1b, we get:

$$QE = (\rho c_p/\gamma)(e^*(T_s)-e_a)/(r_a+r_s) \tag{4.3}$$

With this, we have eliminated surface vapour pressure from the equation, and added $r_s$ as an unknown. Although the number of variables in the equation for QE has not changed, it is assumed that $r_s$ will be easier to measure or estimate.

Equation 4.3 provides the fundamental basis for most evaporation modelling in the literature. The Penman-Monteith combination model (Penman, 1948; Monteith, 1965) can be expressed as a combination of equations 2.17, 4.1a, and 4.3, with the use of the slope of the saturation vapour pressure curve to eliminate surface temperature as a variable. The result is an equation for QE that does not require $T_s$ or $e_s$. An analogous equation for QH can be derived, as indicated by

de Bruin and Holtslag (1982). Further assumptions and simplifications are used to derive the equilibrium evaporation model and the Priestley-Taylor evaporation model (Priestley and Taylor, 1972; Davies and Allen, 1973). The model of Outcalt, et al (1975) uses a simple relative humidity function to calculate surface humidity, while Smith (1975,1977) uses the Priestley-Taylor model. Novak and Black (1985) use equation 4.3. Monteith (1981) provides a good discussion of the various forms of evaporation models, with consideration of the effects of surface temperature.

### 4.2.2 Surface Thermal Resistance

Equation 4.3 is a reasonable approximation when applied to transpiring vegetated surfaces, where leaves are essentially at uniform temperatures throughout their cross-section. For each leaf, the temperature of the water within the leaf is the same as the surface temperature of the leaf, so that the $e*(T_s)$ approximation is valid. The leaf's stomatal resistance is then used to estimate $r_s$. Over a vegetation canopy, the stomatal resistance is integrated to determine a bulk canopy resistance, which is then used in equation 4.3 as if the entire canopy were a single large leaf.

Tanner and Fuchs (1967) and Fuchs and Tanner (1968) point out that evaporation from bare soils occurs in a regime in which the evaporating water can be at a different

temperature from the surface. They outline the modifications required in the Penman-Monteith model to account for this temperature difference. They develop an evaporation equation which includes surface temperature; unfortunately this equation is not suitable for the purpose of this study, as it can be shown to be a simple calculation of QE by residual, using the energy balance equation (2.17), measured values of Q* and Qg, and equation 2.1a for QH. The solution of the energy balance equation for equilibrium surface temperature requires an independent formulation for QE.

The Fuchs and Tanner work, does however lead to a useful modification of the evaporation models outlined above. If the internal evaporation source within the soil is assumed to be saturated with respect to water vapour at a temperature $T_i$, then the evaporation can be expressed by:

$$QE = ( \rho c_p / \gamma) (e*(T_i) - e_a) / (r_a + r_s) \qquad (4.4)$$

where $T_i$ replaces $T_s$ in equation 4.3. In this study, $T_i$ will be referred to as the evaporative surface temperature. The problem with this formulation is that it introduces another unknown, without eliminating any of the previous variables. This adds to the complexity of the modelling effort, but it will be seen that the complexity is of paramount importance.

Although $T_i$ is unknown, it can be related to $T_s$ by defining a second surface resistance: a surface thermal resistance. Just as the $r_s$ term represents the restriction to vapour transfer across a thin surface layer in the soil,

the surface thermal resistance can be used to express the rate of thermal energy transfer across this layer. Choudhury and Monteith (1988) include a resistance of this type in their four-layer heat budget model for land surfaces.

Figure 4.1 illustrates the concept of the surface energy balance combined with a surface layer providing resistance. Figure 4.1a shows a surface layer which provides resistance to vapour transfer only, while figure 4.1b includes both vapour and thermal resistances in the surface layer. Figure 4.1 also shows that the total thermal transfer across the surface layer must be equal to QE+Qg. This is necessary because Q* is assumed to be absorbed at the top of the layer, and the energy for evaporation must be conducted down to the base of the layer where evaporation occurs. At the base of the layer, QE units of thermal energy are consumed in evaporation and are transferred back up through the layer as latent heat, leaving only Qg units as the soil heat flux below this layer. This distinction is irrelevant for the case with no thermal resistance, since it is assumed that all energy is transferred with zero thermal gradient.

The values of the surface vapour and thermal resistances can be calculated by assuming diffusion equations equivalent to those in the air for QH and QE (2.10a, 2.10b), and integrating over the thickness of the surface layer, as was done to derive equations 4.1a and 4.1b. For thermal transfer across the surface layer, both

a)



Surface

Evaporation Source

b)



Surface

Evaporation Source
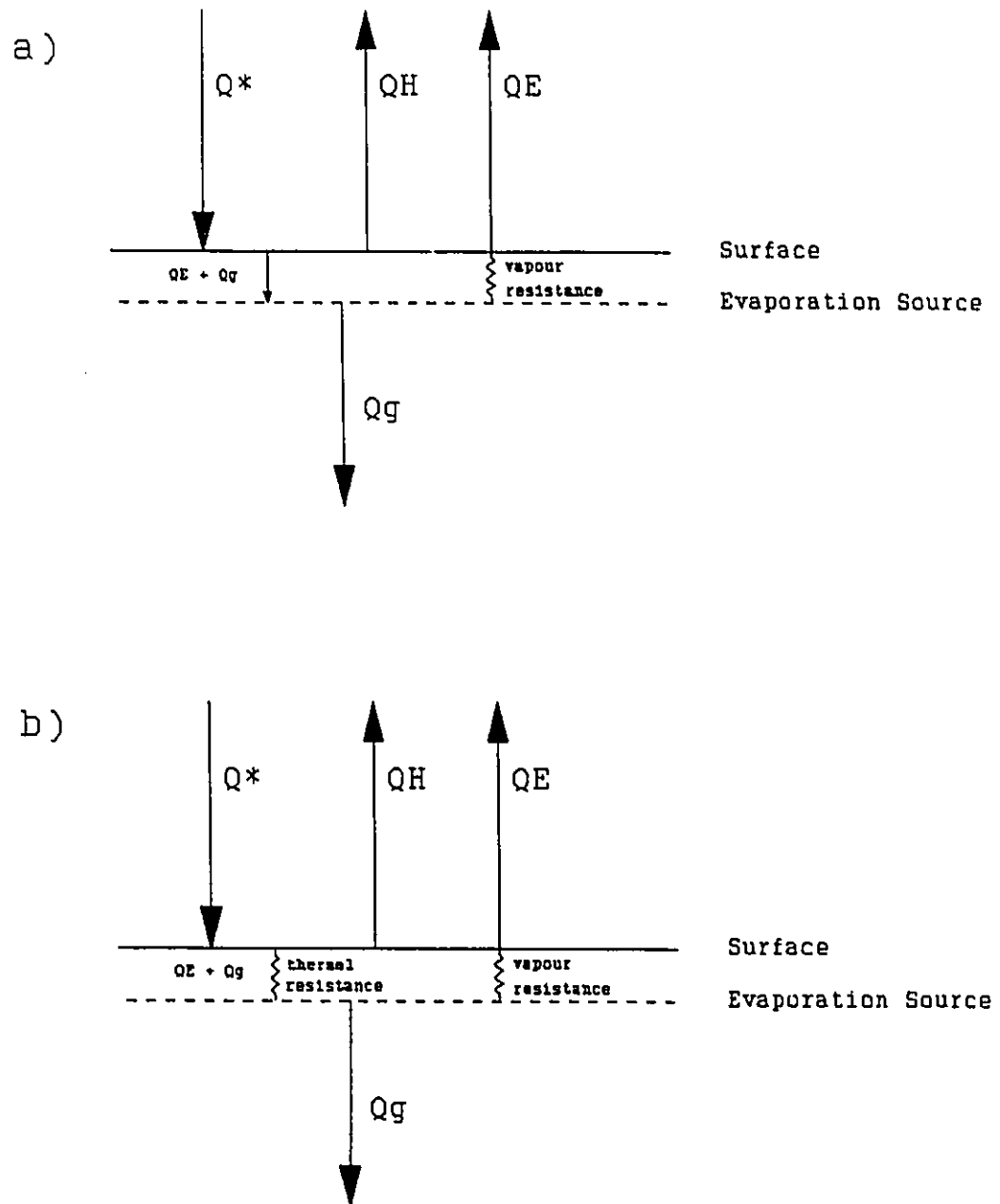
**Figure 4.1:** Surface energy balance fluxes, incorporating a surface resistance layer. a) resistance to vapour only; b) resistance to both vapour and thermal transfer. Direction of arrows indicates positive fluxes.

thermal diffusion through pore air and thermal conduction through the soil (liquid and solid phases) must be included. For the vapour resistance, only diffusion through the pore air is relevant.

Rather than trying to define separate thermal and vapour resistances, it is possible to assume that the two resistances always remain in constant proportion. This follows if we assume that the properties of the layer are uniform, and therefore both resistances change directly in proportion to the thickness of the layer. If the vapour resistance is known, then the thermal resistance is calculated as $k_r r_s$, where $k_r$ is the ratio between thermal and vapour resistances. With this arrangement, the relationship between $T_i$ and $T_s$ is established by:

$$(QE+Qg) = \rho\, c_p (T_s - T_i)/(k_r r_s) \qquad (4.5)$$

which relates the total thermal flux across the layer to the temperature difference and the thermal resistance. With this definition of surface thermal resistance, it is possible to develop a combination-type equation in a fashion similar to the Penman-Monteith model, but for this study it is undesirable to eliminate surface temperature.

The expected range of values for $k_r$ is easily determined. The lowest value is zero, which implies no thermal resistance and is equivalent to the assumption of uniform temperatures across the layer (cf. equation 4.3). The highest value would occur if the soil matrix provides no

thermal conduccion, so that all thermal transfer occurs as diffusion in the pore air. In this case, the value of $k_r$ should be about 1.1, which is the ratio of thermal and vapour diffusion coefficients for still air. (Since the soil has a porosity less than 1, the diffusion coefficient in the soil would be less than that of air, but both the thermal and vapour coefficients would be affected equally.)

This provides the necessary linkage between evaporation and surface temperature for application of the equilibrium surface temperature approach to the surface energy balance. Note that we have replaced one unknown in the evaporation equation (surface vapour pressure, $e_s$) with two other unknowns: a surface vapour resistance ($r_s$), and a ratio between thermal and vapour resistances in the surface layer ($k_r$). The second of these ($k_r$) can be considered a surface property or parameter, rather than a variable.

### 4.3 - Soil Temperature Modelling

#### 4.3.1 - Solutions to Fourier's Law

As covered in chapter 2, thermal transfer in the soil is described by Fourier's equation (2.4). There are many possible solutions to this equation, depending on specified geometry, boundary conditions, and any additional equations to be satisfied in a given problem. The number of existing analytical solutions is limited, and generally use fixed thermal properties, simple geometries, and simple

boundary conditions. Carslaw and Jaeger (1959) is the standard reference source for analytical solutions and solution techniques.

For complex problems, Fourier's equation is usually solved using numerical techniques. The two most widespread techniques are the "finite difference" and "finite element" methods. In the finite difference method, the derivatives in equation 2.4 are replaced by algebraic differences for each of a series of variably-spaced points or nodes within the domain of the problem to be solved. The resulting equation (or system of equations) is then solved to find the temperatures at the specified points, given appropriate boundary conditions. This provides an approximation to the solution of the original problem. Lunardini (1981) reviews finite difference techniques as applied to cold regions.

Generally, finite difference techniques can be divided into two classes: explicit and implicit. In explicit formulations, the new temperature for each node appears in only one equation over the entire grid of nodes, so that rearrangement of the equation for individual nodes allows direct calculation of the new temperature. The calculation of the new temperature for that node uses only the old (known) temperatures for other nodes. In implicit formulations, each new nodal temperature appears in the equations of several nodes, so that a direct solution for a single node is not possible. However, taking the equations

for all nodes together provides a system of equations which can be solved for the new temperatures. The resulting system of equations can be expressed in a matrix form, and solved using standard matrix techniques. Although this is more complicated than the direct solution allowed in explicit formulations, it has the advantage that a much larger time step can be used. Explicit formulations are usually "conditionally stable": small time steps must be used, or rounding errors in the calculations will grown exponentially. (All computer calculations involve rounding error, since computers only store a limited number of significant figures.) The result are only stable and accurate if the size of the time step meets the condition of limited size. The exact limit to the size of the time step depends on the formulation, the node spacing, and the thermal properties used in the calculation.

Implicit formulations are usually "unconditionally stable": rounding errors do not grow with time, regardless of the size of the time step. Although the time step must still be limited so that the numerical approximation accurately duplicates the exact problem, the time step can be much larger than in explicit formulations. The method is stable regardless of time step, node spacing, or thermal properties.

In the finite element method, the solution to equation 2.4 is not considered directly. Instead, the

problem is recast, using either the principles of variational calculus or a weighted residual process, into a form which seeks the temperature distribution that minimizes an appropriate functional (Goodrich, 1982). The nodes are considered only as an assemblage, not on an individual basis. Since the resulting system of equations for some problems is analogous to that derived by application of the finite difference method (Goodrich, 1982), the distinction between the two methods is somewhat hazy. Fundamentally, it is the method used to derive the final system of equations that is different (Goodrich, 1982). Often, finite element techniques are used to derive the numerical equations relating to the depth derivatives, while finite difference techniques are maintained for the time derivatives.

The power of numerical techniques, as opposed to analytical solutions of the Fourier equation , is the ease with which they can handle soil layers of differing thermal properties, latent heat effects, temperature dependent thermal properties, and irregular boundary conditions. The data and observations presented in chapters 2 and 3 indicate that all of these are important at the sites in this study.

## 4.3.2 - Incorporation of Latent Heat Effects

Methods of incorporating latent heat into finite difference formulations are discussed in detail by Hromadka et al (1981), Lunardini (1981) and Goodrich (1982). The most

common method is to distribute the latent heat over a finite temperature range, defining the latent heat to be part of an apparent heat capacity (equation 2.7). The position of the surface separating the frozen and unfrozen phases is then found by interpolating temperatures between the depth nodes. This is the approach used in Nixon and Halliwell (1982).

An alternative approach is to assume that all soil water freezes at a point temperature, and to solve explicitly for the position of the surface dividing the two phases. This second approach involves additional equations in the formulation of the problem, and frequently requires an iterative solution to the resulting non-linear system of equations, leading to longer computation times. Goodrich (1978) presents an efficient variation of this technique which requires iteration only at the nodes on either side of the frozen/unfrozen interface, but it cannot handle more than one interface. This eliminates its application to common ground thermal regimes, where two interfaces are found during thaw of a seasonal frost layer or freeze-back of the active layer.

Hromadka et al (1981) state a preference for modelling phase change in soils as an isothermal process, rather than by the apparent heat capacity method, for models which include water migration due to freezing. This, however, is not consistent with the true state of fine-grained soils. These soils hold significant quantities

of water in the unfrozen state at sub-zero temperatures, and the latent heat is distributed over a range of several degrees.

The choice of technique used to handle the latent heat effect depends, in part, on the choice of numerical solution technique. In an explicit formulation, the temperature-dependency of the apparent heat capacity and thermal conductivity is easily implemented by re-evaluating the thermal properties at each time step using the current nodal temperatures. In an implicit formulation, the thermal properties should be evaluated at the same time step as the depth derivative - i.e. at the unknown nodal temperatures - and an iterative solution technique is required in the matrix equations (Goodrich, 1980). Direct matrix solution techniques are possible if a three-level formulation is used, in which the new nodal temperatures are calculated from the nodal temperatures of the last two time steps. Unconditionally-stable formulations of this type are discussed by Bonacina and Comini (1971), Wood (1978), Goodrich (1980), and Hogge (1981).

### 4.3.3 - Selection of Numerical Method

To allow temperature-dependent thermal properties, inclusion of latent heat as an apparent heat capacity, unconditional stability, and direct matrix solution techniques, it was decided to use a three-time-level

numerical method. Initially, an effort was made to use the scheme described by Bonacina and Comini (1971), Bonacina et al (1973), and Comini et al (1974), with modifications to the heat capacity calculations as suggested by Morgan et al (1978), and modifications to allow variable nodal spacing with depth. However, the Bonacina and Comini scheme showed undesirable oscillations in temperatures when subjected to rapid changes in surface temperature. This behaviour in this scheme is also noted by Goodrich (1980). Goodrich examined two other three-time-level schemes, and recommended a finite element method which he referred to as a quadratic Galerkin scheme. The scheme is expressed by:

$$[C]((T)^{t-\Delta t}-4(T)^{t}+3(T)^{t+\Delta t}) =$$

$$\frac{2}{5} t[\lambda](-(T)^{t-\Delta t}+2(T)^{t}+4(T)^{t+\Delta t}) \qquad (4.6)$$

where [C] and [λ] represent thermal capacitance and conductance matrices, and the (T)$^j$ represent vectors containing the temperature profiles at the indicated times. Temperatures are known for times t and t-Δt. The unknown temperatures to be determined are at time t+Δt. If equation 4.6 is compared to equation 2.4, it can be seen that the capacitance matrix reflects soil heat capacity, while the conductance matrix reflects soil thermal conductivity and nodal spacing. The left side of equation 4.6 relates to the time derivative, while the right side relates to the depth derivative.

To implement equation 4.6, it was first cast in the form of a finite difference representation, following the example of the Bonacina and Comini scheme as outlined in Goodrich (1980) and Bonacina and Comini (1971). After isolating all the thermal parameters and grid spacing terms, the formulation was modified to allow the grid spacing to vary with depth. In the final implementation, thermal conductivity is calculated using temperatures at the middle time point (latest of the two known temperature profiles), using the average temperature between two depths to calculate the conductivity appropriate between the two nodes.

Heat capacity is estimated using the enthalpy approach as discussed in Comini et al (1974) and Morgan et al (1978). This method has already been discussed with respect to soil heat flux calculations in chapter 2. Briefly, the heat capacity is calculated as the difference in enthalpy divided by the difference in temperature. Several possible combinations of the known temperatures at each node were tried for use in the heat capacity calculation. Morgan et al (1978) suggested using the last two known temperatures at each node. In this study, the best results were produced if the temperature difference between the last two known values was used, centred on the last temperature (i.e. $T^m \pm 0.5(T^m - T^{m-\Delta t})$). Thus the enthalpy calculations were based on the latest temperature, but

spread over a range typical of the temperature change between time steps. The advantage of using this varying range, rather than an arbitrary fixed range, is that the heat capacity calculation covers the range of values expected or experienced over one time step. If a large, fixed range were used, the heat capacity could reflect temperatures which may not be experienced at that node for many time steps. If a small, fixed range is used, the temperature could leap across a narrow range where latent heat is released without the latent heat showing up in the heat capacity, because the temperature never actually fell in that narrow range.

Boundary conditions in the numerical scheme use a specified temperature at the surface, and a specified heat flux at the base.

### 4.3.4 - Validation of the Soil Temperature Model

To verify the performance of the numerical method, the numerical scheme was compared to an analytical solution incorporating phase change effects. Normally, Neumann's solution (Carslaw and Jaeger, 1959) is used as an analytical solution with phase change, but it assumes that all phase change occurs isothermally, whereas the numerical solution must liberate the latent heat over a temperature range. Carslaw and Jaeger (1959) also give an analytical solution involving multiple phase changes, originally provided by

Weiner (1955). Use of this solution allows exact comparison with the numerical method. By defining 3 temperature ranges, with zero latent heat at the two points of phase change between ranges, all latent heat can be assigned as an apparent heat capacity in the middle temperature range. This is directly equivalent to the numerical method's approach.

The example problem for which the analytical and numerical methods were compared is very similar to the problem described by Goodrich (1978). The problem considers a semi-infinite solid, initially at T=2°. At time t=0, the surface temperature is instantaneously reduced to -10° and held at this value for t>0, while the temperature at infinite depth is maintained at 2°. Thermal conductivity of the material is 2.25W/m°C for T<0°, and 1.75 W/m°C for T>0°. Latent heat of 100MJ/m$^3$ is liberated over the temperature range 0 to -0.2°C. The step change in surface temperature leads to freezing from the surface downward. Initially, the frost penetration is rapid, but the rate of frost penetration decreases with time.

The numerical scheme was implemented using a time step of 0.25 days. The numerical scheme encounters some difficulty with the abrupt change at t=0, so it was initialized with temperatures from the analytical solution at t=0.25 and t=0.5 days. (These times provide the two initial "known" temperature profiles required by the three-level numerical scheme.) Grid spacing in the numerical model

varied from 0.025m near the surface, to 0.5m at 10m depth, with a total of 59 nodes. The heat flux at 10m was specified to be 0. The model was run for 50 days. (After 50 days, the temperature at 10m, from the analytical solution, is still 2.000°, so that the numerical grid need not be extended beyond this depth and the heat flux at this depth can be ignored.)

Figure 4.2 shows the results of the analytical and numerical computations. Generally the numerical model does well. Small inaccuracies can be seen in the early results at 2 days, due to the rapid changes in the example problem. The early inaccuracies do not affect the results for longer times, as indicated by the excellent comparison after 50 days. The numerical model shows no signs of oscillations. (In simulating this same example problem, the Bonacina and Comini scheme gave similar accuracy after 50 days, but showed large oscillations at early times.) A similar comparison using a freezing range of 0 to -2.0° gave the same excellent results, confirming the accuracy and stability of the numerical method.

## 4.4 - Surface Energy Balance Modelling

The verification of the numerical soil temperature scheme outlined above assures the accuracy of the solution to Fourier's equation. The second stage in the overall numerical model is to develop the equations and algorithms
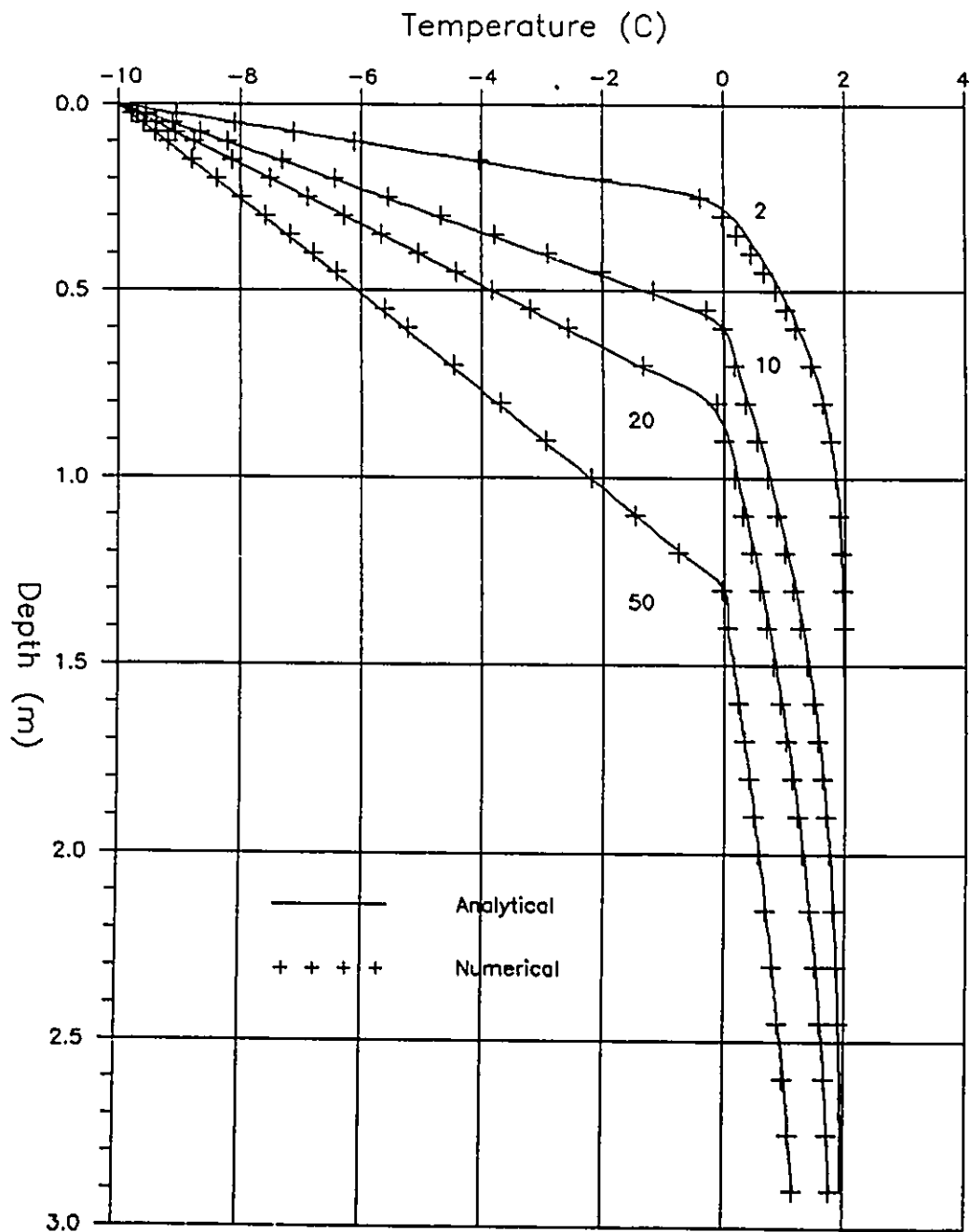
**Figure 4.2:** Comparison of numerical and analytical solutions to the example soil freezing problem. Numbers on curves indicate time in days since start of freezing.

for the surface energy balance calculations which provide the equilibrium surface temperature that forms the surface boundary condition. Each of the four components of the energy balance will be examined individually.

### 4.4.1 - Net Radiation (Q*)

The factors controlling Q* were summarized in equations 2.2 and 2.3, and discussed at the beginning of chapter 4. The only component of Q* which is influenced by surface temperature is the outgoing longwave flux, and this influence is small for small changes in temperature. Since measurements of longwave fluxes and reflected shortwave fluxes (or albedo) were not made at the Marantz site, it was decided to use measured values of Q* in the model rather than trying to calculate Q* using equation 2.3. Although equation 2.3 could be applied at the Churchill site, where the necessary radiation measurements were made, it was felt that it would be better to model the two sites in the same fashion.

### 4.4.2 - Sensible Heat Flux (QH)

The sensible heat flux was modelled using the height-integrated turbulent transfer equation indicated in 4.1a. To evaluate aerodynamic resistance, equation 4.1c was used, which requires wind speed at a reference height and an estimate of $z_0$. Stability corrections were included, using

the Dyer (1974) functions that were described in the data analysis section of chapter 2. Paulson (1970) and Holtslag (1984) provide analytical integrations of the Dyer functions.

Although the stability functions were transformed into functions of Ri for use in chapter 2, they are used in the original form, as functions of $z/L$, for use in the model. There were two reasons for this. First, Ri varies with height in a manner that is not obvious from its defining equation (2.20). On the other hand, L is independent of height, making the dependence of $z/L$ on height quite clear. Therefore, the $z/L$ functions are easily integrated over height. (Height-integrated forms using Ri are not in the literature; forms using $z/L$ are!) Secondly, since L is independent of height, it is very easy to calculate the aerodynamic resistance for QH when the reference height for air temperature is not the same as that for wind speed. This increases the flexibility of the model (and is required for the 1984 data).

Within the model, calculation of aerodynamic resistance depends on $z/L$, which depends on QH (in L), which in turn depends on $r_a$, so an iterative solution is required. A subroutine handles this calculation, independent of the rest of the surface energy balance calculations. First, $r_a$ and QH are calculated assuming neutral stability ($z/L=0$), using the provided values of wind speed, air temperature,

surface temperature, $z_0$, and the reference heights for wind speed and temperature. Then $z/L$ is calculated, and the estimates of $r_a$ and QH are revised. This leads to a revision of $z/L$, and the revision of $r_a$ and QH is continued until $z/L$ is no longer changing. Two exceptions must be handled: if $u*$ is zero (zero wind speed), then ra becomes infinitely large; and if conditions are very stable, then the iterative solution continues with $z/L$ and $r_a$ approaching infinity. In both cases, $r_a$ is set to an arbitrary maximum value. In the model, the maximum is based on integrating equation 2.10a using the thermal diffusivity of still air. This maximum value effectively reduces QH to 0.

### 4.4.3 - Latent Heat Flux (QE)

Latent heat flux is modelled using equation 4.4. This calculation is carried out after the evaluation of QH. so that the value of $r_a$ is known. It is assumed that air temperature and vapour pressure are measured at the same height, and that the value of $r_a$ is the same for both. The value of $T_i$ is calculated from equation 4.6, after making the substitution of $Q*-QH$ for $QE+Qg$. ($Q*$ and QH have been calculated already, whereas neither QE nor Qg are known.)

The complicating factor in modelling QE is the surface resistance, $r_s$. It can be reasonably assumed that this value should be related to soil moisture measured over some depth close to the surface. As water evaporates from

the surface, the thickness of the dry layer at the surface will increase, and $r_s$ will increase. As moisture is brought towards the surface from below, the thickness and $r_a$ should decrease. If precipitation or condensation occur at the surface, then the resistance should become zero. What is needed is a procedure for estimating $r_s$ based on these principles.

Deardorff (1977) describes an algorithm for cycling surface soil moisture in response to surface and subsurface exchanges, recommended for use in evaporation modelling. The algorithm essentially entails a two-layer hydrologic model. The surface layer responds rapidly to evaporation or precipitation quantities at the surface, and slowly to exchanges with the deeper soil layer. The water content in the deep soil layer (which includes the surface layer) also changes in response to precipitation and evaporation, but more slowly due to its greater thickness. If we assume that the value of $r_s$ is linearly related to the surface soil moisture expressed by Deardorff's algorithm, we can derive two expressions which describe the rate of change of $r_s$:

$$\frac{dr_s}{dt} = C_1(E-P) + C_2(\theta_{vmax}(1 - \frac{r_s}{r_{smax}}) - \theta_v) \qquad (4.7)$$

and

$$\frac{d\theta_v}{dt} = -C_3(E-P) \qquad (4.8)$$

In these equations, Deardorff's surface moisture has

disappeared, since we are interested in $r_s$, but soil moisture in the second layer is retained. Additional variables include the maximum soil moisture (saturated value, at which $r_s=0$), and a maximum $r_s$ value (corresponding to dry soil). Evaporation (E) and precipitation (P) are assumed to be rates, rather than absolute values. Equation 4.7 can be considered to cover two processes: the first term of the equation governs rapid surface changes in response to E and P; the second term tends to return $r_s$ to a value consistent with the overall soil moisture level. The two coefficients, $C_1$ and $C_2$, reflect the response rates of these two processes. Equation 4.8 describes the changes in soil moisture resulting from E and P. In the absence of subsurface drainage at the base of the deep soil layer, coefficient $C_3$ is related directly to the depth of the soil layer.

Equations 4.7 and 4.8 are used to vary $r_s$ within the numerical model. Changes in $\theta_v$ due to equation 4.8 can be calculated directly using the time step in the model, but changes in $r_s$ due to equation 4.7 cannot use 4.7 in its current form. Equation 4.7 is an ordinary differential equation, wich $r_s$ on both sides of the equation. The second term describes an exponential process, by which $r_s$ tends towards an equilibrium value. If the time step in the model is sufficiently small, then equation 4.7 would provide a satisfactory approximation in a difference form. However,

for model time steps which are long in comparison to the length of time involved in the exponential decay, direct use of 4.7 will overestimate the change in $r_s$.

To eliminate this problem, equation 4.7 was solved to find the exact value of $r_s$ after any time. Given the value of $r_s$ at time 0, the solution is:

$$r_s(t) = (r_s(0) - X)\ e^{-C_2 \frac{\theta_{vmax}}{r_{smax}} t} + X \qquad (4.9a)$$

$$\text{where} \quad X = \frac{C_1(E-P) + C_2(\theta_{vmax} - \theta_v)}{C_2 \frac{\theta_{vmax}}{r_{smax}}} \qquad (4.9b)$$

Within the model, $r_s$ and $\theta_v$ are kept between the limits of zero and their maximum values. The various coefficients and parameters involved in equations 4.9a and b will be discussed in detail when the model is used to simulate the research sites.

### 4.4.4 - Soil Heat Flux (Qg)

Although surface temperature has been selected as the boundary condition for the numerical soil temperature scheme, surface soil heat flux must be estimated independently for the energy balance and equilibrium surface temperature calculations. In the search for equilibrium surface temperature, it is not practical to solve the

numerical scheme for all soil temperatures repeatedly, so an approximation for Qg is required. Hopefully, the approximation will give the same soil heat flux that corresponds to the results of the numerical scheme when the detailed soil temperature calculations are completed.

The surface soil heat flux is proportional to the temperature gradient and thermal conductivity at the surface, as indicated by equation 2.6. Using a finite difference approximation to this equation, we get:

$$Qg(0) = -\lambda \Delta T / \Delta z \tag{4.10}$$

where the temperature and depth differences are calculated between the surface and first internal nodes in the numerical grid. In the numerical scheme, the thermal conductivity is calculated using the properties and temperature of this first soil layer. The "surface" temperature is taken to be that of the evaporative surface (i.e. $T_i$), rather than the surface temperature in contact with the atmosphere.

To use this formula, both temperatures must be known at the new time. The new surface temperature is known from the equilibrium surface temperature estimation procedure, but the temperature within the soil is not known. Since the numerical scheme is not explicit, it cannot be used to calculate this one temperature alone. An alternate method must be employed to estimate the internal soil temperature at the new time.

The selected method must be explicit, so that the internal soil temperature can be calculated directly from known values. Three methods were tried: a simple explicit procedure, using the surface, first, and second nodes from the previous time step; the DuFort-Frankel method, using the surface and second nodes from the previous time step, and the first node from the time step before that; and the Saul'yev method, using the first and second nodes from the previous time step, and the surface temperature from the new time. All methods are discussed in Lunardini (1981). The simple explicit method is conditionally stable, while the other two methods are unconditionally stable.

The three methods were evaluated by using them in the numerical model with hourly and daily time steps, and then comparing the estimated internal soil temperature with the temperature subsequently calculated by the complete numerical scheme. The results of linear regression analysis for each of the three methods is given in table 4.1. All methods worked reasonably well for hourly data, but the simple explicit and DuFort-Frankel methods were inaccurate using a daily time step. The Saul'yev method gave the best results, and was selected for use in the model.

The likely reason for the Saul'yev method's success is that it is the only one of the three to include the new surface temperature in the estimation of the new internal soil temperature. One possible concern in using the Saul'yev

Table 4.1:  Regression analysis, internal soil temperature
estimation versus numerical scheme.

a)  Hourly simulation, 463 hours. Mean temperature at
first internal node (from numerical scheme) =
7.027°.

| Method | Mean Est. | Slope | Int. | $r^2$ | SE |
|---|---|---|---|---|---|
| Simple Explicit | 7.034 | 1.014 | -0.091 | 0.9959 | 0.240 |
| DuFort-Frankel | 7.028 | 1.022 | -0.153 | 0.9955 | 0.254 |
| Saul'yev | 7.032 | 0.980 | 0.143 | 0.9962 | 0.226 |

b)  Daily simulation, 111 days. Mean temperature at
first internal node (from numerical scheme) =
7.800°.

| Method | Mean Est. | Slope | Int. | $r^2$ | SE |
|---|---|---|---|---|---|
| Simple Explicit | 7.864 | 1.132 | -0.961 | 0.8681 | 1.421 |
| DuFort-Frankel | 7.846 | 1.116 | -0.860 | 0.8139 | 1.693 |
| Saul'yev | 7.793 | 0.991 | 0.062 | 0.9898 | 0.324 |

method is that its unconditional stability normally only is
maintained when it is used as an alternating direction
method. This means that for alternate time steps the
direction of calculation is reversed: i.e. using the new
temperatures at node n-1, and existing temperatures at nodes
n and n+1 for one time step, then using the existing
temperatures at nodes n-1 and n, and the new temperatures at
node n+1 for the next time step. The method is explicit in
both directions because the boundary conditions provide the
necessary new temperature at one end, and calculations can
then proceed one node at a time to the other boundary.

In the current scheme, the direction is always from the surface downward. However, the internal soil temperature calculated using the Saul'yev method is used only for estimating Qg, and does not feed directly into the numerical grid calculations. The temperatures used in the next application of the Saul'yev method were calculated using the Quadratic Galerkin scheme, so the Saul'yev method does not have the opportunity to magnify its own errors and stability is not a concern.

The soil heat flux calculated from equation 4.10 represents an instantaneous value at the new time, at a depth half way between the surface and the first internal node. To accommodate the surface layer above this depth, and to include the effects of the change in soil temperature since the last time step, the calorimetric heat storage in this layer between time steps is added to the value from equation 4.10. The heat storage is calculated using the enthalpy function for the first soil layer, and the old and new surface temperatures. The depth used to calculate storage is half the depth of the first soil node. Normally, the heat storage term is small relative to the value of equation 4.10. Exceptions occur when the surface temperature change is unusually large, or the surface undergoes a freeze/thaw transition. The main purpose for including the storage term is to prevent unrealistic changes in surface temperature when freezing or thawing occurs.

## 4.5 - Equilibrium Temperature Solution

The methods described above for the surface energy balance must be used to calculate each term and find the equilibrium surface temperature. Rearrangement of the energy balance equation (2.17) gives:

$$Q* - QH - QE - Qg = 0 \qquad (4.11)$$

For any given surface temperature, all four terms can be calculated. If the four terms do not add up to zero, then the temperature used is not the equilibrium surface temperature, and the estimate must be revised. The search for equilibrium surface temperature then becomes a simple root-finding procedure.

The method used to find the root of equation 4.11 starts with a secant algorithm. With two initial guess at surface temperature, the left hand side of equation 4.11 is used to calculate a residual energy balance term. A straight line is then fitted between the two residual values, and the temperature at which the line goes through 0 is used as the next estimate. The oldest of the two previous estimates is then discarded, and the procedure repeated using the two remaining values. For each iteration, one evaluation of the energy balance terms is required, since the residual is retained for the previous estimate. One advantage of the secant algorithm is that the two estimates need not bracket the root. However, if the two temperatures have residuals

that are very close in value, then a large change in estimated temperature can result, throwing the calculations far from the region of the desired root. For this reason, the surface temperature estimate is never allowed to change by more than +20° or -19°. (The use of different positive and negative values avoids the possibility of returning directly to the previous estimate and starting an endless loop.)

Normally, the secant algorithm converges to the solution after 6 to 8 iterations. However, if freezing or thawing is occurring at the surface, then the residuals from equation 4.11 become highly non-linear when plotted against temperature. Under these conditions, the secant algorithm can become very slow to converge, or may not converge at all. To avoid this problem, if the secant method takes more than 10 iterations to converge on the root, then the model switches to the false-position method (Press et al, 1986).

The false-position method is very similar to the secant method. Given two estimates, the new estimate is found in the same manner: by fitting a straight line between the two points. The difference in the false-position method is in the retention of old estimates: the secant method always discards the oldest estimate, whereas the false position method always retains the old estimate which is on the other side of the root from the new estimate, discarding the old estimate which is on the same side of the root.

Therefore the two estimates in use will always bracket the root (indicated by the opposite signs of the residuals). Often, the false-position method and the secant method retain the same value, so the false position method formally converges nearly as fast as the secant method. However, the false-position method must be started with two estimates that bracket the root. The slower convergence of the false-position method is offset by its guarantee of convergence on the root.

In any root-finding procedure, the better the initial estimate, the more rapidly the root is found. In the model, the first guess is always taken to be the equilibrium surface temperature from the last time step. The second guess is based on a very simplified energy balance approach. Equation 4.1a relates the difference in temperature between the air and the surface to QH. QH can also be calculated from the Bowen ratio, using equation 2.18a. If we assume that Qg is a constant fraction of Q*, e.g. 10%, then we can eliminate Qg from the equation. If we then assume a value for $\beta$, we can get QH as a function of Q*. Substitution of this value for QH into equation 4.1a using a typical value for $r_a$ then yields an estimated temperature difference. SInce Q* usually varies more rapidly than $\beta$ or $r_a$, this gives us a very simple estimate of $T_S$. In practice, it was found that using $T_S = T_a + 0.02Q*$ gave a reasonable second estimate for $T_S$. The next iteration then uses the secant

algorithm.

The root-finding procedure is assumed to have converged when two conditions are satisfied: the surface temperature is changing less then a prescribed limit (0.0001° is used), and the residual from the energy balance calculation is less than a second limit ($1.0 Wm^{-2}$).

Once the equilibrium surface temperature has been determined, the evaporative surface temperature is used as the boundary condition in the numerical soil temperature model. Once the soil temperatures have been calculated, the model interpolates the temperature profile to find the depths of the 0° isotherm, outputs the energy balance and soil temperature results, and moves on to the next time step.

Chapter 5: Model Performance with Field Data

## 5.1 - Model Inputs

To run the model, two data sets are required. The first data set specifies site conditions, parameters, and temperature profiles at the start of the simulation. The second data set specifies meteorological conditions for the duration of the simulation.

Initialization data includes the time step, anemometer and air temperature/humidity heights, surface roughness length, parameters for surface vapour resistance cycling, information on the soil profile (including the number of layers, the depths, water contents, and thermal properties), the spacing for the thermal grid, initial soil temperatures for two times prior to the start of the simulation, and the heat flux at the base of the thermal grid.

Meteorological data required during the simulation are date and time (for identification purposes only), net radiation, air temperature and vapour pressure, wind speed, and precipitation.

All initialization data are printed out for verification at the start of the simulation. At each time step, the printout includes the read-in meteorological data,

Table 5.1:  Site initialization data.

|  | Churchill | Marantz |
|---|---|---|
| Anemometer height (m) - 1984 | 3.55 | 3.66 |
| - 1985 | 2.00 | 2.00 |
| Temperature/humidity height (m) | 2.00 | 2.00 |
| Surface roughness ($z_0$) (m) | 0.014 | 0.014 |
| Depth of thermal grid (m) | 1.5 | 1.5 |
| Grid node spacing (m) - surface | 0.02 | 0.02 |
| - base | 0.10 | 0.10 |
| Number of nodes in grid | 50 | 50 |
| Heat flux at base (W/m$^2$) | 7.0 | 7.0 |

calculated energy balance values, residual in the energy balance equation, calculated u*, $r_a$, z/L, $r_s$, and $\theta_v$, surface temperature, evaporative surface temperature, the estimated soil temperature at the first soil node (used in Qg), interpolated 0° isotherm depths, and the soil temperature profile.

In the initialization data, instrument heights, surface roughness length, soil properties and initial temperatures are based on direct field measurements. The majority of this information is given in tables 5.1 and 5.2. Field observations indicated that the heat flux at a depth of 1.5m was fairly uniform over the field season, so the thermal grid was extended only to this depth, with a constant basal heat flux imposed as the boundary condition.

Table 5.2:    Soil profiles for simulation.

Churchill:

| Depth (m) | Soil | Solid Fraction | Solids Heat Cap. | Volumetric Water Content | Unfr. Water Param. A | B | C | Thermal Cond. Thawed | Frozen |
|---|---|---|---|---|---|---|---|---|---|
| .30 | Peat | .150 | .25E+07 | .850 | .076 | .782 | .042 | .60 | 1.60 |
| 1.00 | Clay (act.1) | .650 | .19E+07 | .350 | .070 | .772 | .125 | 2.30 | 2.90 |
| 2.50 | Clay (Perma) | .570 | .19E+07 | .430 | .070 | .772 | .125 | 2.30 | 2.90 |

Marantz:

| Depth (m) | Soil | Solid Fraction | Solids Heat Cap. | Volumetric Water Content | Unfr. Water Param. A | B | C | Thermal Cond. Thawed | Frozen |
|---|---|---|---|---|---|---|---|---|---|
| .05 | Peat | .120 | .25E+07 | .400 | .067 | .525 | .064 | .20 | .50 |
| .10 | Peat | .100 | .25E+07 | .600 | .067 | .525 | .064 | .35 | .80 |
| .25 | Peat | .120 | .25E+07 | .800 | .067 | .525 | .064 | .50 | 1.60 |
| 1.00 | Peat | .130 | .25E+07 | .870 | .067 | .525 | .064 | .57 | 1.60 |
| 1.50 | Sand | .720 | .19E+07 | .280 | .010 | 1.000 | .000 | 2.70 | 3.75 |

### 5.1.1 - Surface Resistance Coefficients

One important set of parameters which could not be based on direct field measurements is the coefficients for $r_s$ cycling. In all, six values are required in the resistance cycling procedure. These are the thermal/vapour resistance ratio ($k_r$), the three cycling coefficients ($C_1$, $C_2$, and $C_3$), and maximum and initial values for surface vapour resistance and water content ($r_s$ and $\theta_v$). Water contents could be based on the 1985 TDR measurements, but it is not known over what depth $\theta_v$ should be measured to provide a reasonable estimate of $r_s$.

The approach that was taken was to look at the entire range of values of $k_r$, and to fit the cycling coefficients to apparent values of $r_s$ determined from the measured energy balance values. As mentioned in chapter 3, $k_r$ should fall between 0 (no thermal resistance) and 1.1 (thermal and vapour diffusion in still air). If textbook values of properties of dry peat are used, then the thermal conductivity and porosity characteristics correspond to a $k_r$ value of about 0.3. For this reason, $k_r$ values of 0.0, 0.3, 0.6, and 1.1 were selected.

Rather than trying to fit cycling coefficients to the entire data set, the month of July 1985 was selected. The measured hourly values of QH and wind speed were used to determine $r_a$, and then the measured value of QE was used to calculate an apparent $r_s$ value for all values of $k_r$. The

time series of $r_s$ values was then used to fit the coefficients $C_1$ and $C_2$. Initially, $C_3$ was fitted to the Churchill TDR measurements of $\theta_v$ using the 0-0.15m vertically-oriented probe.

Apparent values of $r_a$ derived from the field measurements for the various $k_r$ were highly correlated. It appears that for any given QE value, the four apparent $r_a$ values remain in fairly constant proportion. Plotting $r_s$ for one value of $k_r$ against that for another $k_r$ yields a near-linear relationship. The apparent $r_s$ value is highest for $k_r=0$ and lowest for $k_r=1.1$. This is expected, because the introduction of a thermal resistance reduces the temperature at the evaporative surface, reducing the saturation vapour pressure and the evaporation. To "explain" a particular evaporation rate, the value of $r_s$ is less when combined with a thermal resistance than when used alone. The ratios between $r_s$ values are about 1.4 for each step from $k_r=1.1$ to 0. (The relative constancy of the ratio between steps simply indicates that the four $k_r$ values represent an even selection of possible $k_r$ values.)

In fitting the cycling coefficients to equations 4.8 and 4.9, it becomes apparent that several of the parameters are also highly correlated. The reason for this is seen in examining the characteristics of the equations. As mentioned in chapter 4, equation 4.7 (differential form for $dr_s/dt$) includes a surface response term and soil moisture term.

Each term represents a source or sink of moisture. In equation 4.9 (analytical solution for $r_s(t)$), there are also two terms, but the arrangement is slightly different. The second of the two terms (X in 4.9b) represents the ultimate equilibrium value of $r_s$, while the first term (involving the exponential function) represents the time-dependent approach towards equilibrium.

In the absence of evaporation or precipitation, the equilibrium value will be $r_s = r_{smax}(1-\theta_v/\theta_{vmax})$, which corresponds to our assumption that $r_s$ is a linear function of $\theta_v$, ranging from 0 at saturation to a maximum in dry soil. Therefore, $r_{smax}$ simply indicates how quickly $r_s$ changes with $\theta_v$. Since the time-dependent change in $\theta_v$ is indicated by $C_3$ (equation 4.8), changes in the value of $C_3$ or $r_{smax}$ will have the same effect on equilibrium values of $r_s$. $\theta_{vmax}$ simply provides an arbitrary reference point corresponding to $r_s=0$, and is also tied directly to $\theta_v$ and $r_{smax}$. Since $\theta_v$ is the only variable amongst these, it is the dominant control over long term variability of $r_s$. In view of the correlation between $C_3$ and $r_{smax}$, the fitting of $C_3$ to field measurements of $\theta_v$ is superfluous, since any value of $C_3$ could be used when $r_{smax}$ is fitted.

In the transient portion of equation 4.9, $C_1$ represents the response to E and P, while $C_2$ represents the rate of return towards the equilibrium value dictated by soil moisture at depth. The size of these two coefficients

must balance. If $C_1$ is too large, evaporation will dry the surface (in the algorithm) more rapidly than soil moisture moves upward, and $r_s$ will rise continuously. If $C_2$ is too large, the effects of evaporation and precipitation will be damped. Therefore, in practice, $C_1$ and $C_2$ tend to increase and decrease proportionally. Since these two parameters relate $r_s$ to changes in surface moisture content, they are affected by the size of $r_{smax}$.

Fitting of parameters was done by eye. Since water contents and $C_3$ could be based on field measurements, most of the fitting is carried out using $C_1$, $C_2$, and $r_{smax}$. For initial values, $\theta_v$ is more important than $r_s$, because it influences long term values. An odd initial value of $r_s$ affects initial transient terms, but not the long term results.

The fitted values, using the July 1985 hourly data, are given in table 5.3. The Churchill values were fitted first, and the reason that the Marantz values are the same is simply because they seemed to work there as well. The Marantz surface is quite different in terms of surface vegetation cover and near surface water content, but appears to react in a very similar manner in terms of changes in $r_s$. It would be nice to think that the coefficients in table 5.3 are somewhat universal, but the similarity between the Churchill and Marantz sites is probably a coincidence.

Table 5.3:  Resistance  cycling  coefficients  fitted  to
July 1985 hourly data.

| $k_r$ | $c_1$ | $c_2$ | $c_3$ | $r_{smax}$ | $\theta_{vmax}$ |
|---|---|---|---|---|---|
| | $(s/m^2)$ | $(/m)$ | $(/m)$ | $(s/m)$ | |
| Churchill: | | | | | |
| 0.0 | 230,000 | 0.22 | 1.5 | 800 | 0.87 |
| 0.3 | 160,000 | 0.18 | 1.5 | 600 | 0.87 |
| 0.6 | 90,000 | 0.11 | 1.5 | 400 | 0.87 |
| 1.1 | 50,000 | 0.06 | 1.5 | 275 | 0.87 |
| Marantz: | | | | | |
| 0.0 | 230,000 | 0.22 | 1.5 | 800 | 0.87 |
| 0.3 | 160,000 | 0.18 | 1.5 | 600 | 0.87 |
| 0.6 | 90,000 | 0.11 | 1.5 | 400 | 0.87 |
| 1.1 | 50,000 | 0.06 | 1.5 | 275 | 0.87 |

A  comparison  of  the  transient  and  equilibrium
portions of equation 4.9 indicate that the coefficients in
table 5.3 are consistent with a fairly rapid approach to
equilibrium. The transient term dissipates after several
hours.  On  a  diurnal  basis,  this  means  that  daytime
evaporation causes a rapid increase in $r_s$, with a fairly
rapid return to lower values at night. Precipitation inputs
cause a rapid drop in $r_s$, followed by a rapid rise after the
rain stops. These characteristics of the resistance cycling
algorithm  are  consistent  with  the  patterns  of  apparent
surface relative humidity presented in chapter 3.

The ultimate test of the cycling algorithm is in the
results from the numerical model.

## 5.2 - Modelling the Field Data

### 5.2.1 - Simulations of July 1985

The fitting of resistance cycling coefficients completes the initialization data requirements. Meteorological data for the model are taken directly from field measurements. The first step in modelling the field data was to simulate the July 1985 conditions using all combinations of coefficients. The purpose of this was two-fold: to see if the resistance cycling algorithm works, and to see if the results could help determine what value of $k_r$ was best.

In comparing the model results to observed data, it was decided to examine the energy balance terms (QH, QE, and Qg) and the thaw depth. The energy balance terms indicate whether or not the model is adequately simulating the surface boundary conditions. Although it would appear that a comparison between measured and modelled surface temperature may be more appropriate, it was felt that the measured surface temperature may not be a reliable value. Although there is confidence that the thermocouples accurately measured the surface temperature where they were located, the comparison between thermocouple measurements and extrapolated temperature profiles suggested that the thermocouples may not be representative (figure 3.9). The 1987 data on surface temperature (figure 3.10) indicated a fair degree of spatial variation could be expected.

The surface temperature calculated by extrapolating the air temperature profiles should give a better estimate of the areal average, but using this value for comparison with the model is equivalent to comparing the measured and modelled QH values anyway. The extrapolation technique is based on the same aerodynamic theory that is used to model QH. Since the model is provide with one of the measured air temperatures and wind speeds, a comparison of QH becomes a comparison of temperature gradients, and thus a comparison of surface temperatures.

For the same reason of spatial variability, the modelled soil temperatures are not compared directly to the measured values. Near-surface comparisons would suffer the same degree of possible error. In addition, the apparent upward motion of the Churchill temperature sensors relative to ground level would require interpolation of the temperature profiles in order to match "measured" depths with modelled depths. The distance between sensors on the thermocouple rod is not small enough to provide good short-term interpolated values. As depth increases, the measured soil temperatures are influenced by a greater surface area, so they automatically become more representative of the average conditions. Diurnal fluctuations are also small, easing the interpolation problem. The calorimetric calculations of soil heat flux (chapter 2) indicate that most of the soil heat flux is used to thaw frozen soil, so

Table 5.4:   Error   values,   July   1985   hourly   model
             simulations.  (Thaw  values  are  actual  modelled
             depth at end of simulation.) Values in W/m$^2$ and
             m.

Churchill.   Initial thaw depth = 0.35m.
             Final observed thaw depth = 0.73m
             Observed means: QH= 45.4, QE= 75.1, Qg= 21.9

| $k_r$ | QH | | QE | | Qg | | Final thaw |
|---|---|---|---|---|---|---|---|
| | MBE | RMSE | MBE | RMSE | MBE | RMSE | |
| 0.0 | -3.5 | 31.4 | 5.5 | 25.6 | -1.1 | 24.9 | 0.771 |
| 0.3 | 1.5 | 33.5 | 2.2 | 24.7 | -2.8 | 22.8 | 0.725 |
| 0.6 | -0.4 | 34.0 | 4.9 | 23.5 | -3.6 | 25.0 | 0.709 |
| 1.1 | -0.2 | 35.5 | 5.4 | 22.9 | -4.3 | 27.9 | 0.692 |

Marantz      Initial thaw depth = 0.27m.
             Final observed thaw depth = 0.40m
             Observed means: QH= 45.7, QE= 64.7, Qg= 21.7

| $k_r$ | QH | | QE | | Qg | | Final thaw |
|---|---|---|---|---|---|---|---|
| | MBE | RMSE | MBE | RMSE | MBE | RMSE | |
| 0.0 | -1.8 | 32.9 | 4.3 | 36.7 | -4.8 | 19.3 | 0.374 |
| 0.3 | 6.2 | 34.9 | -1.7 | 36.8 | -6.8 | 16.7 | 0.365 |
| 0.6 | 4.0 | 34.8 | 1.5 | 36.0 | -7.8 | 16.9 | 0.349 |
| 1.1 | 4.2 | 35.4 | 2.1 | 35.4 | -8.6 | 17.8 | 0.348 |

the position of the frost line (0° isotherm) provides a good
reference value for the soil temperature comparison. In
essence, rather than picking a single depth to compare
modelled and measured temperatures, we are picking a single
temperature and comparing modelled and measured depths.

Table 5.4 shows the results of the model
simulations, compared to the field measurements of the
surface energy balance and thaw depth. The error statistics
used are Mean Bias Error MBE) and Root Mean Square Error

(RMSE) as described in chapter 2. In general, the energy balance values are good. At the Churchill site, QE tends to be overestimated at the expense of QH and Qg. At the Marantz site, both QH and QE are overestimated, with Qg being significantly underestimated. Although the absolute errors are similar for all fluxes, the relative error is much larger for Qg. The MBE and RMSE values for QH and QE are similar to the values mentioned in chapter 2, when comparing the aerodynamic and Bowen ratio methods. Since the two measurement methods show an error this large when compared together, it is unreasonable to expect the model to do better.

The modelled thaw depths at the Churchill site bracket the observed thaw depth at the end of July. The tendency is for less thaw as $k_r$ increases. This is consistent with the pattern of Qg. At the Marantz site, Qg and the thaw depth are underestimated. The pattern between Qg, thaw depth, and $k_r$ is the same as for the Churchill site. The increase in thaw depth for $k_r=1.1$ is little more than half what it should be, which corresponds to the error in Qg.

Table 5.4 suggests that the model works fairly well. However, it provides no information on the model's performance on a daily basis, or at specific times of the day. Figures 5.1 to 5.3 use the Churchill simulation for $k_r=0.3$ as an example to show how the modelled and measured
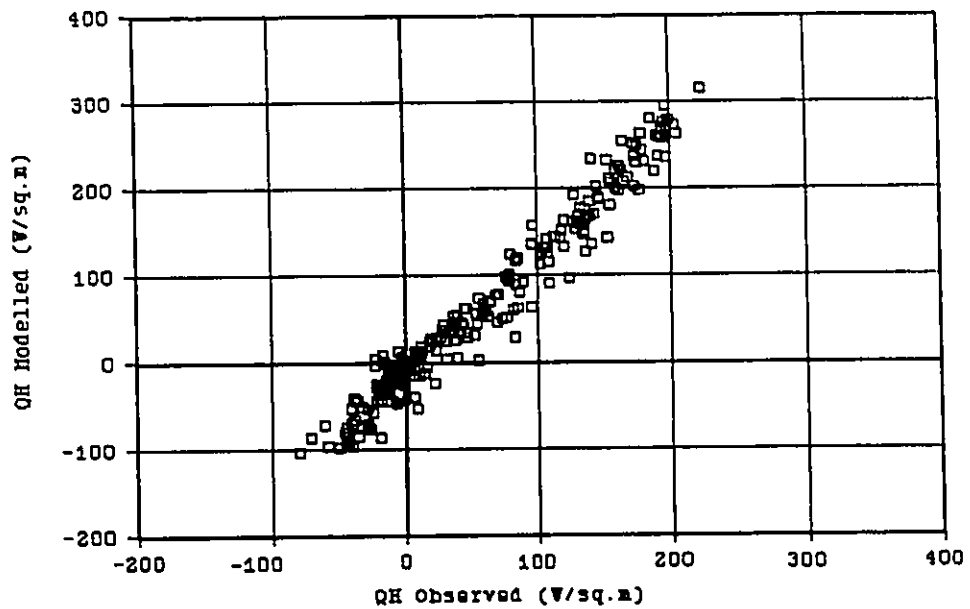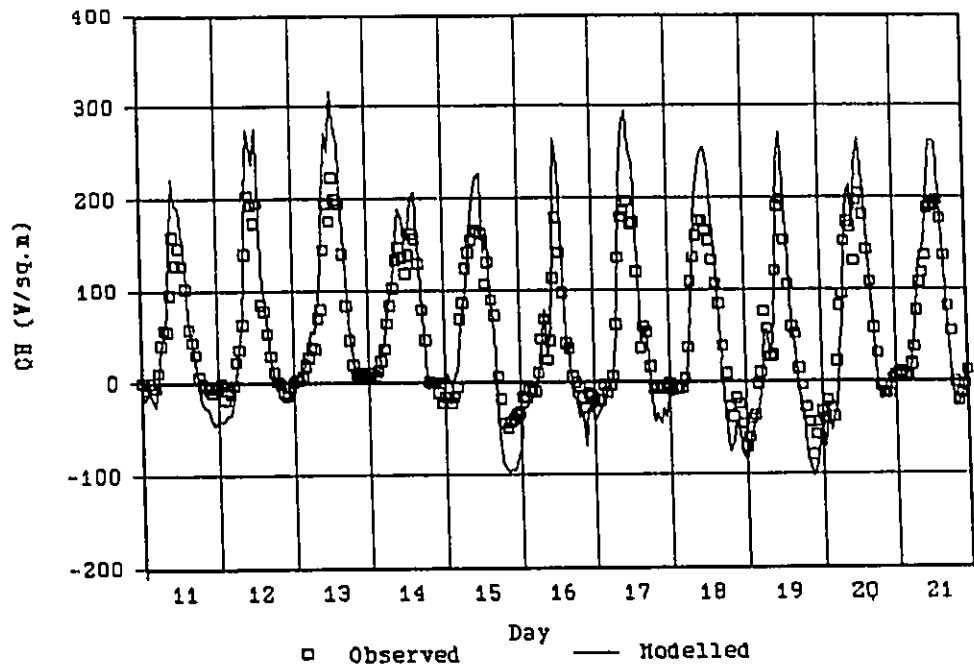
Figure 5.1: Comparison of modelled QH ($k_r$=0.3) to observed values. Churchill Site, July 11-21, 1985. Top: time series. Bottom: scatter diagram.
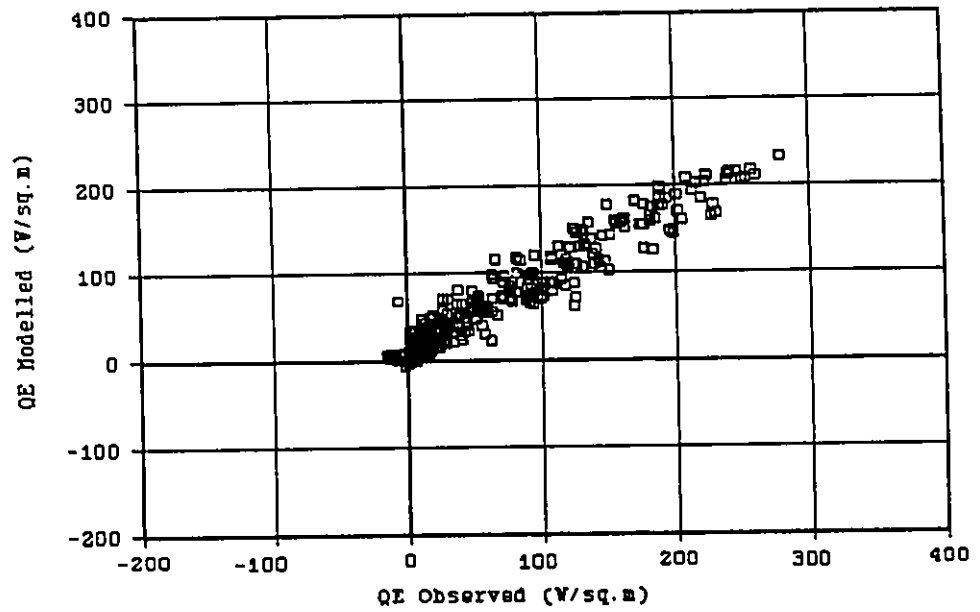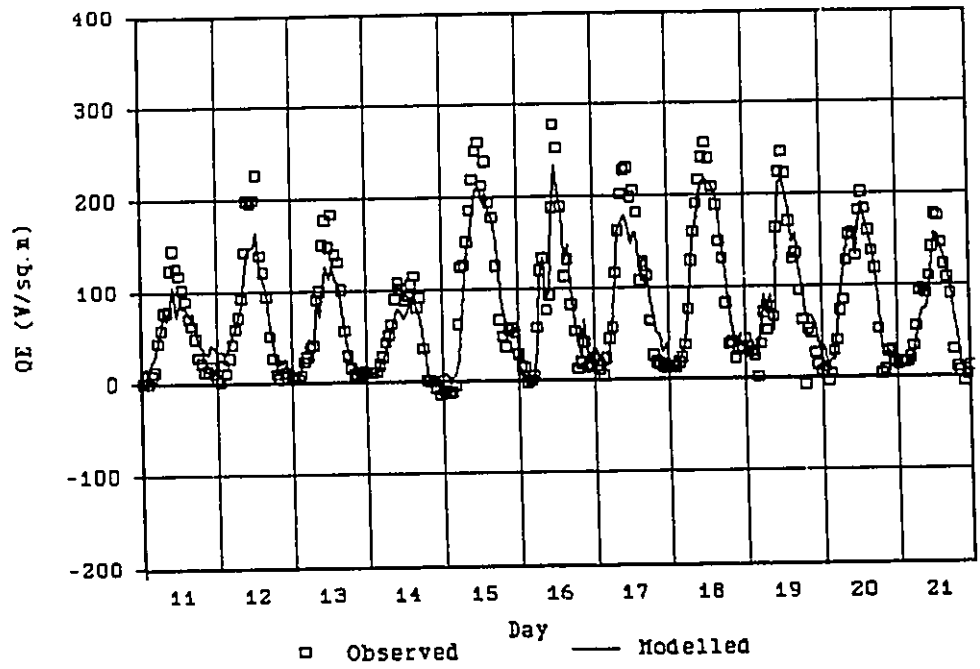
Figure 5.2: As for figure 5.1, for QE.
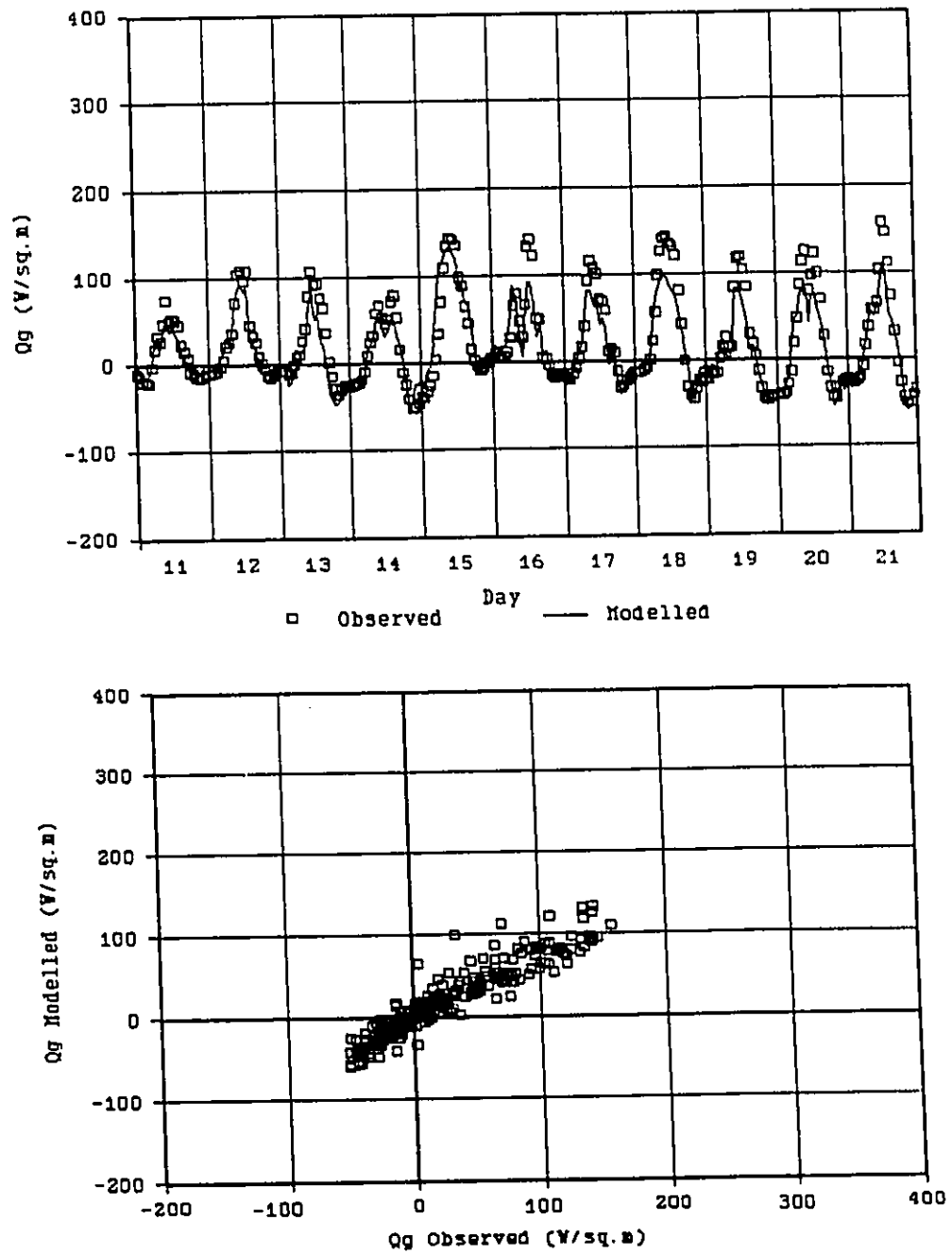
Figure 5.3: As for figures 5.1 and 5.2, for Qg.

values compare, in the form of time series and a scatter diagrams. The scatter diagrams show that QE is modelled equally well at all times, whereas QH tends to be overestimated primarily at high values, and Qg is underestimated at high values. The time series graphs illustrate that the error in the model is not entirely random: on some days the model does consistently well, while on other days it overestimates or underestimates consistently. The simulations for other $k_r$ values are similar.

Figure 5.4 shows the MBE values for all $k_r$ values on an hourly basis. Strong diurnal patterns are evident. Results for all $k_r$ values show the same pattern, but the amplitudes vary. For QH, $k_r=0$ shows the smallest errors at all times of day. For QE, errors for all $k_r$ values are similar. For Qg, the "best" value for $k_r$ depends on the time of day. The sign of the error term tends to follow the sign of the flux for QH, is opposite for Qg, and varies for QE. This can be seen by comparing Figure 5.4 with Figure 5.5, which shows the mean measured fluxes by hour for the Churchill site in July 1985.

These figures do not help much in determining the most appropriate value of $k_r$ to use in a "real" simulation. Part of the diurnal pattern is likely due to the use of an aerodynamic calculation in the model and a Bowen ratio calculation (mostly) in the observed values. If the Bowen
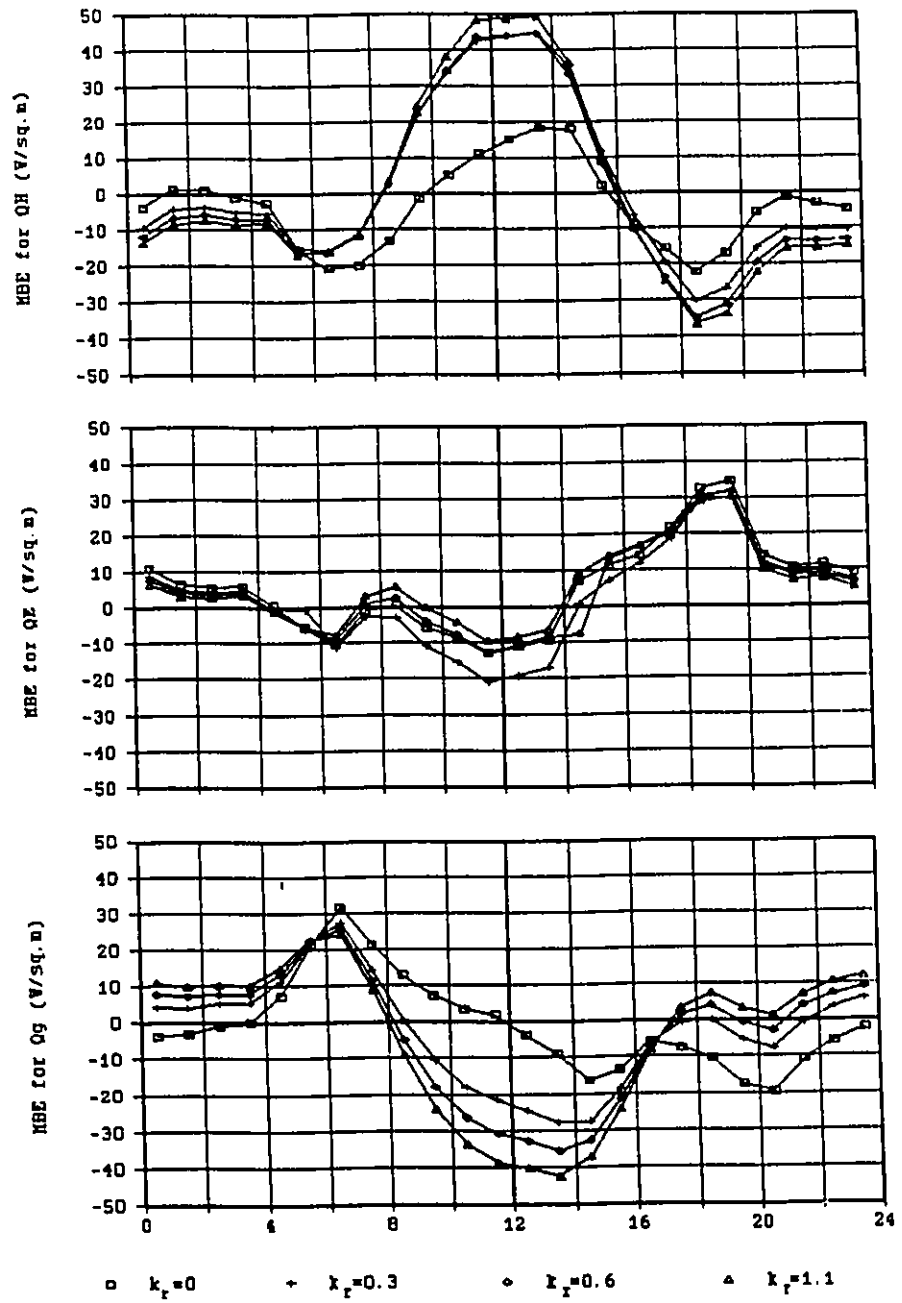
Figure 5.4: Model errors (MBE) by time of day.
Churchill Site, July 1985.
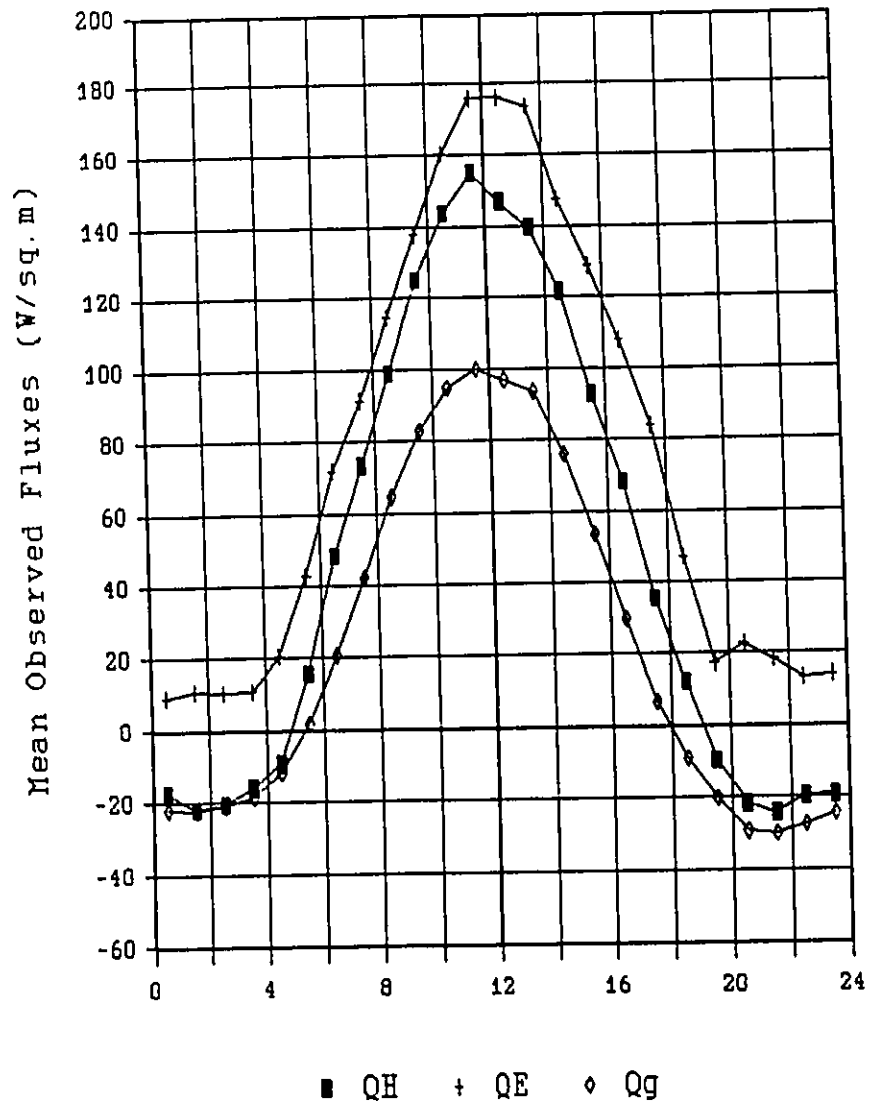
Figure 5.5: Mean observed energy balance fluxes by time of day. Churchill Site, July 1985.
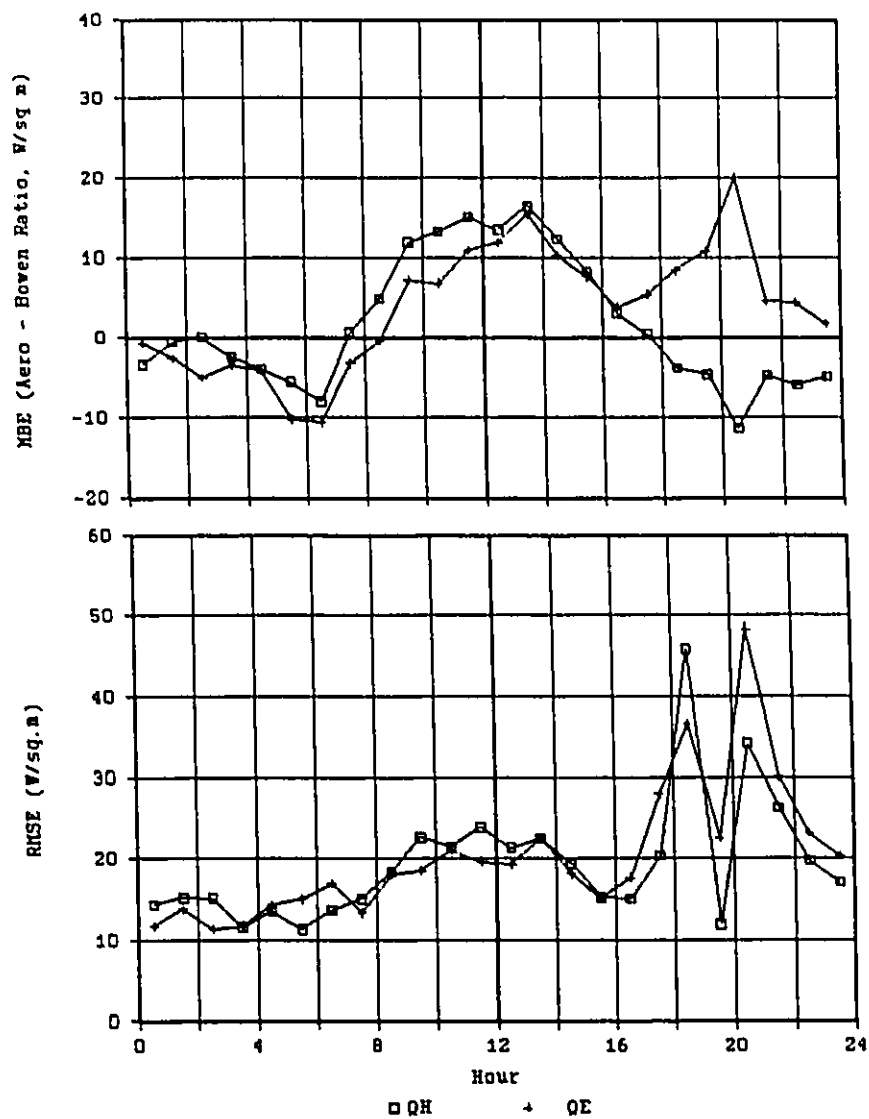
Figure 5.6: Errors between aerodynamic and Bowen Ratio
measurements of QH and QE, by time of day.
Churchill Site, June/July 1985.

ratio and aerodynamic methods for analyzing the field data are compared on an hourly basis, a similar diurnal pattern appears. This is shown in figure 5.6, using Churchill data from June and July 1985. The magnitude of the error is similar to the smaller errors in figure 5.4. The same holds true for the Marantz site. Figure 5.6 also shows RMSE values, indicating that the largest MBE values (late in the day) occur when there are also large RMSE values. At this time of day, when temperature gradients are inverting, the Bowen ratio method is unreliable.

Some comments apply to this error comparison. Generally, the model duplicates QE the best. This is not surprising, since the main determinant in partitioning Q* (which is provided) into QH, QE, and Qg is the surface resistance, $r_s$. Since $r_s$ was fitted to reproduce the observed QE values, it should at least work for this. However, the good comparison for QH and Qg confirm the validity of the overall modelling approach. The use of $r_s$ does link the evaporation process to surface temperature, and the resulting equilibrium surface temperature does give reasonable values for QH and Qg.

### 5.2.2 - Simulations of the 1984 and 1985 seasons

Since we so far have only looked at July 1985, it is not yet known if the resistance cycling coefficients are truly representative of the surface in general, or whether

they apply only to the conditions in the month from which they were derived. We only know that if we derive resistance values from the measured data and use them in the model, we can get the same measured data back again. If the resistance cycling coefficients are characteristic of the surface rather than July 1985, the model should also do well for other times. This will be examined by using the same coefficients to simulate the 1984 and 1985 seasons, from the start of June to the end of the energy balance measurements.

Detailed soil moisture measurements were not available at the start of June in 1985, or at all in 1984. At the Churchill site, rain and snow up to the beginning of June 1985 had left the site in a very wet state. The moisture content at the start of the 1985 simulation was set to be 0.86 - just slightly below the maximum value of 0.87. For the Marantz site, the soil was assumed to be saturated at the maximum of 0.87. In the 1984 simulations, both sites were assumed to be saturated at the start of June.

Table 5.5 provides MBE and RMSE values for the model simulation on a monthly basis. The model was run in one-month periods, to provide error statistics on a monthly basis. However, the model conditions were not reset to observed values for each month: the results of each simulation were saved and the following month initialized with the model output, assuring that the season's values were the result of a continuous simulation. For this reason,

Table 5.5:  Error  values,  hourly  model  simulations  for
$k_r$=0.3.  (Thaw  values  are  actual  modelled  depth
at end of simulation.) Values in $Wm^{-2}$ and m.


Churchill, 1984     June 1 thaw depth = 0.18m.
                    Final observed thaw depth = 0.72m

| Month | QH | | QE | | Qg | | Final thaw |
|---|---|---|---|---|---|---|---|
| | MBE | RMSE | MBE | RMSE | MBE | RMSE | |
| June | 4.4 | 43.6 | 4.8 | 27.3 | -3.1 | 31.7 | 0.345 |
| July | 10.2 | 30.4 | -8.5 | 30.3 | -3.9 | 27.1 | 0.796 |
| Aug. | 6.4 | 30.0 | -3.7 | 30.7 | -2.1 | 28.0 | 1.048 |

(Ends on August 21)

Churchill, 1985     June 1 thaw depth = 0.13m.
                    Final observed thaw depth = 0.95m

| Month | QH | | QE | | Qg | | Final thaw |
|---|---|---|---|---|---|---|---|
| | MBE | RMSE | MBE | RMSE | MBE | RMSE | |
| June | -3.4 | 29.4 | 6.4 | 22.3 | -2.3 | 27.4 | 0.270 |
| July | 3.4 | 34.6 | -1.8 | 25.7 | -0.7 | 22.2 | 0.569 |
| Aug. | -1.4 | 32.1 | 4.9 | 23.1 | -1.6 | 21.8 | 0.826 |
| Sept. | -5.2 | 26.7 | 6.4 | 22.5 | 0.3 | 17.6 | 0.898 |

(Ends on September 19)


Marantz, 1984       June 1 thaw depth = 0.11m.
                    Final observed thaw depth = 0.50m

| Month | QH | | QE | | Qg | | Final thaw |
|---|---|---|---|---|---|---|---|
| | MBE | RMSE | MBE | RMSE | MBE | RMSE | |
| June | -13.1 | 30.8 | 10.5 | 28.7 | 0.5 | 19.4 | 0.199 |
| July | -1.9 | 33.1 | 0.8 | 37.3 | 0.5 | 23.8 | 0.299 |
| Aug. | -2.7 | 30.4 | 1.9 | 34.5 | -0.5 | 20.9 | 0.348 |

(Ends on August 18)

Marantz, 1985       June 3 thaw depth = 0.10m.
                    Final observed thaw depth = 0.49m

| Month | QH | | QE | | Qg | | Final thaw |
|---|---|---|---|---|---|---|---|
| | MBE | RMSE | MBE | RMSE | MBE | RMSE | |
| June | -9.2 | 33.9 | 10.7 | 33.7 | -3.2 | 21.4 | 0.174 |
| July | 2.8 | 34.1 | -2.0 | 36.4 | -3.2 | 16.0 | 0.275 |
| Aug. | -1.1 | 28.7 | 2.8 | 30.9 | -1.6 | 13.9 | 0.309 |

(Ends on August 15)

the July 1985 values in table 5.5 are not the same as in table 5.4. The simulations presented in table 5.4 were initialized using observed data.

Since all $k_r$ values provided similar results for the original July 1985 simulations, only the results for $k_r=0.3$ are provided in table 5.5. This value was chosen for two reasons: it simply represents an intermediate value of $k_r$, and because it is also the value suggested by textbook thermal properties of peat.

In comparing the July 1985 errors from table 5.5 (seasonal simulation) to table 5.4 (monthly simulation), we see that there are some small differences. For the Churchill site, QH and Qg are slightly higher for the seasonal simulation, while QE is a bit lower. The change in thaw depth is less in the seasonal simulation, but this simulation starts will a shallower thaw depth (0.27m, from the June simulation) than the monthly simulation (0.35m). This shallower depth is in the high-water-content peat layer, so that 0.03m of peat must thaw before the 0° isotherm enters the clay. Therefore the thaw depths in the two simulations are not directly comparable.

For the Marantz site, the seasonal simulation has lower QH, higher Qg, and a similar value of QE. The change in thaw depth is similar, although the actual depths are deeper in the monthly simulation.

In looking at all months from the seasonal

simulations, we can see that the model generally does well. For the 1985 Churchill simulation, the size of the errors in the energy balance values tends to be similar for all months. The thaw depth is underestimated in June, and then lags behind the observed values (figure 3.4) for the rest of the summer. The 1984 simulation is somewhat worse, with larger errors in the energy balance values (especially July). The thaw depth is well-predicted at the end of June, but is overestimated in July and August.

For the Marantz site, the 1985 simulation shows higher errors in June, but good values in July and August. The 1984 simulation shows the same pattern. In both years, the thaw depth is significantly underestimated. The 1985 Qg values tend to be low, but the 1984 Qg values agree well with observations. It seems that for both the Churchill and Marantz sites, the model tends to underpredict the rate of thaw in the peat soils, where the latent heat requirement is large.

For the Marantz site, efforts were made to improve the agreement between the simulation and observations by adjusting the near surface soil profile. If the uppermost soil layers are given lower water contents and thermal conductivities, then the modelled soil heat flux and thaw depth are reduced. Conversely, increasing the values from those given in table 5.2 increases Qg and thaw depth. Tuning the model in this fashion may be justified in an effort to

Table 5.6: Daily simulations versus hourly simulations (daily averages). Churchill and Marantz sites 1985, $k_r$=0.3. Residuals calculated as (daily simulation – hourly simulation). Units are $W/m^2$, °C, and m.

Churchill

|      | QH   | QE   | Qg   | $T_s$ | $T_i$ | Thaw |
|------|------|------|------|------|------|------|
| MBE  | -5.1 | 5.0  | 0.1  | 0.31 | 0.44 | 0.01 |
| RMSE | 15.4 | 15.0 | 14.5 | 0.62 | 0.67 | 0.03 |

Marantz

|      | QH   | QE   | Qg   | $T_s$ | $T_i$ | Thaw |
|------|------|------|------|------|------|------|
| MBE  | -6.3 | 6.3  | 0.0  | 0.57 | 0.71 | 0.04 |
| RMSE | 13.0 | 14.3 | 7.9  | 0.82 | 0.94 | 0.05 |

---

improve prediction in some cases, but the purpose of this section is to assess the model's capabilities given independent measurements where available. Sensitivity of the model to these characteristics will be discussed in chapter 6.

### 5.2.3 - Daily Simulations

In order to assess the performance of the model with a daily time step, the 1985 simulations with $k_r$=0.3 were repeated. All initialization data were identical to the hourly simulations, except for the time step. The meterological data was averaged on a daily basis as well.

Table 5.6 compares the two simulations, using the daily averages from the hourly simulations as the base

values. The use of the same initialization parameters results in an under-estimation of QH and an over-estimation of QE. At the same time, Qg remains relatively constant, but both the surface temperature and evaporative surface temperature are raised slightly. Thaw depth remains fairly constant. (The constancy of thaw depth and Qg are related to the use of $k_r=0.3$, as will be seen in chapter 6.) Figures 5.7 and 5.8 show comparisons of daily values from the Churchill simulations. The scatter is evident on the energy balance graphs (figure 5.7), whereas the temperature graphs (5.8) show very good results.

The reason for the systematic shift from QH to QE in the daily simulation has to do with two factors. First, the evaporation modelling involves saturation vapour pressure, which is a non-linear function of temperature. When temperatures and vapour pressures are averaged on a daily basis, the correlation between the two is shifted. The second factor, which appears to dominate, is the characteristics of the resistance cycling algorithm. In the hourly simulations, the high daytime evaporation rates cause a significant increase in $r_s$, which limits the peak evaporation rates. At night, subsurface moisture reduces $r_s$ back towards its equilibrium value. In the daily simulation, the diurnal cycle of $r_s$ is lost. Overall, $r_s$ is lower, so QE is greater.
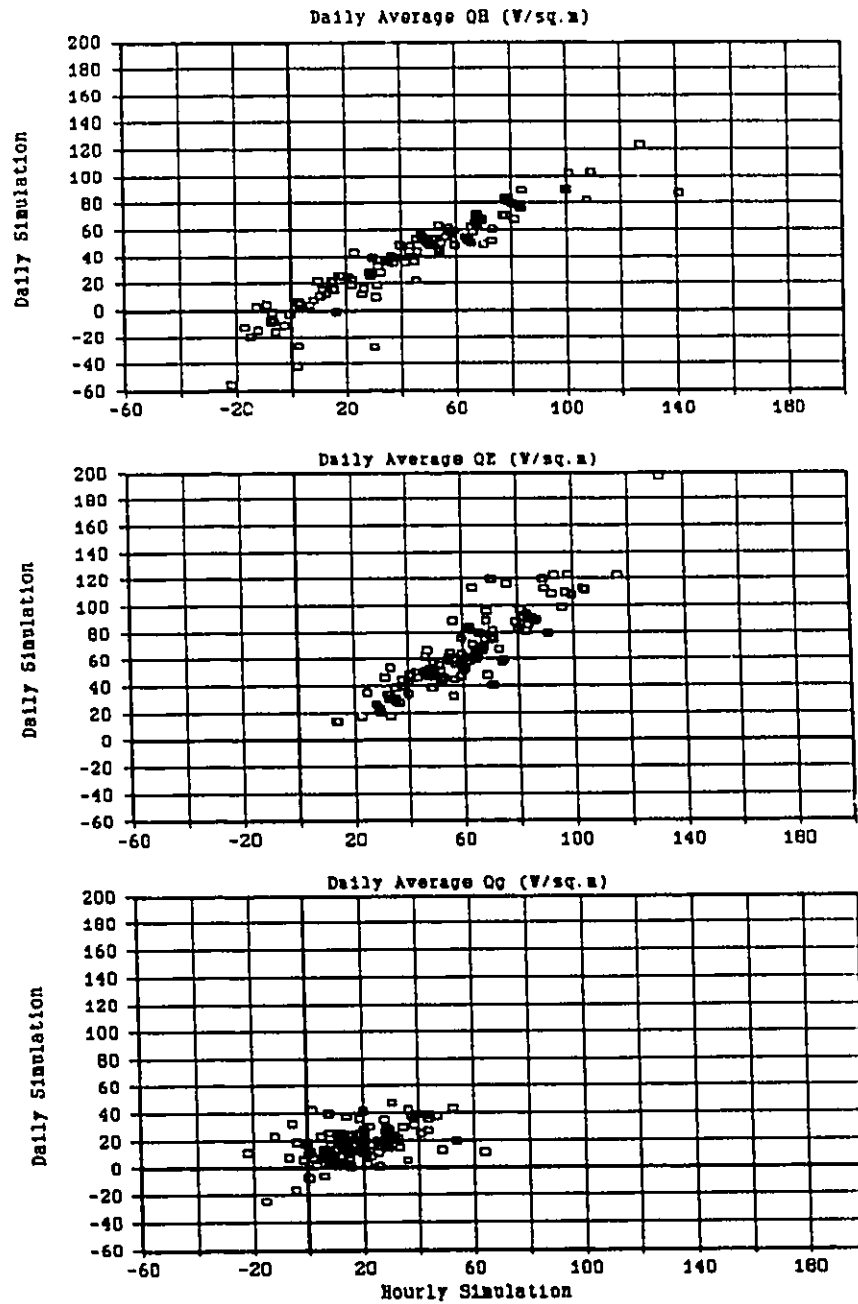
**Figure 5.7:** Comparison of daily mean energy balance values from hourly and daily simulations. Churchill Site, 1985. ($k_r$=0.3)
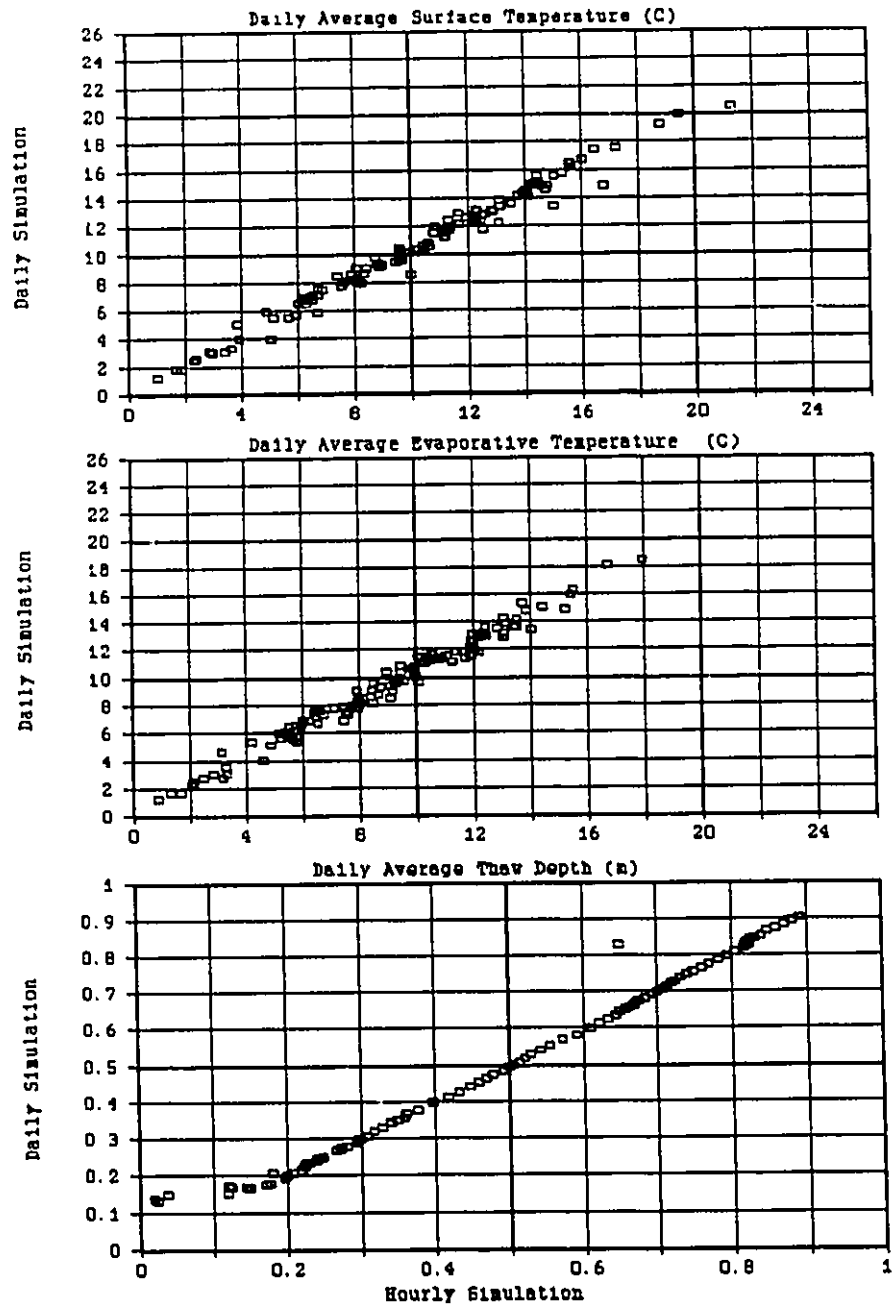
**Figure 5.8:** Comparison of daily mean $T_s$, $T_j$, and thaw depth for the simulations in figure 5.7.

Table 5.7: Resistance cycling coefficients for daily simulations.

Churchill:

| $k_r$ | $c_1$ (s/m$^2$) | $c_2$ (/m) | $c_3$ (/m) | $r_{smax}$ (s/m) | $\theta_v$ (initial) |
|---|---|---|---|---|---|
| 0.0 | 300,000 | 0.18 | 1.5 | 1050 | 0.87 |
| 0.3 | 300,000 | 0.18 | 1.5 | 700 | 0.87 |
| 0.6 | 300,000 | 0.18 | 1.5 | 550 | 0.87 |
| 1.1 | 300,000 | 0.18 | 1.5 | 400 | 0.87 |

Marantz:

| $k_r$ | $c_1$ (s/m$^2$) | $c_2$ (/m) | $c_3$ (/m) | $r_{smax}$ (s/m) | $\theta_v$ (initial) |
|---|---|---|---|---|---|
| 0.0 | 300,000 | 0.18 | 1.5 | 900 | 0.85 |
| 0.3 | 300,000 | 0.18 | 1.5 | 600 | 0.85 |
| 0.6 | 300,000 | 0.18 | 1.5 | 450 | 0.85 |
| 1.1 | 300,000 | 0.18 | 1.5 | 300 | 0.85 |

For this reason, it is apparent that a daily time step cannot be used with "hourly" resistance cycling coefficients. Separate "daily" coefficients were then determined, and the 1984 and 1985 seasons modelled again. Table 5.7 shows the resistance cycling coefficients for these simulations. Since $c_1$ and $c_2$ control the diurnal cycle, which is absent in the daily simulations, they have little effect and are the same for all values of $k_r$. The change from the hourly to daily coefficients must increase the calculated $r_s$ to reduce QE. In the Churchill coefficients, this was done by increasing $r_{smax}$. This leads to a larger value of $r_s$ given the same water content. In the

Table 5.8:   Error  values,  daily  model  simulations  for
             $k_r=0.3$.  (Thaw  values  are  actual  modelled  depth
             at end of simulation.) Values in $Wm^{-2}$ and m.

Churchill, 1985   June 1 thaw depth = 0.13m.
                  Final observed thaw depth = 0.95m

| Month | QH MBE | QH RMSE | QE MBE | QE RMSE | Qg MBE | Qg RMSE | Final thaw |
|-------|--------|---------|--------|---------|--------|---------|------------|
| June  | -3.8   | 16.1    | 7.1    | 15.9    | -3.2   | 10.6    | 0.252      |
| July  | 0.3    | 24.3    | 4.2    | 23.5    | 1.3    | 13.4    | 0.553      |
| Aug.  | -3.6   | 23.9    | 5.4    | 22.4    | 0.0    | 11.3    | 0.830      |
| Sept. | -6.0   | 13.3    | 6.1    | 10.6    | 1.3    | 8.0     | 0.903      |

(Ends on September 19)

Marantz, 1985   June 3 thaw depth = 0.10m.
                Final observed thaw depth = 0.49m

| Month | QH MBE | QH RMSE | QE MBE | QE RMSE | Qg MBE | Qg RMSE | Final thaw |
|-------|--------|---------|--------|---------|--------|---------|------------|
| June  | -9.3   | 18.8    | 8.3    | 18.1    | -0.8   | 11.5    | 0.167      |
| July  | -0.3   | 20.8    | -0.5   | 21.5    | -1.7   | 4.9     | 0.286      |
| Aug.  | -3.7   | 17.4    | 3.6    | 16.7    | 0.3    | 4.3     | 0.324      |

(Ends on August 15)

---------------------------------------------------------------

Marantz coefficients, $r_{smax}$ values have been increased less
than the Churchill ones, but the initial water content was
reduced slightly. This also tends to increase $r_s$, as the
different water content influences the entire simulation.

Table 5.8 provides the error statistics for the
daily simulations using "daily" coefficients for 1985, with
$k_r=0.3$. The MBE values are very comparable with the values
for the hourly simulations (table 5.5). The RMSE values are
somewhat lower than table 5.5, but table 5.7 is based on
daily rather than hourly means. If the RMSE is calculated on

a daily basis for the hourly simulations, then the daily simulations give higher RMSE values. On average, the daily simulations do as well as the hourly simulations, albeit with a slightly greater variance. Given the economy of calculation using a daily time step, the extra inaccuracy is small.

Figures 5.9, 5.10, and 5.11 show time plots and scatter diagrams from the Marantz 1985 daily simulation. The model results do follow the observed trends, but the differences are noticeable. The model appears to under-estimate day-to-day changes on some occasions, and over-estimate the changes on others. A comparison between these figures and those for the hourly simulations (figure 5.1-5.3) is difficult: the hourly graphs are smoother, and this makes it easier to identify similarities between modelled and observed patterns.

## 5.3 - Possible Model Improvements

At this point, it is worth conjecturing on how the model may be improved. Earlier, mention was given to the possibility of adjusting soil thermal properties, but this type of parameter adjustment does not represent an improvement of the model: it would only improve the fit of a given simulation.

The greatest uncertainty in the current model has to do with the surface resistance cycling. It appears that when
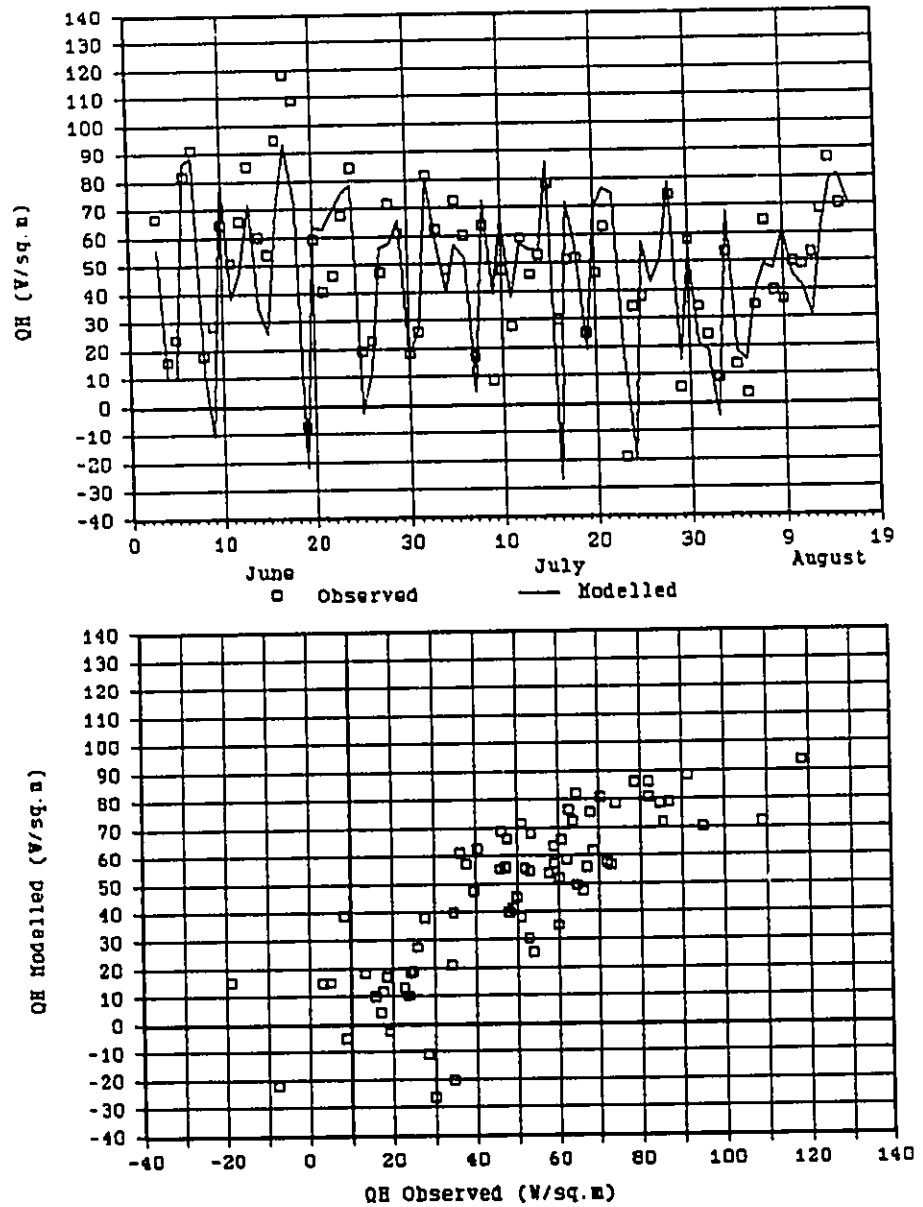
Figure 5.9: Comparison of modelled QH ($k_r=0.3$) to observed values. Marantz Site, 1985, daily simulation. Top: time series. Bottom: scatter diagram.
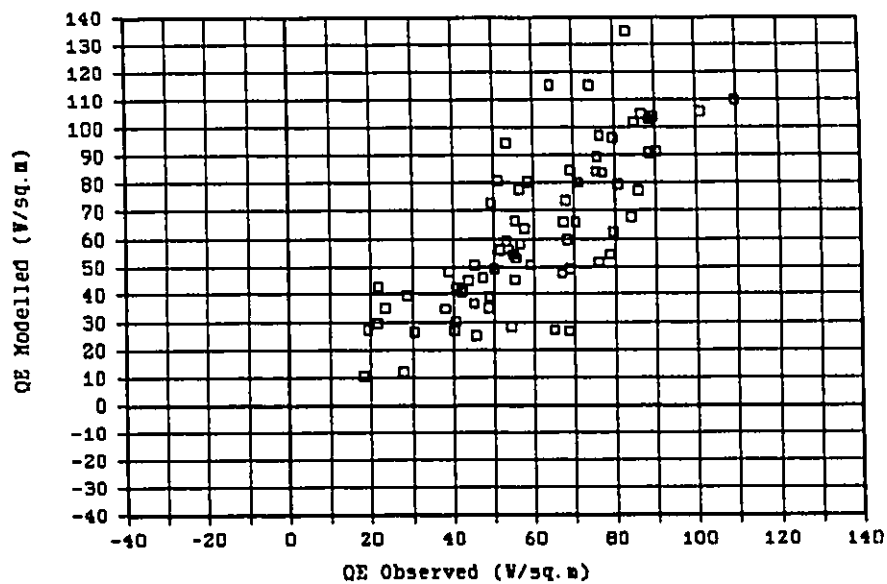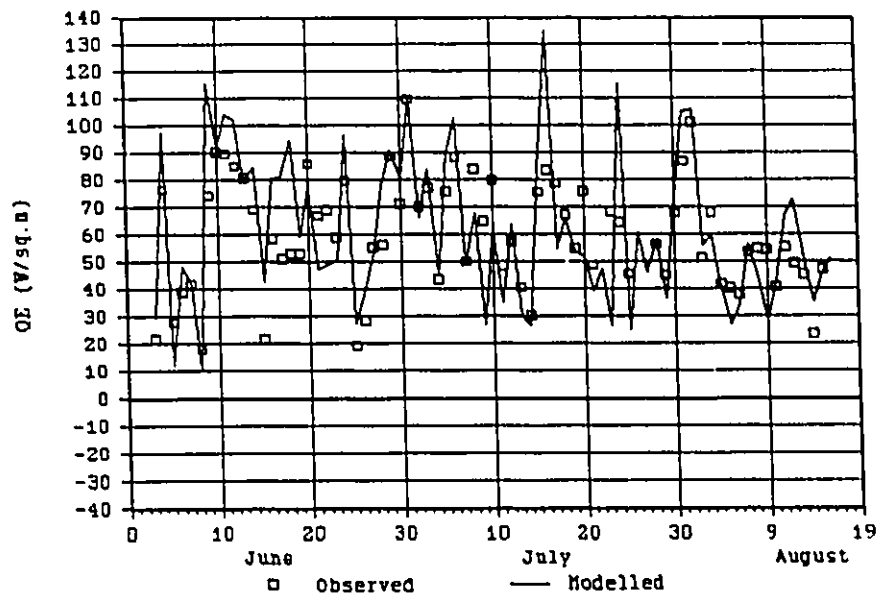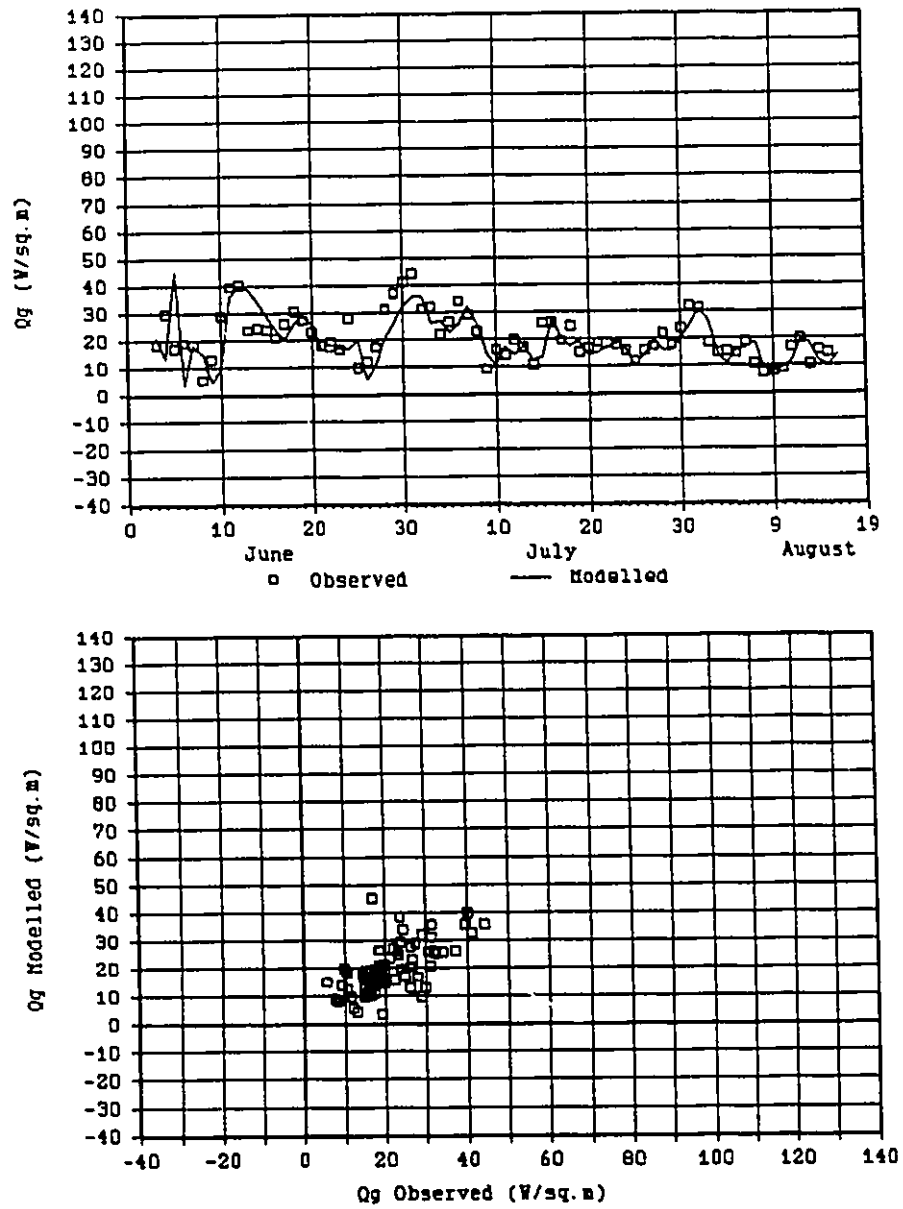
Figure 5.10: As for figure 5.9, for QE.

**Figure 5.11:** As for figures 5.9 and 5.10, for Qg.

the "correct" surface resistance is supplied to the model (i.e. the $r_s$ value that gives the correct QE) then the model will do well in estimating QH and Qg. The theoretical framework of the model appears sound. However, in spite of the resistance cycling scheme being based on a logical analysis of the physical processes involved, in practice it is essentially empirical. A great deal of the characteristics of the physical system are duplicated, but systematic variations remain.

It is tempting to try to improve upon the description of surface resistance. However, the results from the 1987 field measurement indicate a great deal of spatial variability in surface soil moisture and temperature. Temperature values were given in figure 3.10; moisture values are given in table 5.9. It is apparent that modelling this type of system in a one-dimensional model on a physical basis would be very difficult.

In the current model, the source of QH at the surface and the source of QE at the evaporation point within the soil are displaced vertically, whereas in the real world it is apparent that they will be displaced horizontally. A theoretical framework to incorporate this characteristic in a one-dimensional model is lacking. Attempts to improve the physical basis of the evaporation model would likely have to attack this problem, rather than refine the representation of an apparent one-dimensional resistance value.

Table 5.9: Vertical TDR Readings, 1987 site. Values are the range of volumetric water content, in %, measured at each location, and are the average over the indicated depth.

| Date | Location | 0-2.5cm | 0-5cm | 0-10cm |
|------|----------|---------|-------|--------|
| July 6 | Dry | 15-24 | 19-46 | 50-68 |
| | Mesic | 78-83 | 83-93 | 81-86 |
| | Wet | 83-100 | 69-98 | 79-88 |
| July 9 | Dry | 24-37 | 37-55 | 47-70 |
| | Mesic | 69-92 | 84-90 | 86-90 |
| | Wet | 69-100 | 74-95 | 82-93 |
| July 24 | Dry | 19-30 | 37-54 | 60-67 |
| | Mesic | 74-97 | 81-88 | 76-89 |
| | Wet | 45-75 | 74-88 | 73-87 |
| July 29 | Dry | 17-34 | 28-44 | 44-54 |
| | Mesic | 40-86 | 72-82 | 54-79 |
| | Wet | 30-68 | 78-84 | 80-83 |
| Aug 2 | Dry | 21-29 | 30-45 | 43-71 |
| | Mesic | 68-74 | 72-82 | 44-82 |
| | Wet | 41-70 | 57-77 | 62-80 |
| Aug 9 | Dry | 28-35 | 31-40 | 49-62 |
| | Mesic | 69-85 | 71-81 | 59-76 |
| | Wet | 37-82 | 49-77 | 73-79 |
| Aug 16 | Dry | 28-39 | 34-45 | 58-67 |
| | Mesic | 60-85 | 69-85 | 71-82 |
| | Wet | 52-69 | 67-81 | 67-73 |

NOTE: The water contents are based on calibration of the peat samples from the 1985 sites (Churchill and Marantz).

In spite of this criticism, the characteristics of the one-dimensional model should be valid on a very local scale, so that experimentation with the model is appropriate. In chapter 6, the effects of varying surface moisture will be examined.

Before moving on to the sensitivity analysis of the model, the 1987 temperature data can be used to examine the spatial variability we might expect in QH and QE. Briefly, if we assume that Q*-Qg is constant, then any vertical divergence in QH would be offset by divergence in QE, and local advection would occur. The horizontal energy flux could be calculated at any height if the horizontal temperature or vapour pressure gradient was known along with the wind speed. Unfortunately, the 1987 values only provide surface temperatures - at which point wind speed is zero- and air temperatures at a single location above 0.5m, where the horizontal temperature gradient is assumed to be negligible. However, an alternate approach is possible using the surface and air temperature values.

Equation 4.1a gives QH as a function of the surface-air temperature difference. Using this equation with the observed values of surface and air temperature provides an estimate of the variation in QH, which is equivalent to the quantity of energy which must be advected from dry to wet locations. If $\rho$ , $c_p$, and $r_a$ do not vary spatially, then the ratio of QH(dry) to QH(wet) is the same as the ratio of the

temperature differences.

Taking one example from the 1987 data, on July 14 for the 10-minute period ending at 13:30, we have $T_a$=22.65°, and $T_s$=40.04° at the warmest and 27.94° at the coolest location. The vertical temperature differences are 17.39° and 5.29° respectively, for a ratio of 3.29. Measured wind speed was 1.7m/s, and estimated $z_0$ is 0.02m. Measured QH over the hour ending at 14:00 was 170Wm$^{-2}$. This would correspond to a surface temperature of about 28.7° and $r_a$ of 42s/m. The value of QH calculated for the wet location would be 150Wm$^{-2}$, and the dry location would be 494Wm$^{-2}$.

In fact, equation 4.1a was derived assuming that QH is constant with height, so it is not valid for this calculation. However, the effect of flux divergence on the temperature profiles would be to increase the gradient at the surface over the dry location and decrease it at the wet location. Thus the values just calculated represent the minimum difference between the two locations. This confirms that the spatial variability in QH and QE is very high. The difference is large enough that the assumptions of constant Q*-Qg and $r_a$ may also be invalid. The fact that the mean measured QH is closer to the "wet" QH value suggests that wet areas cover more of the surface than dry areas on this particular day.

## Chapter 6: Model Sensitivity to Moisture Variations

In this chapter I will examine the model response to changes in moisture content. As was shown in chapter 5, changes in soil thermal properties in the model lead to changes in soil heat flux and thaw depth at the Marantz site. However, changes of this type influence the internal nodes of the thermal grid in the model. The purpose of this chapter is to examine the effects on the surface boundary conditions, without changing the soil thermal properties. Other authors - e.g. Goodrich (1978), Smith (1984), Smith and Riseborough (1983, 1985) - have examined the sensitivity of similar numerical models in this respect and their work will not be duplicated here.

In the present work, the most radical departure from previous models is in the evaporation component. As mentioned in chapter 4, Novak and Black (1985) use equation 4.3, which is equivalent to the one used in the present study (equation 4.4) for the case of no thermal resistance. The models described by Outcalt et al (1975) and Smith (1975, 1977) use relatively simple methods which can be derived from Novak and Black's evaporation model. Therefore, all these previous works use evaporation models which represent one specific case of the model used here. The

present work includes a more rigorous description of the surface evaporation process, without incorporating separate vapour diffusion terms in the entire soil column, as is done by van Bavel and Hillel (1976) and Outcalt and Nelson (1985).

The sensitivity analysis will seek to determine the influence of using the more detailed evaporation model. The analysis will assess the differences in model response under varying evaporation rates for the possible range of $k_r$ values.

### 6.1 - Methods

The evaporation model uses several parameters and variables. Changing evaporation rates in the model could be accomplished by any one of several methods, such as changing the cycling coefficients, changing the limits for $r_s$ or water content ($\theta_v$), changing the initial value of $\theta_v$, or changing the atmospheric conditions. Since the cycling coefficients and maximum $r_s$ should be properties of the surface, and the atmospheric conditions are a complex function of local and regional conditions, changes in these values would introduce complexities in the analysis. The simplest and most reasonable variable to change is the initial value of $\theta_v$. This is easily interpreted in terms of the natural field conditions, where the 1987 data indicated wide variations in surface soil moisture over short

distances. The nature of the resistance cycling algorithm is such that a change in initial $\theta_v$ will have a continuous influence for the duration of the simulation.

In the sensitivity analysis, the moisture conditions ranged from saturated to extremely dry. All but the saturated simulations used the same coefficients as were used in the comparisons with field data. The saturated simulation also had the resistance cycling coefficients changed to maintain a saturated surface, by eliminating the changes in $r_s$ due to evaporation or precipitation. Each simulation spanned the period from the start of June to the end of the field season.

For each value of $k_r$ (0.0, 0.3, 0.6, and 1.1), five simulations were performed: saturated ($r_s$=0.0 at all times), normal (as used in the model evaluation, giving the best fit to observed conditions), dry (initial $\theta_v$ 0.1 less than normal), very dry ($\theta_v$ 0.3 less than normal), and extremely dry ($\theta_v$ 0.5 less). The "normal" conditions always started within 0.02 of saturation, so the lowest initial water content was 0.35. Although this may not seem dry, at this water content the simulations exhibited very low evaporation rates.

## 6.2 - Results

The simulations were compared on the basis of the mean seasonal energy balance values (QH, QE, and Qg), the surface

temperature, evaporative surface temperature, and thaw depth
at the end of the simulation. For each value of $k_r$, the same
change in initial water content led to similar changes in
QH, QE, and $T_s$. The differences were in Qg, $T_i$, and thaw
depth. Since the surface temperature is the factor which
links the energy balance and soil thermal regime together,
it will be treated as the independent variable in examining
the differences between simulations.

### 6.2.1 - Hourly Simulations

The first set of simulations used the Churchill 1985
data, with an hourly time step. Figure 6.1 shows the model
response for QH, QE, and Qg. All $k_r$ values give the same
results for saturated conditions (lowest surface
temperature) since the surface vapour and thermal
resistances are continuously zero. As the initial soil
moisture decreases, surface temperature increases in a
similar fashion for all $k_r$. QH and QE show the same trend
for all $k_r$ values, with a continuous shift of energy from QE
to QH as surface temperature increases. The results cover a
range of conditions from QH<0 for saturated conditions to QE
approaching zero for extremely dry conditions.

Qg does not show the same sensitivity to soil moisture
for all values of $k_r$. For $k_r=0$, the trend is a consistent
increase in Qg as $T_s$ increases. At the other extreme, for
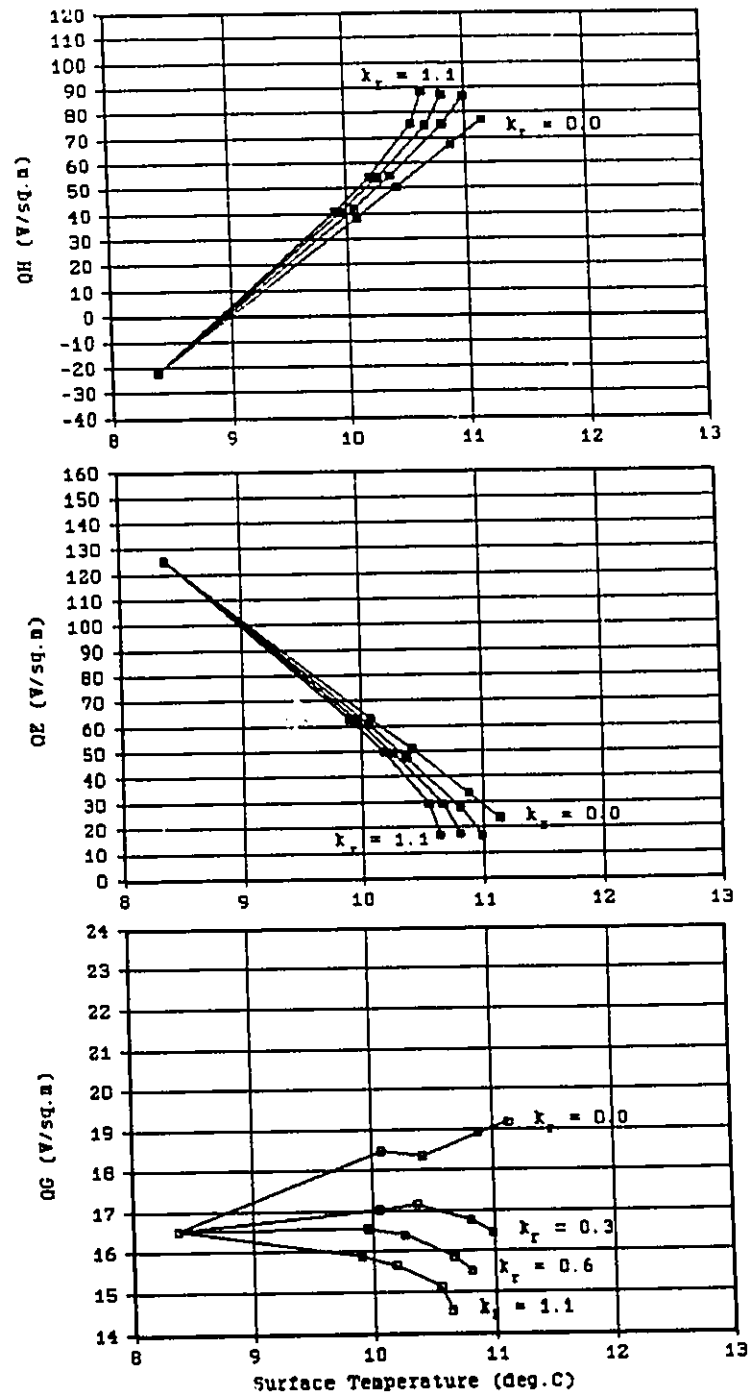$k_r=1.1$, Qg decreases as $T_s$ increases. For intermediate $k_r$

**Figure 6.1:** Energy balance response to soil moisture sensitivity analysis, Churchill Site 1985, hourly simulation.
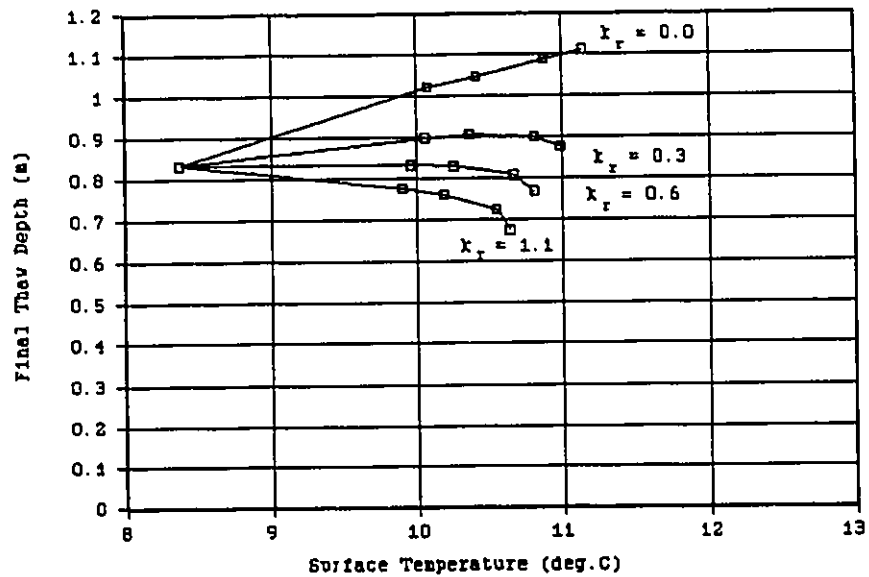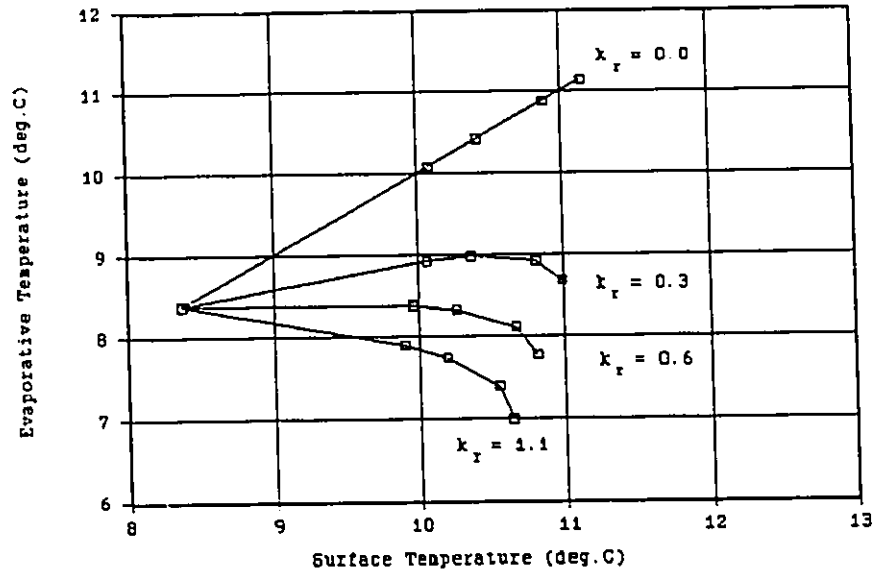
**Figure 6.2:** Evaporative temperature and thaw depth response to soil moisture sensitivity analysis, Churchill Site 1985, hourly simulation.

values, $Qg$ increases slightly or remains constant, then decreases as soil moisture decreases.

The reason for this can be seen in figure 6.2a, where evaporative surface temperature is plotted against surface temperature. For $k_r=0$, $T_i=T_s$ so the line is a 1:1 relation. However, for $k_r>0$, $T_i<T_s$, and as soil moisture decreases the difference between the two increases. For $k_r=1.1$, $T_i$ is always decreasing as soil moisture decreases. For intermediate $k_r$ values, the effect is the same as for $Qg$. Figure 6.2b shows the various thaw depths at the end of the simulations, illustrating the same pattern.

This series of simulations illustrates the importance of $k_r$ in the behaviour of the model. For intermediate values, the sensitivity depends on the range of water content examined. At extreme values of $k_r$, the directions of sensitivity are opposite. Interestingly, at $k_r=0.3$, the subsurface temperatures and thaw depth are nearly independent of the surface moisture conditions. The partitioning of energy between QH and QE has little influence on soil temperature. In verifying the model performance (chapter 5), the use of $k_r=0.3$ means that the model would predict much the same soil temperatures and thaw depths even if it did poorly with QH and QE! Therefore any errors in soil temperature or thaw depth in this portion of the model are due to errors in thermal characteristics of the soil (or an inappropriate $k_r$ value!).

### 6.2.2 - Daily Simulations

The sensitivity analysis using the Churchill 1985 data was also carried out with a daily time step. The results of this analysis are given in figures 6.3 and 6.4. Overall, the changes in surface temperature and energy balance are close to the changes in the hourly simulations. QH and QE show almost identical patterns, while $T_i$ and thaw depth are very similar. Qg shows some differences, including an unusually high value for the driest simulation using $k_r=1.1$.[1]

Sensitivity analyses of the model using Marantz data and Churchill 1984 data were also carried out with a daily time step. All demonstrate the same sensitivity as the Churchill 1985 results, indicating that the results are not due to the characteristics of the Churchill site, or the 1985 meteorological data. The Marantz 1984 results are given in figures 6.5 and 6.6.

---

[1]This odd value appears to be the result of problems estimating Qg in the equilibrium surface temperature procedure, for high thermal resistances at low water contents. The mean value has been unduly influenced by one or two days with irregular Qg values in the simulation. The Qg value shown is the estimation from the energy balance, rather than a value from the soil thermal model, and the approximation appears to break down in this case. It is caused by rapid changes in surface temperature from day-to-day, combined with a fine thermal grid in the model. The hourly simulation does not have this problem because changes are more gradual.

Figure 6.3: Energy balance response to soil moisture sensitivity analysis, Churchill Site 1985, daily simulation.

**Figure 6.4:** Evaporative temperature and thaw depth response to soil moisture sensitivity analysis, Churchill Site 1985, daily simulation.
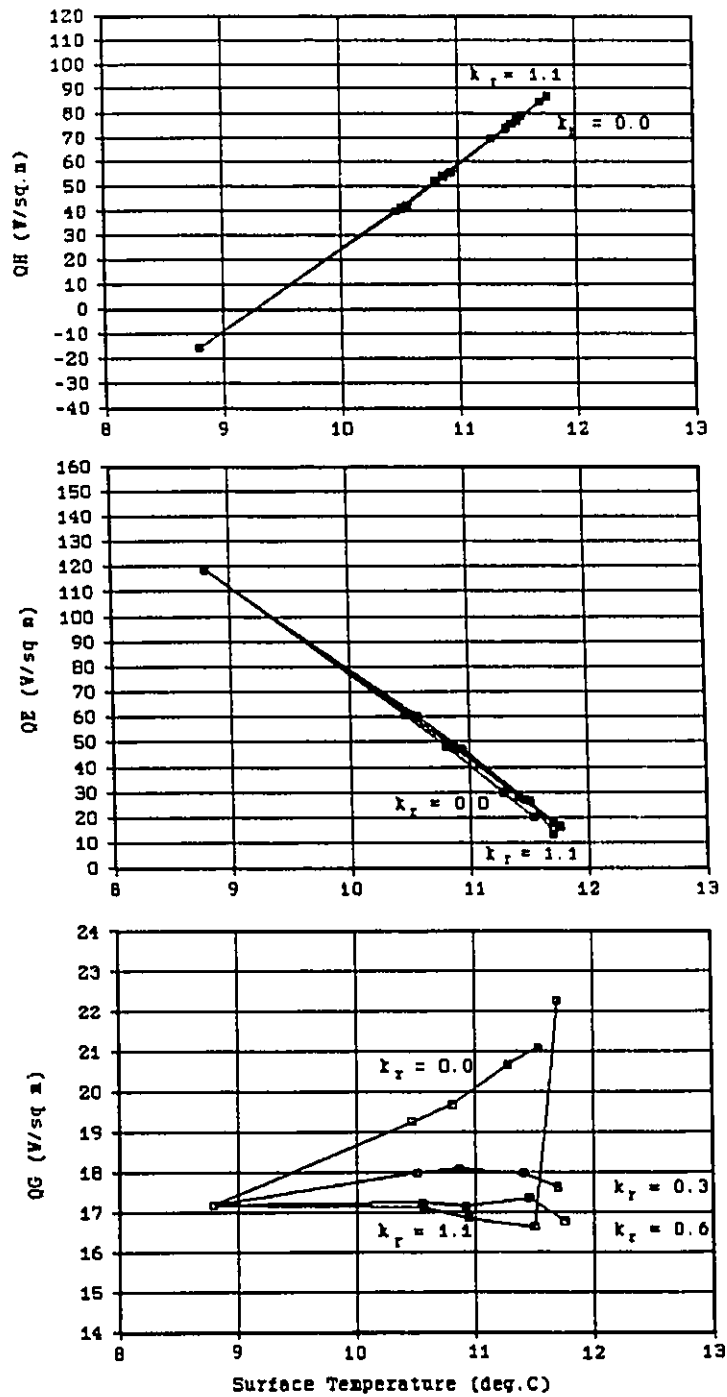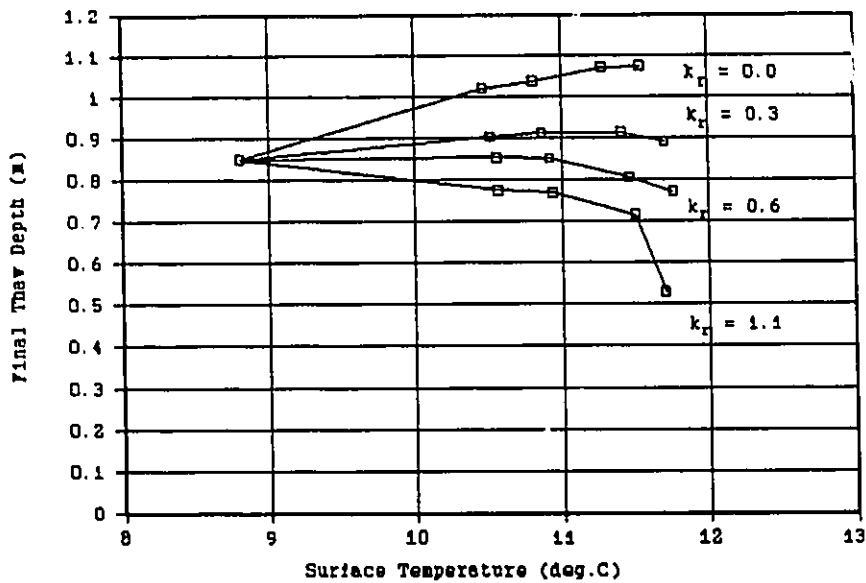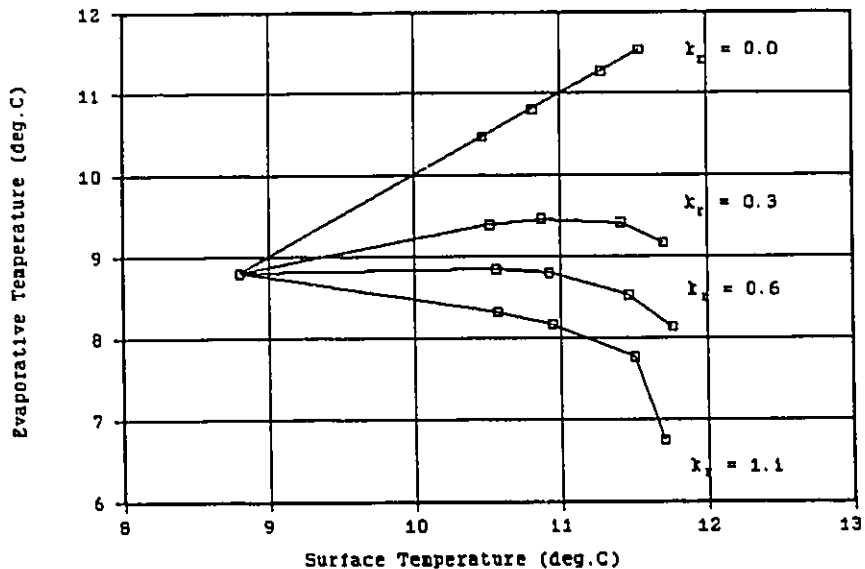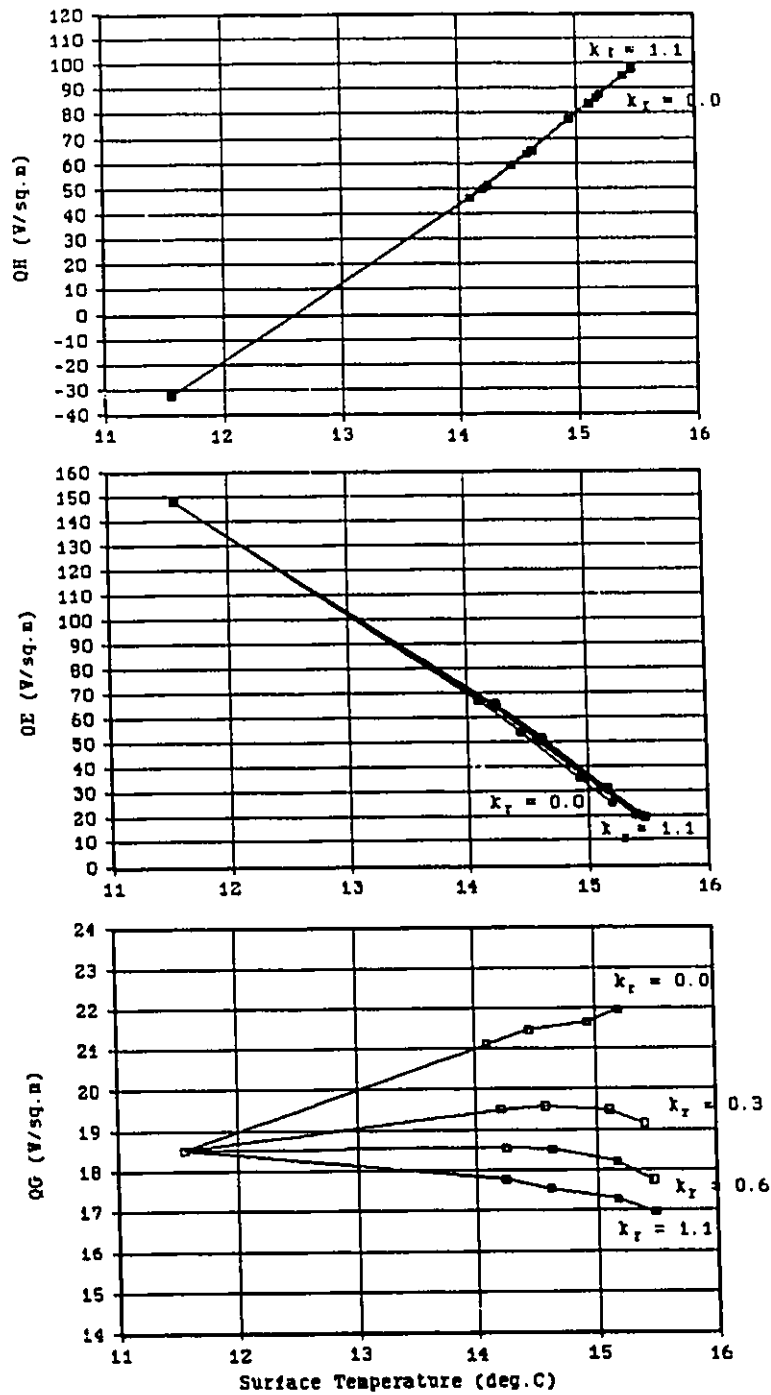
**Figure 6.5:** Energy balance response to soil moisture sensitivity analysis, Marantz Site 1984, daily simulation.
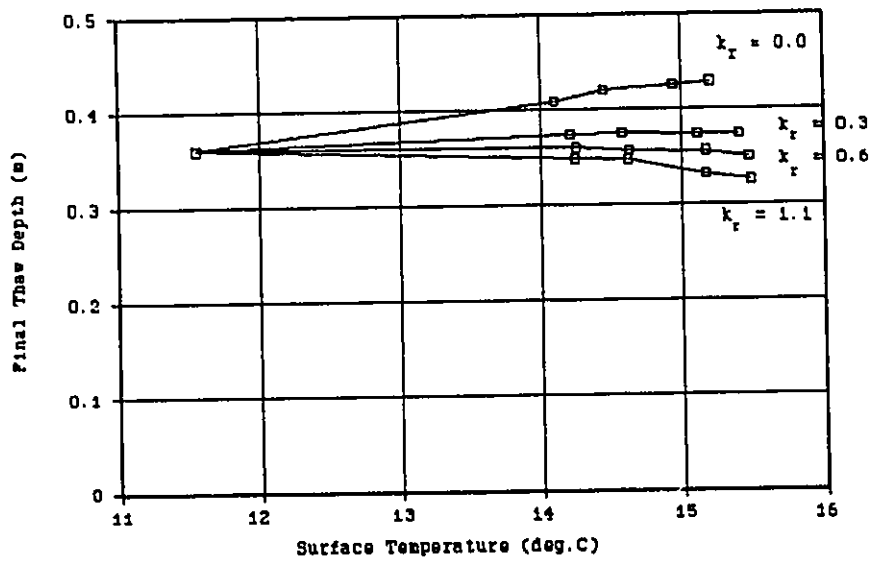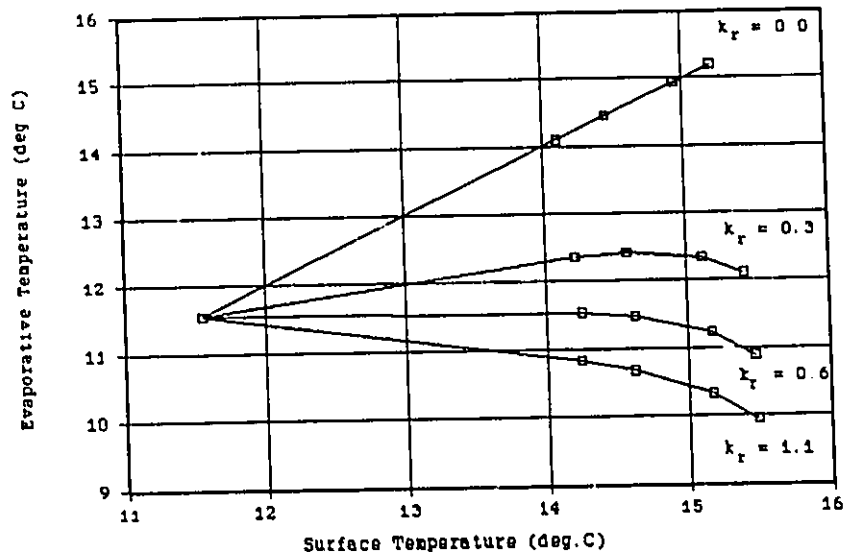
**Figure 6.6:** Evaporative temperature and thaw depth response to soil moisture sensitivity analysis, Marantz Site 1984, daily simulation.

6.3 - Discussion

The results presented in section 6.2 indicate that the value of $k_r$ is critical in the response of the model. When a thermal resistance exists, the direction of sensitivity is reversed. This is consistent with two field observation at the Churchill Site: greater thaw depths in 1985 (cool, wet) than 1984 (warm, dry); and greater thaw depths at the thermocouple rod location (wet) than at the thermistor rod (dry). The Marantz Site shows little difference in thaw depth between the two years, in spite of differences in the partitioning between QH and QE. If the model is to be believed, then this suggests that a thermal resistance could be playing an important role at these two sites. Riseborough (1985) also observed a lack of variation in sub-surface temperatures in response to variations in surface moisture at sites with organic surface covers near Mayo, Yukon Territory.

Previous model sensitivity studies have indicated that soil temperature shows a strong dependence on evaporation rate. Using the Smith (1977) model, Smith and Riseborough (1983) showed that changes in evaporation rate from 0 to potential (i.e. a saturated surface) led to a reduction in mean annual surface temperature of 10.2°C. This was the most sensitive parameter in the model. (The analysis included the type of surface cover, surface roughness $(z_0)$, albedo, wetness, slope and slope aspect, and snow cover.)

The model presented here shows a shift in surface temperature of nearly 3° for the change from low evaporation to potential evaporation. This is less than the Smith and Riseborough (1983) result because their value represents an equilibrium value, after ground temperatures stabilize over a period of years. The model results presented here are a transient response over one summer season, with all simulations starting at the same temperature. Since the difference between simulations is 0° at the start, it must approach 6° at the end for the averages to differ by 3°. Warming would continue from summer to summer, until the mean annual Qg value becomes zero, further increasing the difference.

Applying the seasonal sensitivity of this model to annual periods is not unreasonable. In the winter season, temperatures would reduce evaporation to very low rates, and snow cover would eliminate any soil surface control on the evaporation process. All of the influence of the evaporation characteristics will be felt during the summer months. In extrapolating summer warming to annual mean temperatures, one would have to weight the changes according to the length of season. Since little sensitivity in winter temperatures would be expected, the change in mean annual temperature would be less than the summer change alone.

## Chapter 7: Summary and Conclusions

The stated purpose of this thesis was four-fold: the description of the microclimatic and ground thermal regimes, development of the model, use of the model for interpretation, and assessment of the modelling approach for predictive purposes. This chapter summarizes and discusses the thesis in this light.

The database accumulated during the field portions of the study represents a significant accomplishment in itself. The data set is detailed, comprising hourly measurements of meteorological and soil conditions on an almost continuous basis for two summers. The time period included covers almost the entire summer thaw period at Churchill. The concurrent collection of climatic data and soil thermal and moisture regimes facilitates the modelling effort. The completeness of the data set encourages confidence in any interpretation of the descriptive values.

At a technical level, part of the confidence in the data is the result of innovations in analysis of the data: the assessment of the accuracy of the soil heat flux plates, and the analytical method combining the Bowen ratio and aerodynamic methods of evaluating the turbulent energy exchanges. These methods were discussed fully in Chapter 2.

Chapter 3 provided a summary of the field

observations. Of particular interest are the observations of high soil moisture just below the surface at the same time that the surface appears quite dry, and the very large variability in surface soil moisture and surface temperature at the 1987 site. The variability in surface temperature had not been anticipated prior to the 1984 and 1985 field seasons, so detailed measurements were not made at the Churchill and Marantz sites.

Chapter 4 presents the development of the numerical model. This model is very similar to the models of Outcalt et al (1975) and Smith (1975, 1977), except for the detail of the evaporation modelling. Outcalt et al (1975) and Smith (1975, 1977) used very simple evaporation models, whereas this study uses a much more detailed parameterization of the surface evaporation layer. The inclusion of a thermal resistance, suggested by the field observations of temperature gradients and thermal properties of the soils, constitutes a radical alteration of the evaporation model. Since evaporation is one of the most dominant and variable factors in the surface energy balance, changes in the evaporation model are important.

Chapter 5 illustrated the ability of the model to emulate the observed characteristics of the field sites. In general, the model behaves in a manner consistent with observations. Systematic variations in energy balance partitioning do occur, and appear to be related to

inadequacies of the evaporative resistance cycling. Although the behaviour of the resistance cycling parameters can be explained in physical terms, they remain an empirical approximation. The data from the 1987 site indicated a wide variation in surface temperature over horizontal distances of only a few metres. This variation must be coincident with variations in the sensible and latent heat fluxes. In view of this, there remains a question regarding the validity of using a one dimensional model over this type of surface.

In chapter 6, the sensitivity of the model to variations in soil moisture was examined. The purpose of this was to examine the effects of the new evaporative model. If no thermal resistance was used, the model showed subsurface warming in response to decreased soil moisture and evaporation, consistent with the sensitivity reported by Smith and Riseborough (1983). When an intermediate thermal resistance was incorporated, the soil warming was eliminated. At high thermal resistance values, the effect was reversed: although the reduced evaporation led to higher surface temperatures, the evaporative surface temperature at the base of the resistance layer decreased, yielding cooler subsurface temperatures and less thaw.

The results of this sensitivity analysis are very important. In using models for the purpose of prediction, the first hope is that the model will get the sign of the change correct. Refinements to the model will then improve

the ability to predict the quantity of the change. The sensitivity analysis states that we cannot predict the sign of the change unless we know the relative importance of the thermal and vapour resistances of the surface layer. Outcalt and Nelson (1985) conclude that internal evaporation can retard soil warming. This is an area which requires further research.

The surface layer is actually a very complex layer. In porous materials such as peat, penetration of solar radiation into the surface may be important, in addition to the characteristics of thermal conduction, and thermal and vapour diffusion. This study has pointed out the importance of the thermal properties of this layer, which likely extends only a few millimetres below the surface. Previous discussions of the thermal effects of peat have considered much greater thicknesses, where moisture conditions vary seasonally rather than hourly or daily. These descriptive works have not recognized the possible influence on the evaporative regime.

The sensitivity analysis also demonstrates that previous models in the literature which ignore thermal resistance in the evaporation process may mislead us in their predicted response to climate change. Kellogg and Zhao (1988) examined the sensitivity of soil moisture in North America to doubling of $CO_2$ in five Global Circulation Models (GCMs). The GCMs generally showed decreased summer soil

moisture over most of the arctic and subarctic regions. (Winter changes were predicted less consistently.) In considering the effect on permafrost conditions, the changes in soil moisture could either augment or reduce the effect of increasing atmospheric temperature.

Similar arguments could be made regarding predictions associated with construction projects in the arctic. Changes in surface hydrology could lead to changes in surface soil moisture which may have an important effect. Depending on the characteristics of the surface, increased soil moisture could lead to either increased or decreased sub-surface temperatures.

On a final note, it is recommended that further research look in greater detail at the properties of the surface layer. However, it may not be worth pursuing this to any great degree unless it can be demonstrated that a one-dimensional approach is appropriate. The concept of surface thermal and vapour resistances in a surface layer applies to an homogeneous surface. The 1987 field observations demonstrate that peat surfaces are far from homogeneous. Changes in energy balance values and ground temperatures resulting from soil moisture changes may be completely different in reality from changes predicted in a one-dimensional model. There is a need to model the system on a two- or three- dimensional basis, to see how (or if) these effects can be incorporated into a one-dimensional model.

## Appendix I - Nomenclature

a,b,c   -    parameters for unfrozen water content vs. temperature relationship.

C   -    volumetric heat Capacity $(MJ/m^3C\cdot)$.

$C_1$, $C_2$, $C_3$ - resistance cycling coefficients $(s/m^2,/m,/m)$

$c_p$   -    specific heat of air at constant pressure (= 1010 J/kgK)

$c_s$   -    volumetric heat capacity of soil solids

C'   -    apparent volumetric heat capacity.

d   -    deviation or difference between values measured by two methods

e   -    vapour pressure (kPa), or base of natural logarithms.

$e_a$   -    air vapour pressure

$e_s$   -    surface vapour pressure

E   -    evaporation (m or m/s)

$e*(T)$   -    saturation vapour pressure at T (kPa)

g   -    acceleration due to gravity (= 9.8 $m/s^2$)

H   -    soil enthalpy $(MJ/m^3)$.

k   -    von Karman's constant (= 0.4)

$K\downarrow,K\uparrow,K*$ - incoming, outgoing, net shortwave radiation $(W/m^2)$

$k_r$   -    ratio between surface thermal and vapour resistances. (dimensionless)

$K_h$, $K_m$, $K_w$ - turbulent transfer coefficients for heat, momentum, and water vapour $(m^2/s)$

187

L       -     Monin-Obukhov stability length $(= \dfrac{u_*^3 \, \rho \, c_p T}{k \, g \, QH})$ (m)

L↓,L↑,L* -    incoming, outgoing, net longwave radiation $(W/m^2)$

$L_v$      -     latent heat of vaporization of water   (J/kg)

MBE     -     mean bias error

p       -     atmospheric pressure (kPa)

P       -     precipitation (m or m/s)

Q       -     turbulent flux density (generic)   $(W/m^2)$

QE      -     latent heat flux density   $(W/m^2)$

Qg      -     soil heat flux density   $(W/m^2)$

QH      -     sensible heat flux density   $(W/m^2)$

Q*      -     net all-wave surface irradiance   $(W/m^2)$

r       -     correlation coefficient (dimensionless)

Ri      -     gradient Richardson number   $(= \dfrac{g \; (dT/dz)}{T \; (du/dz)^2})$
              (dimensionless)

RMSE    -     root mean square error

$r_a$      -     aerodynamic resistance (s/m)

$r_s$      -     surface vapour resistance (s/m)

$r_{smax}$   -     maximum value for $r_s$

SE      -     correlation standard error

t       -     time (seconds).

T       -     temperature (°C).

$T_a$      -     air temperature

$T_i$      -     temperature at source of evaporation within soil

$T_s$      -     surface temperature

u — mean wind speed (m/s)

$u_*$ — friction velocity (m/s)

VPD — vapour pressure deficit, $= e^*(T)-e$ (kPa)

$X_s$ — volume fraction of soil solids.

z — height or depth (m).

$z_0$ — surface roughness length (m)

$\beta$ — Bowen ratio, $= QH/QE$ (dimensionless)

$\Delta$ — difference operator in numerical methods

$\varepsilon$ — surface emissivity (dimensionless)

$\gamma$ — psychrometer constant $\left(= \dfrac{p\, c_p}{0.622\, L_v}\right)$ (kPa/K)

$\lambda, \lambda_t, \lambda_f$ — thermal conductivity (thawed, frozen) (W/mC°).

$\varnothing_h, \varnothing_m, \varnothing_w$ — dimensionless stability functions for transfer of heat, momentum, and water vapour.

$\rho$ — density of air (kg/m$^3$)

$\sigma$ — standard deviation, or Stefan-Boltzman constant.

$\theta_v$ — water content (volume fraction).

$\theta_{uf}$ — unfrozen water content at sub-zero temperature.

$\tau$ — momentum flux density (N/m$^2$)

# References

Alados-Arboledas, L., J. Vida, and J.I. Jimenez (1988) "Effects of solar radiation on the performance of pyrgeometers with silicon domes" <u>J. Atmos. Ocean. Tech.</u> <u>5</u>, 666-670.

Baker, T.H.W. and L.E. Goodrich (1984). "A probe for measuring both thermal conductivity and water content of soils." <u>Proc. 3rd Intl. Cold Regions Engineering Specialty Conf. Vol.2,</u> (sponsored by ASCE), 835.

Bonacina, C. and G. Comini (1971) "On a numerical method for the solution of the unsteady heat conduction equation with temperature dependent parameters", <u>IIR, XIII Int. Congr. of Refrig., 2-28,</u> Washington

Bonacina, C., G. Comini, A. Fasano, and M. Primicerio (1973) "Numerical solution of phase-change problems", <u>Int. J. Heat Mass Transfer 16,</u> 1825-1832.

Brown, R.J.E. (1978) "Influence of climate and terrain on ground temperatures in the continuous permafrost zone of northern Manitoba and Keewatin District, Canada", in <u>Proc. 3rd Intl. Conf. on Permafrost, Vol. 1,</u> Nat. Res. Council Canada, Ottawa, Ont., 16-21.

Brown, R.J.E. and T.L. Péwé (1973) "Distribution of permafrost in North America and its relationship to the environment: a review, 1963-1973", in <u>North American Contribution, Permafrost: Second International Conference,</u> National Academy of Sciences, Washington, 71-100.

Brown, R.J.E. and G.P. Williams (1972) <u>The Freezing of Peatland,</u> NRCC DBR Tech. Paper 381, Ottawa.

Carslaw, H.S. and J.C. Jaeger (1959) <u>Conduction of Heat in Solids,</u> Oxford University Press, Oxford, 510pp.

Choudhury, B.J. and J.L. Monteith (1988) "A four-layer model for the heat budget of homogeneous land surfaces", <u>Q. J. Roy. Met. Soc. 114,</u> 373-398.

Comini, G., S. Del Guidice, R.L. Lewis, and O.C. Zienkiewicz (1974). "Finite element solution of non-linear heat conduction problems with special reference to phase change." <u>Intl. J. for Numer. Methods in Eng. 8,</u> 613.

Davies, J.A. and C.D. Allen (1973) " Equilibrium, potential and actual evaporation from cropped surfaces in southern Ontario", J. Appl. Met. 12, 649-657.

Davies, J.A., M. Abdel-Wahab, and D.C. Mackay (1984) "Estimating Solar Irradiation on Horizontal Surfaces", Int. J. Solar Energy 2, 405-424.

de Bruin, H.A.R. and A.A.M. Holtslag (1982) "A simple parameterization of the surface fluxes of sensible and latent heat during daytime compared with the Penman-Monteith Concept", J. Appl. Met. 21, 1610-1621.

Deardorff, J.W. (1977) "A parameterization of ground-surface moisture content for use in atmospheric prediction models", J. Appl. Met. 16, 1182-1185.

Dyer, A.J. (1974) "A review of flux-profile relationships", Boundary-Layer Met. 7, 363-372.

Enz, J.W., J.C. Klink, and D.G. Baker (1975) "Solar radiation effects on pyrgeometer performance", J. Appl. Met. 14, 1297-1302.

Fritschen, L.J. and L.W. Gay (1979). Environmental Instrumentation, Springer-Verlag, New York.

Fuchs, M. and C.B. Tanner (1967) "Evaporation from a drying soil", J. Appl. Met. 6, 852-857.

Fuchs, M. and C.B. Tanner (1970) "Error Analysis of Bowen Ratios Measured by Differential Psychrometry", Agricultural Met. 7, 329-334

Goodrich, L.E. (1978) "Efficient numerical technique for one-dimensional thermal problems with phase change", Int. J. Heat Mass Transfer 21, 615-621.

Goodrich, L.E. (1980) "Three-time-level methods for the numerical solution of soil freezing problems", Cold Regions Sci. Tech. 3, 237-242.

Goodrich, L.E. (1982) An Introductory Review of Numerical Methods for Ground Thermal Regime Calculations, N.R.C.Can., D.B.R. Paper No. 1061, Ottawa, 33pp.

Halliwell, D.H. and W.R. Rouse (1987) "Soil heat flux in permafrost: characteristics and accuracy of measurement", J. of Climatology 7, 571-584.

Halliwell, D.H. and W.R. Rouse (1989) "A comparison of sensible and latent heat flux calculations using the Bowen ratio and aerodynamic methods", J.Oceanic Atmos. Tech. 6, 563-574.

Hogge, M.A. (1981) "A comparison of two- and three-level integration schemes for non-linear heat conduction", in Numerical Methods in Heat Transfer, R.W. Lewis, K. Morgan, and O.C. Zienkiewicz, eds. John Wiley and Sons, Ltd.

Holtslag, A.A.M. (1984) "Estimates of Diabatic Wind Speed Profiles From Near-Surface Weather Observations", Boundary-Layer Met. 29, 225-250.

Hromadka, T.V. II, G.L. Guymon, and R.L. Berg (1981) "Some approaches to modelling phase change in freezing soils" Cold Regions Sci. Tech. 4, 137-145.

Kellogg, W.W. and Z-C Zhao (1988) "Sensitivity of soil moisture to doubling of carbon dioxide in climate model experiments. Part I: North America", J. Climate 1, 348-366.

Kimball, B.A. and R.D. Jackson (1975). "Soil heat flux determination: a null-alignment method." Agricultural Meteorology 15, 1.

Lunardini, V.J. (1981) Heat Transfer in Cold Climates, Van Nostrand Reinhold Co., New York, 731pp.

Luthin, J.N. and G.L. Guymon (1974) "Soil moisture-vegetation-temperature relationships in central Alaska", J. Hydrology 23, 233-246.

McCaughey, J.H. and D.M. Brintnell (1984) "Evaluation of a Bowen Ratio Measurement System over Forest and Clear-Cut Sites at Petawawa, Ontario", J. Atmospheric and Oceanic Technology 4, 276-282.

Monteith, J.L. (1965) Evaporation and Environment, Symp. Soc. Exp. Biol., XIX, Cambridge Univ. Press, 205-234.

Monteith, J.L. (1981) "Evaporation and surface temperature", Q. J. Roy. Met. Soc. 107, 1-27.

Morgan, K., R.W. Lewis, and O.C. Zienkiewicz (1978) "An improved algorithm for heat conduction problems with phase change", Int. J. for Num. Meth. Engng. 12, 1191-1195.

Nixon, J.F. and D.H. Halliwell (1982) "Practical applications of a versatile geothermal simulator", ASME Winter Annual Meeting, Phoenix, Arizona, Nov. 1982.

Novak, M.D. and T.A. Black (1985) "Theoretical determination of the surface energy balance and thermal regimes of bare soils", Bound. Lay. Met. 33, 313-333.

Ohmura, A. (1982) "Objective Criteria for Rejecting Data for Bowen Ratio Flux Calculations", J. Applied Met. 21, 595-598.

Oke, T.R. (1978) Boundary Layer Climates, Methuen and Co., London, 372pp.

Outcalt, S.I., C. Goodwin, G. Weller, and J. Brown (1975) "Computer simulation of the snowmelt and soil thermal regime at Barrow, Alaska", Water Resources Research 11, 709-715.

Outcalt, S., and F. Nelson (1985) "A model of near-surface coupled-flow effects on the diurnal thermal regime of a peat-covered palsa", Arch. Met. Geoph. Biocl., Ser. A 33, 345-354.

Patterson, D.E. and M.W. Smith (1981) "The measurement of unfrozen water content by Time Domain Reflectometry: results from laboratory tests", Can. Geotech. J. 18, 131-144.

Paulson, C.A. (1970) "The mathematical representation of wind speed and temperature profiles in the unstable atmospheric surface layer", J. Appl. Met. 9, 857-861.

Penman, H.L. (1948) "Natural evaporation from open water, bare soil, and grass", Proc. Roy. Soc. London, Ser. A 193, 120-146.

Penney, C.L. (1979). "The ground heat flux dependence on size and depth of implantation of a transducer." Arch. Met. Geoph. Biokl., Ser. B 27, 23.

Press, W.H., B.P. Flannery, S.A. Teukolsky, and W.T. Vetterling (1986) Numerical Recipes, Cambridge University Press, Cambridge, 818pp.

Priestley, C.H.B. and R.J. Taylor (1972) "On the assessment of surface heat flux and evaporation using large-scale parameters", Mon. Wea. Rev. 106, 81-92.

Riseborough, D.W. (1985) Modelling Climatic Influences on Permafrost at a Boreal Forest Site, M.A. Thesis, Dept. of Geography, Carleton University, Ottawa, Ont. 172pp.

Rouse, W.R. (1984) "Microclimate at arctic tree line II. Soil microclimate of tundra and forest", Water Resources Research 20, 67-73.

Schwerdtfeger, P. (1976). Physical Principles of Micro-meteorological Measurements. Developments in Atmospheric Science 6, Elsevier Scientific Publishing Company, Amsterdam.

Sellers, W.D. (1965) Physical Climatology, U. of Chicago Press, Chicago, 272pp.

Smith, M.W. (1975) Numerical Simulation of Microclimatic and Active Layer Regimes in a High Arctic Environment, ALUR 74-75-72, Ministry of Indian and Northern Affairs, Ottawa, 29pp.

Smith, M.W. (1977) Computer Simulation of Microclimatic and Ground Thermal Regimes: Test Results and Program Description, ALUR 75-76-72, Ministry of Supply and Services Canada, Ottawa, 74pp.

Smith, M.W. (1984) "Climate change and other effects on permafrost", In Permafrost: Fourth International Conference, Final Proceedings, National Academy Press, Washington, D.C., 153-155.

Smith, M.W. and D.W. Riseborough (1983) "Permafrost sensitivity to climatic change", In Permafrost: Fourth International Conference, Proceedings, National Academy Press, Washington, D.C., 1178-1183.

Smith, M.W. and D.W. Riseborough (1985) "The sensitivity of thermal predictions to assumptions in soil properties", in Proceedings, Fourth International Symposium on Ground Freezing, Sapporo, Japan, Balkema, Rotterdam, 17-23.

Tanner, C.B. and M. Fuchs (1968) "Evaporation from unsaturated surfaces: a generalized combination method", J. Geophys. Res. 73, 1299-1304.

Thom, A.S. (1975) "Momentum, Mass and Heat Exchange of Plant Communities", in Vegetation and the Atmosphere, Vol. 1, Principles, J.L. Monteith, ed., Academic Press, London, 57-109.

Topp, G.C., J.L. Davis, and A.P. Annan (1980). "Electromagnetic determination of soil water content: measurements in coaxial transmission lines." Water Resources Research 16, 574.

van Bavel, C.H.M. and D.I. Hillel (1976) "Calculating potential and actual evaporation from a bare soil surface by simulation of concurrent flow of water and heat" Agric. Met. 17, 453-476.

Viellette, J.J. and F.M. Nixon ((1980) Portable Drilling Equipment for Shallow Permafrost Sampling, Geological Survey of Canada Paper 79-21,

Weiner, J.H. (1955) "Transient heat conduction in multiphase media" Brit. J. Appl. Phys. 6, 361-364.

Weller, G. and B. Holmgren (1974) "The microclimates of the arctic tundra", J. Appl. Met. 13, 854-862.

Williams, P.J. (1977). "Thermal properties of soils", in Soil Freezing and Highway Construction, P.J. Williams and M. Fremond, eds., Paterson Centre, Carleton University, Ottawa, p34.

Wood, W.I. (1978) "On the Zienkiewicz three- and four-time-level schemes applied to the numerical integration of parabolic equations", Int. J. Num. Meth. Engnrg. 12, 1717-1726.

Yaglom, A.M. (1977) "Comments on wind and temperature flux-profile relationships", Boundary-Layer Met. 11, 89-102.